DTIC FILE COPY

AD-A199 717

OBJECTIVE ANALYSIS OF THE GULF STREAM THERMAL FRONT: METHODS AND ACCURACY

by

Karen L. Tracey
Amy I. Friedlander
D. Randolph Watts

University of Rhode Island
Graduate School of Oceanography
Narragansett, R.I. 02882

GSO Technical Report 87-2
December 1987

DTIC
ELECTE
JUL 22 1988
S D
H

DISTRIBUTION STATEMENT A
Approved for public release;
Distribution Unlimited

88

OBJECTIVE ANALYSIS

OF THE

GULF STREAM THERMAL FRONT:

METHODS AND ACCURACY

by

Karen L. Tracey

Amy I. Friedlander

D. Randolph Watts

Graduate School of Oceanography
University of Rhode Island
Narragansett, Rhode Island 02882

GSO Technical Report No. 87-2

December, 1987

This research program has been sponsored by the
National Science Foundation under grants OCE82-01222 and OCE85-17746
and by the Office of Naval Research under contract N00014-81-C-0062.

ABSTRACT

The objective analysis (OA) technique was adapted by Watts and Tracey in order to map the thermal frontal zone of the Gulf Stream. Here, we test the robustness of the adapted OA technique to the selection of four control parameters: mean field, standard deviation field, correlation function, and decimation time. Output OA maps of the thermocline depth are most affected by the choice of mean field, with the most realistic results produced using a time-averaged mean. The choice of the space-time correlation function has a large influence on the size of the estimated error fields, which are associated with the OA maps. The smallest errors occur using the analytic function, ρ_{WT}, which is based on four years of inverted echo sounder data collected in the same region of the Gulf Stream. Variations in the selection of the standard deviation field and decimation time have little effect on the output OA maps.

We determine the accuracy of the output OA maps by comparing them with independent measurements of the thermal field. Two cases are evaluated: standard maps and high temporal resolution maps, with decimation times of 2 days and 1 day, respectively. Standard deviations (STD) between the standard maps at the 15% estimated error level and the XBTs (AXBTs) are determined to be 47-53 m. The comparisons of the high temporal resolution maps at the 20% error level with the XBTs (AXBTs) give STD differences of 47 m.

DTIC COPY INSPECTED 6

DTIC COPY INSPECTED

n For
A&I

By
Distribution/
Availability Cod
Dist | Avail and/o Special
A-1

TABLE OF CONTENTS

Page

LIST OF TABLES

LIST OF FIGURES

SECTION 1. INTRODUCTION

1.1 Background

Objective analysis (OA) is a technique that statistically determines the optimal estimate of a quantity from a limited number of measurements of that quantity. The optimal estimate is the one, of all possible linear estimates, that has the least error. The optimal estimate is determined from the observations by knowing the space-time correlation function of the quantity being estimated. The first use of objective analysis was in meteorology when Gandin (1965) analyzed atmospheric pressure and wind fields. The technique was later introduced to oceanography by Bretherton et al. (1976), who demonstrated its use with simulated temperature and velocity data. Additionally, Freeland and Gould (1976) applied the method to velocity measurements obtained in the MODE region to produce stream function maps.

Several generalizations to the OA technique are presented in Carter (1983) and Carter and Robinson (1987). They extended its application to include spatial anisotropy by defining the correlations as functions of both x and y distances. Additionally, they introduced correlation functions that were dependent on the time lag as well. This allowed estimates of the field to be obtained from data collected over long periods of time.

In these applications, a necessary condition for performing objective analysis on the oceanographic data sets is that the fields being estimated must have homogenous statistics; that is, the mean must be zero and the variance must be uniform throughout. To satisfy these requirements, typically the technique could be applied only to data

obtained from mid-ocean regions, areas that were away from strong boundary currents.

Watts and Tracey (1985; hereafter referred to as WT85) extended the use of the OA method to frontal regions, where the homogenous statistics are not found. They overcame this difficulty by preconditioning the input data prior to performing the objective analysis (described below). This report documents a series of tests on the consistency and accuracy of our objective analysis work on the Gulf Stream.

1.2 Special Application to the Gulf Stream Frontal Zone

We have performed objective analyses on a set of inverted echo sounder (IES) observations taken in the Gulf Stream region near Cape Hatteras, NC (Section 2). For example, in WT85 and in three data reports (Tracey et al., 1985; Tracey and Watts, 1986b; and Friedlander et al., 1986) we have produced a series of maps of the 12°C isotherm depth (Z_{12}) at daily intervals, in which each map consisted of a full grid of points at regular (20-km) spacing.

To estimate the value at each output grid point, the OA mapping technique selects from all the available data within a specified maximum time lag (T) and maximum radial distance (R), the number of points (N) which had the highest correlations (ρ). By using an assumed noise level (E), smoothing is permitted and the method is not required to fit all the observations exactly. For example, the output maps shown in WT85 result from specifying N = 9, T = ±4 days, R = 120 km, and E = 0.05.

Since the measurements were made in a frontal region, we must always precondition the data. First, the mean field is removed from the observations, and the resulting perturbation field is then normalized by the standard deviation. In this way, the perturbation field has

homogeneous statistics and is appropriate for objective analysis. Both the mean and standard deviation are restored to the output field after running the OA, thus mapping the Gulf Stream Z_{12} field. In WT85, the "mean field" that was removed approximated the instantaneous cross-stream profile, in that it sloped steeply through the main portion of the thermocline. The standard deviation field was defined as the first derivative of the mean field, scaled to agree in magnitude with the observed variance. Both of these fields are shown below in Section 3.

A crucial input to the OA mapping technique is the correlation function. The Appendix to this report describes how the correlation function was determined empirically from nearly 5 years of measurements obtained in our study region of the Gulf Stream. An important result of this work is that after the mean field is removed from the observations, the resulting correlation function is isotropic. We typically use an analytic correlation function that was obtained by fitting a decaying (temporal and spatial) cosine function to the observed correlations. This function is shown in Section 3. This report compares results from other functions as well.

Additionally, the input time series of Z_{12} measurements had a sampling interval of one day. However, in our earlier mapping work we subsampled these input data at two-day intervals to use more independent measurements.

The OA technique also produces error estimates of the output Z_{12} field. The error associated with each output grid point depends only on the locations, in space and time, of the input data and the correlation function; it is independent of the measurements themselves. We have used these estimated error fields to mask out regions of the Z_{12} maps where the map quality is predicted to be poor (estimated errors

≥15-20%). Examples of these error fields are presented in Section 4.

1.3 Purpose of this Report

It is evident that the choices for the OA control parameters used by WT85 are not the only ones possible. For example, where WT85 used the instantaneous Gulf Stream profile to approximate the mean field, a temporally averaged thermocline profile might also have been used. Is the objective mapping technique robust to variations in these choices? Do the OA maps accurately represent the "true" field? In this report, we document the effects of varying the control parameters on the output maps. Then we determine the accuracy of these OA maps by comparing them with other independent measurements of the Gulf Stream thermocline field.

An array of inverted echo sounders was deployed in the Gulf Stream northeast of Cape Hatteras from July 1982 through May 1985 in order to monitor changes in the path of the current. In previous investigations (Watts and Rossby, 1977; Watts and Johns, 1982), IESs have been shown to be reliable instruments for monitoring the thermal structure of the water column with high temporal resolution. However, the instruments have been located at only a limited number of sites and were separated by relatively large distances (60-65 km). Since observations which provide both high temporal and spatial resolution are desired, the method of objective analysis was employed on the three-year-long set of IES data to produce daily maps of the Gulf Stream thermocline depth field on a highly resolved horizontal grid. The mapped region (Figure 2.1) extended 240 km across the Gulf Stream and 460 km downstream, with grid point spacings of 20 km.

The IES OA maps are tested against concurrent measurements of the Gulf Stream thermocline depth field obtained using ship- and

aircraft-deployed expendable bathythermographs (XBTs and AXBTs, respectively). The IES, XBT, and AXBT data are described in Section 2.

In Section 3, we test the robustness of the OA technique to variations in the selection of (a) mean field, (b) standard deviation field, (c) correlation function, and (d) subsampling interval of the input time series. For these tests, objective maps have been produced for both the IES and AXBT data. First we check the output maps for internal consistency by comparing them with the actual observations. Then we examine the differences between the OA maps produced with different choices of the above parameters, repeating these comparisons for a representative selection of maps.

In Section 4, we further test the accuracy of the IES OA maps by comparing them with independent measurements of the thermocline depth field. The Z_{18}s are extracted from over 500 XBT and AXBT records taken in the Gulf Stream frontal region throughout the three-year period. We also determined the Z_{18} from the corresponding objective maps, using a linear interpolation scheme whenever an XBT or AXBT site did not correspond to an output grid point. The differences between these observed and estimated values were calculated and these were subsequently compared at different levels of estimated mapping errors.

Finally, in Section 5, we present a summary of the important conclusions.

SECTION 2. DESCRIPTION OF THE DATA

2.1 IES Measurements

For the period July 1982 through May 1985, thermocline depth records of the Gulf Stream downstream of Cape Hatteras were collected using inverted echo sounders. The array, shown in Figure 2.1, was configured such that the lines of instruments were approximately normal to the historical mean axis of the current. The IESs were deployed on various subsets of the lines during several deployments throughout the three-year period. Typically, the instruments were placed about 60 km apart across the Gulf Stream and 65 km apart downstream. The number of IESs in the water at any given time varied from 8 to 20 (Figure 2.1), depending on the deployment and recovery schedules.

Using the techniques described in Watts and Johns (1982) and Tracey and Watts (1986a), the travel times measured by the IESs were scaled to thermocline depths. For many practical purposes the main thermocline depth can be represented by the depth of an individual isotherm. We have chosen the 12°C isotherm since it is situated near the highest temperature gradient of the main thermocline. In this report, we refer to the main thermocline depth and the depth of the 12°C isotherm (Z_{12}) interchangeably. The Z_{12} measurements for each instrument were smoothed using a 40-hour low-pass filter to remove the tidal and internal wave signals.

Objective maps of the thermocline field in the array area were produced from these Z_{12} records at daily intervals for July 1982 to May 1985. The boxed region in Figure 2.1, oriented 064°T, is the 240 km by 460 km region which has been mapped. Two complete sets of maps were generated. The first set of maps (case A) was produced using the

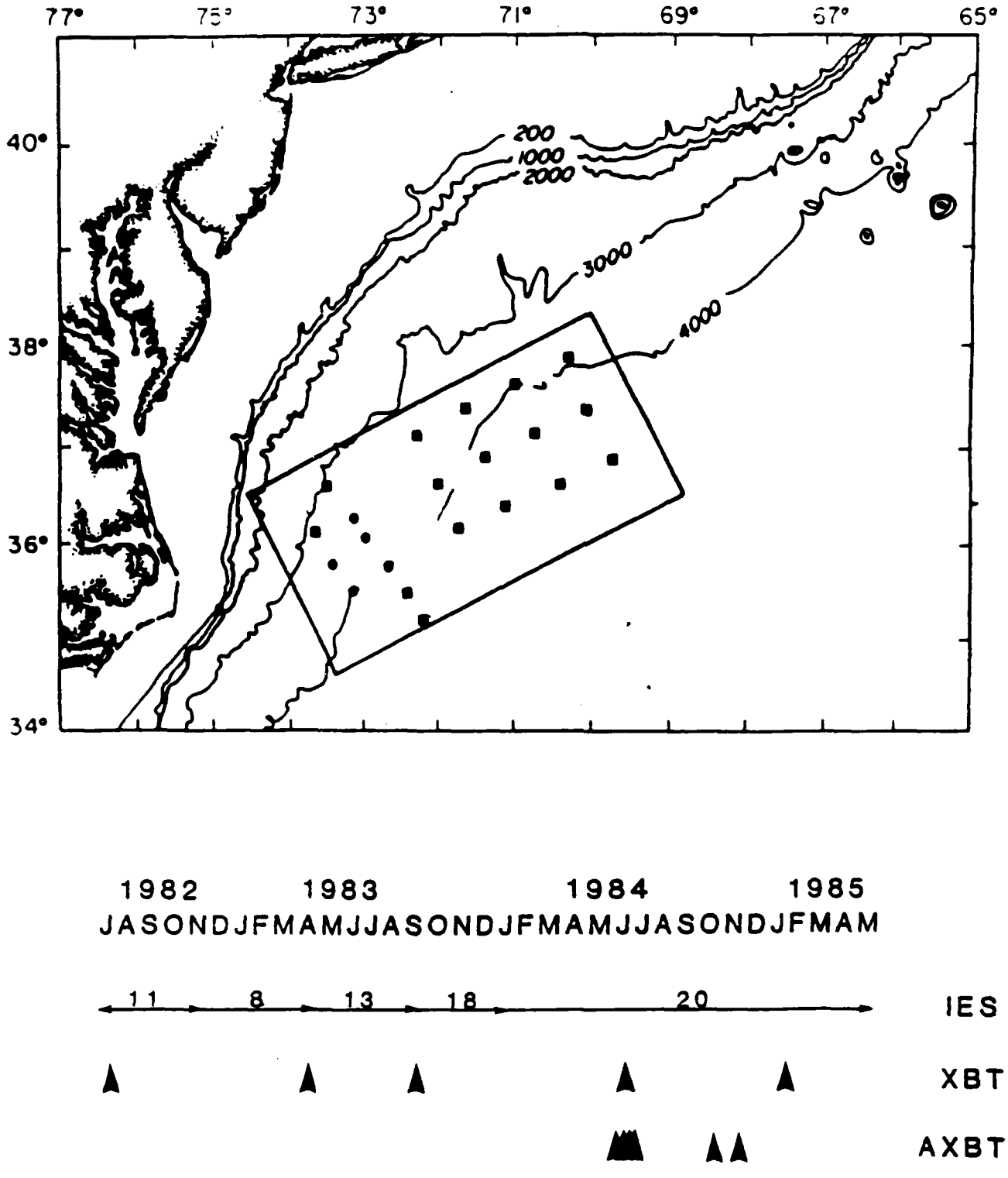

Figure 2.1 Map of IES array (top) and timeline of XBT and AXBT surveys (bottom). IES locations are shown by the solid circles and squares; the box outlines the 240 km by 460 km region mapped by objective analysis. The number of IESs deployed in the study area between July 1982 and May 1985 are indicated on the timeline. The dates of the XBT shipboard surveys and AXBT flight surveys are indicated by the arrows below the timeline.

special objective analysis (OA) techniques described in Section 1.2, together with the control parameters listed below (Section 3.1.1) for the "standard" maps. The second set (case B) was produced using different control parameters (described in Section 4.1.1), which gave higher temporal resolution. The complete set of case A IES OA maps for the three-year period is documented in three data reports (Tracey et al., 1985; Tracey and Watts, 1986b; and Friedlander et al., 1986).

In Section 3 of this report, the IES OA maps produced for 12 June and 17 October 1984 are used for the sensitivity tests of the mapping technique to the choices of control parameters. These two dates were selected because they coincided with two of the seven AXBT surveys (described below) that were conducted in the same region, and because the Gulf Stream path on these two dates typified two different cases.

In June 1984, the Gulf Stream flowed along a relatively straight path through the center of the IES array. At that time, we were conducting a cruise in the array area to recover and redeploy the instruments. Since some of the IESs were out of the water during that period, no real-time $Z_{1,2}$ measurements were available at those sites for 12 June. Thus, it was necessary to use time-lagged data in order to map the complete area. As a result, the estimated error fields associated with the IES OA maps for this day are slightly larger than those obtained when real-time measurements were available at all sites. The fourth AXBT survey was conducted on this day.

In contrast, on 17 October, the path of the Gulf Stream through the study area was arched by the passage of a meander. The strong thermal front associated with the Gulf Stream was located far to the north and almost out of the region mapped by the IES array. Since all the instruments were in the water at that time, the estimated error fields

associated with the IES OA maps are representative of those obtained during the three-year period. The fifth AXBT survey was conducted on this day. However, since the drop sites are typically concentrated in the frontal region, the spatial overlap between the AXBT survey and the IES array is limited.

In Section 4, the accuracy of both the case A ("standard") and case B (high temporal resolution) IES OA maps are assessed by comparing them with concurrent Z_{12} measurements obtained from XBT and AXBT (described below) probes deployed in the same region of the Gulf Stream. The Z_{12} value was determined from each IES OA map for exactly the same location as the XBT or AXBT drop site. When the drop site was not located at an output grid point, the Z_{12} value was found by linear interpolation.

Of the daily IES OA maps, the one that was closest in time to the probe launch was used for the comparison. Since the flight time required to complete an AXBT survey was usually less than eight hours, only one IES OA map was needed for comparison with each survey. However, several maps were needed for the comparisons with the XBT measurements, since ship surveys take several days to complete.

2.2 AXBT Measurements

During 1984, John Bane (University of North Carolina) flew seven AXBT survey flights mapping areas of the Gulf Stream thermal field from Cape Hatteras to 65°W. For six of these, there was sufficient overlap in the coverage to allow us to compare the Z_{12} measurements with those obtained from the IESs.

The AXBT probes, manufactured by Sippican Corporation, measured the temperature structure to a depth of 760 m. The depth of the 12°C isotherm was extracted from each record; the deepest Z_{12} was used when

there were shallower temperature inversions. All probes dropped in regions where the water was too cold (Slope Water) or too warm (Sargasso Sea) to have Z_{12} values were excluded from the tests described in Sections 3 and 4.

Of the six flights, the first four were conducted during June 1984. These occurred on 1, 4, 6, and 12 June. The fifth and sixth surveys were flown on 17 October and 13 November 1984. These survey flights are indicated on the timeline in Figure 2.1. Approximately 100 probes were launched per flight, with spacings of about 18 km cross stream and 55 km downstream. Since the primary purpose was to resolve the thermal front associated with the Gulf Stream, the survey region changed with each flight, depending on the location of the current. As a result, the survey region did not always coincide completely with the region mapped by the IES array.

In Section 3, the Z_{12} measurements determined for the AXBTs were used to generate objective maps for 12 June and 17 October using the same techniques as those used to produce the IES OA maps. However, because the surveys were conducted intermittently, the AXBT OA maps were produced without using time-lagged measurements. In order to compare them with the IES OA maps for the same dates, the AXBT OA maps encompass the same region as shown in Figure 2.1. Although many of the AXBT drop sites were actually outside this region, all Z_{12} measurements obtained on a given survey were used to produce the map.

The data from all six of the AXBT surveys are used in Section 4. As described above, the thermocline depths were determined from the IES OA maps at the same locations as the AXBT drop sites. For this comparison, we excluded all probes that were outside the boxed region

shown in Figure 2.1 to avoid excessive extrapolation outside the IES array.

2.3 XBT Measurements

Five research cruises were conducted to the study area between July 1982 and May 1985 (Figure 2.1). Four of these took place aboard the R/V ENDEAVOR: EN087 (5-25 July 1982), EN106 (22-30 September 1983), EN118 (1-18 June 1984), and EN124 (11-20 January 1985). The remaining cruise was aboard the R/V COLUMBUS ISELIN (C8304, 16-27 April 1983).

In all, nearly 300 XBT probes were launched during that time period. There were three main goals for the surveys: (a) to calibrate the IES measurements, (b) to map short segments of the path of the Gulf Stream, and (c) to determine the cross-stream structure of the thermocline.

All XBTs were T-7 probes manufactured by Sippican Corporation; they measured the temperature structure down to 800 m. The depth of the 12°C isotherm was extracted for each probe in the same manner as described above for the AXBTs.

These data are used in Section 4 of this report to test the accuracy of the IES OA maps. Since the XBT surveys were often concentrated near the IES sites, essentially the only probes excluded from this study were those dropped in regions where the waters were either too warm or too cold to obtain Z_{12} values.

SECTION 3. TESTS FOR ROBUSTNESS OF THE OBJECTIVE ANALYSIS METHOD

3.1 General Information for All Tests

In this section we report the results of several tests conducted on the objective analysis method in which we varied the selection of several control parameters. We produced OA maps (Table 3.1) of both the IES and AXBT data for two dates, 12 June and 17 October 1984. The Gulf Stream paths on these two dates were considered to be representative of its positions during 1984-1985. In June, the Gulf Stream was flowing along a relatively straight path through the center of the IES array. By contrast, during October a large meander deflected the Gulf Stream to the north and nearly out of the IES array.

3.1.1 Standard maps

In order to compare the results from the various tests, we produced a set of OA maps, which we considered to be accurate representations of the true fields, to be used as the 'standard maps' against which other maps would be tested. One IES OA map and one AXBT OA map were generated for each of the two dates analyzed. These four maps were used in each of the tests described in the following sections.

Each of these standard OA maps (Table 3.1) was made using the following set of control parameters: (a) the temporal mean field, Z_T (described in Section 3.2); (b) the Gaussian-shaped standard deviation field, σ_T (Section 3.3); (c) the analytic correlation function, ρ_{WT} (Section 3.4); and (d) a decimation time of 2 days (Section 3.5). Additionally, each standard map was produced using a maximum radial distance R = 120 km and an assumed noise level E = 0.05. The IES OA maps were generated using N = 9 points and maximum time lag T = ±4 days. However, due to the closer station spacing, the AXBT OA maps were

Table 3.1 OA map abbreviations and the associated control parameters. The maximum radial distance of R = 120 km and the assumed noise level of E = 0.05 are used for all of the objective maps listed.

Map Type	Map Number	Data Type	Date (1984)	Mean Field	Standard Deviation Field	Correlation Function	Decimation Time (days)	N*	T† (± days)
Standard Maps	I4T	IES	12 Jun	Temporal	Gaussian	WT Analytic	2	9	4
	I5T	IES	17 Oct	Temporal	Gaussian	WT Analytic	2	9	4
	A4T	AXBT	12 Jun	Temporal	Gaussian	WT Analytic	0	6	0
	A5T	AXBT	17 Oct	Temporal	Gaussian	WT Analytic	0	6	0
Mean and Standard Deviation Fields	I4C	IES	12 Jun	Constant	Constant	WT Analytic	2	9	4
	I4I	IES	12 Jun	Instantaneous	Derivative	WT Analytic	2	9	4
	I4CS	IES	12 Jun	Temporal	Constant	WT Analytic	2	9	4
	I5C	IES	17 Oct	Constant	Constant	WT Analytic	2	9	4
	I5I	IES	17 Oct	Instantaneous	Derivative	WT Analytic	2	9	4
	I5CS	IES	17 Oct	Temporal	Constant	WT Analytic	2	9	4
	A4C	AXBT	12 Jun	Constant	Constant	WT Analytic	0	6	0
	A4I	AXBT	12 Jun	Instantaneous	Derivative	WT Analytic	0	6	0
	A4CS	AXBT	12 Jun	Temporal	Constant	WT Analytic	0	6	0
	A5C	AXBT	17 Oct	Constant	Constant	WT Analytic	0	6	0
	A5I	AXBT	17 Oct	Instantaneous	Derivative	WT Analytic	0	6	0
	A5CS	AXBT	17 Oct	Temporal	Constant	WT Analytic	0	6	0
Correlation Function	I4EMP	IES	12 Jun	Temporal	Gaussian	Empirical	2	9	4
	I4HM	IES	12 Jun	Temporal	Gaussian	HM Analytic	2	9	4
	I5EMP	IES	17 Oct	Temporal	Gaussian	Empirical	2	9	4
	I5HM	IES	17 Oct	Temporal	Gaussian	HM Analytic	2	9	4
	A4EMP	AXBT	12 Jun	Temporal	Gaussian	Empirical	0	6	0
	A4HM	AXBT	12 Jun	Temporal	Gaussian	HM Analytic	0	6	0
	A5EMP	AXBT	17 Oct	Temporal	Gaussian	Empirical	0	6	0
	A5HM	AXBT	17 Oct	Temporal	Gaussian	HM Analytic	0	6	0
Decimation Time	I41D	IES	12 Jun	Temporal	Gaussian	WT Analytic	1	7	1
	I44D	IES	12 Jun	Temporal	Gaussian	WT Analytic	4	9	8
	I48D	IES	12 Jun	Temporal	Gaussian	WT Analytic	8	11	8
	I51D	IES	17 Oct	Temporal	Gaussian	WT Analytic	1	7	1
	I54D	IES	17 Oct	Temporal	Gaussian	WT Analytic	4	9	8
	I58D	IES	17 Oct	Temporal	Gaussian	WT Analytic	8	11	8

* N is number of points.
† T is maximum time lag

produced using N = 6. Since the AXBT survey flights were conducted intermittently, the AXBT OA maps were produced by specifying T = 0 days (no time lag).

In the following tests, other IES OA and AXBT OA maps for the same two days were produced by varying just one of these parameters at a time, keeping all of the others the same.

3.1.2 The OA map evaluations

For each test described below, we performed several comparisons in order to assess the sensitivity of the OA method to the parameter choices. An "internal consistency" check was performed in which the IES and AXBT OA maps were evaluated at the instrument sites, and then compared with the actual observations. Since both spatial and temporal smoothing were permitted, the estimated values did not need to agree exactly with the measurements. However, we expected the mapped fields to differ minimally from the input data at these sites.

Secondly, we compared pairs of OA maps by determining the differences between the estimated values at grid points. We limited the comparisons to include only those grid points for which the OA error field was predicted to be small (<15%). (The full estimated error field for a representative date is shown in Figure 4.1.) In the figures shown below, grid points which have been excluded from the analyses (predicted errors ≥15%) are shaded by the crosshatchings. For each test, we compare IES OA maps against other IES OA maps produced using different choices of the one parameter being tested. We repeat the same analyses for the AXBT OA maps. Subsequently, we intercompare the IES and AXBT OA maps produced using the same parameter choices.

The differences, ΔZ, between the estimated values at grid points are calculated as:

$$\Delta Z = (\text{OA Field 2}) - (\text{OA Field 1})$$

The first column in Tables 3.2-3.18 show the two OA maps being compared. For the internal consistency checks, OA Field 2 is replaced with the observations (abbreviated as OBS). The mean, range, and root-mean-square (RMS) differences of those grid points comparisons (NPTS) are listed in the tables, where

$$\text{range} = \max(\Delta Z) - \min(\Delta Z)$$

$$\text{mean} = \frac{\Sigma(\Delta Z)}{\text{NPTS}}$$

$$\text{RMS} = \left[\frac{\Sigma(\Delta Z)^2}{\text{NPTS}} \right]^{1/2}$$

Additionally, we report the residual RMS (STD), which was determined as:

$$\text{STD} = [(\text{RMS})^2 - (\text{Mean})^2]^{1/2}$$

3.1.3 Naming conventions

The IES and AXBT OA map numbers used in this report were formulated in the following way. The first letter, 'I' or 'A', indicates whether the map is derived from IES or AXBT data, respectively. Then a number (4 or 5) indicates the date of the map (the fourth AXBT survey was conducted on 12 June 1984; thus, the number '4' has been selected as the code for both the IES and AXBT maps for this day. Likewise, the fifth AXBT survey was made on 17 October 1984, and '5' has been used as its code number). The remaining symbols indicate the choices of the various parameters being tested. The abbreviations are listed in Table 3.1 along with the control parameters used to generate the maps.

3.2 Mean Field Selection

3.2.1 Description of the test

We chose to test the OA method sensitivity by using three different 'mean fields'. These three fields were: (a) a broad sloping profile, which represented the time-averaged thermocline, (b) a steeply sloping profile, which approximated the instantaneous thermocline running straight down the middle of the array, and (c) a constant mean throughout the entire mapping region.

To represent the time-averaged mean field, $Z_T(x,y)$, a third order polynomial was fitted to the mean Z_{ij} values observed at the IES sites during the June 1984 to May 1985 deployment period (Tracey et al., 1985). The functional form of the polynomial was:

$$Z_T(x,y) = B_0 + B_1x + B_2y + B_{11}x^2 + B_{12}xy + B_{22}y^2 + B_{111}x^3 + B_{112}x^2y + B_{122}xy^2 + B_{222}y^3$$

where (x,y) is the position in kilometers from the origin at 36°00'N, 73°30'W and the x axis is along 064°T. B_0 is 5.997880E+02, B_1 is 6.122714E-01, B_2 is -3.145789E+00, B_{11} is -1.427472E-03, B_{12} is 5.780502E-03, B_{22} is -7.886405E-03, B_{111} is -3.748734E-07, B_{112} is -1.383396E-05, B_{122} is 5.646291E-06, and B_{222} is 2.626524E-05. Figure 3.1 shows this 'temporal mean' field in plan view.

The 'instantaneous mean' field, Z_I, was approximated by an asymmetric tanh-like function of cross-stream distance y of the form:

$$Z_I(y) = Z_i + \left[\frac{Z_B - Z_A}{1 + \frac{1}{D}}\right]\left[\frac{1 - e^{\frac{-2(y-C)}{A}}}{1 + De^{\frac{-2(y-C)}{A}}}\right]$$

where Z_i is 350 m, Z_A is 100 m, Z_B is 850 m, D is 2.0, A is 40 km, and C is 25 km, determined from observational results. It should be noted that Z_I does not vary in the downstream direction and is identical to

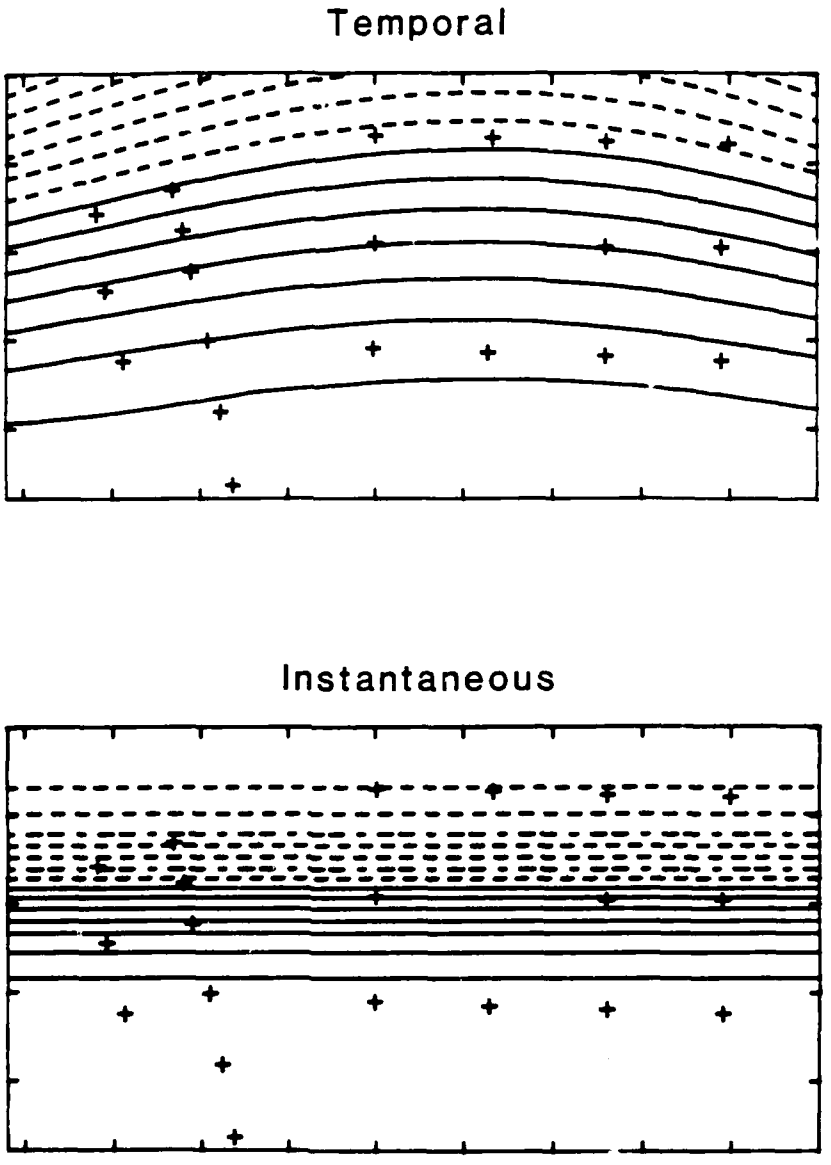

Figure 3.1 The temporal mean field, Z_T (top), and the instantaneous mean field, Z_I (bottom), are contoured in plan view. Contours indicate the depth of the 12°C isotherm (Z_{12}), with dashed contours indicating depths shallower than 500 m. The contour interval is 50 m. The frames, corresponding to the boxed region of Figure 2.1, have been rotated so that the long sides lie across the page.

the mean field used in WT85. This instantaneous mean field is also shown in Figure 3.1.

The third mean field used in this test is typical of the mean fields removed in traditional applications of objective analysis (c.f., Carter, 1983). We defined the third mean field as Z_C = 400 m. It is unlike the temporal and instantaneous means, which slope down across the mapping region, in that it is constant throughout the entire area.

Associated with each of these mean fields is a different standard deviation field (σ). Since these σ fields are defined as functions of the mean fields, they were varied during this test as well. However, as will be shown in Section 3.3, the choice of σ alone has minimal effect on the output fields; thus, the comparisons presented here are primarily affected by the choice of mean field, not σ.

3.2.2 Description of the AXBT and IES OA maps

The AXBT and IES OA maps for 12 June are shown in Figures 3.2 and 3.3, respectively. The corresponding maps for 17 October are shown in Figures 3.4 and 3.5. In each figure, the three maps were produced from identical set of observations and the standard control parameters, except for the choices of mean fields (and their associated standard deviation fields).

The overall impression of the output maps produced by removing the various mean fields is that they are somewhat different from one another. However, their similarities, especially in the <u>interpolated</u> regions (between the instrument sites), are apparent on closer examination. In general, both the shape of the Gulf Stream path and the steepness of the thermocline are similar for maps constructed from the same observations (c.f., Figure 3.2). The obvious exceptions are maps A5I (Figure 3.4) and I5I (Figure 3.5), for which the combined usage of

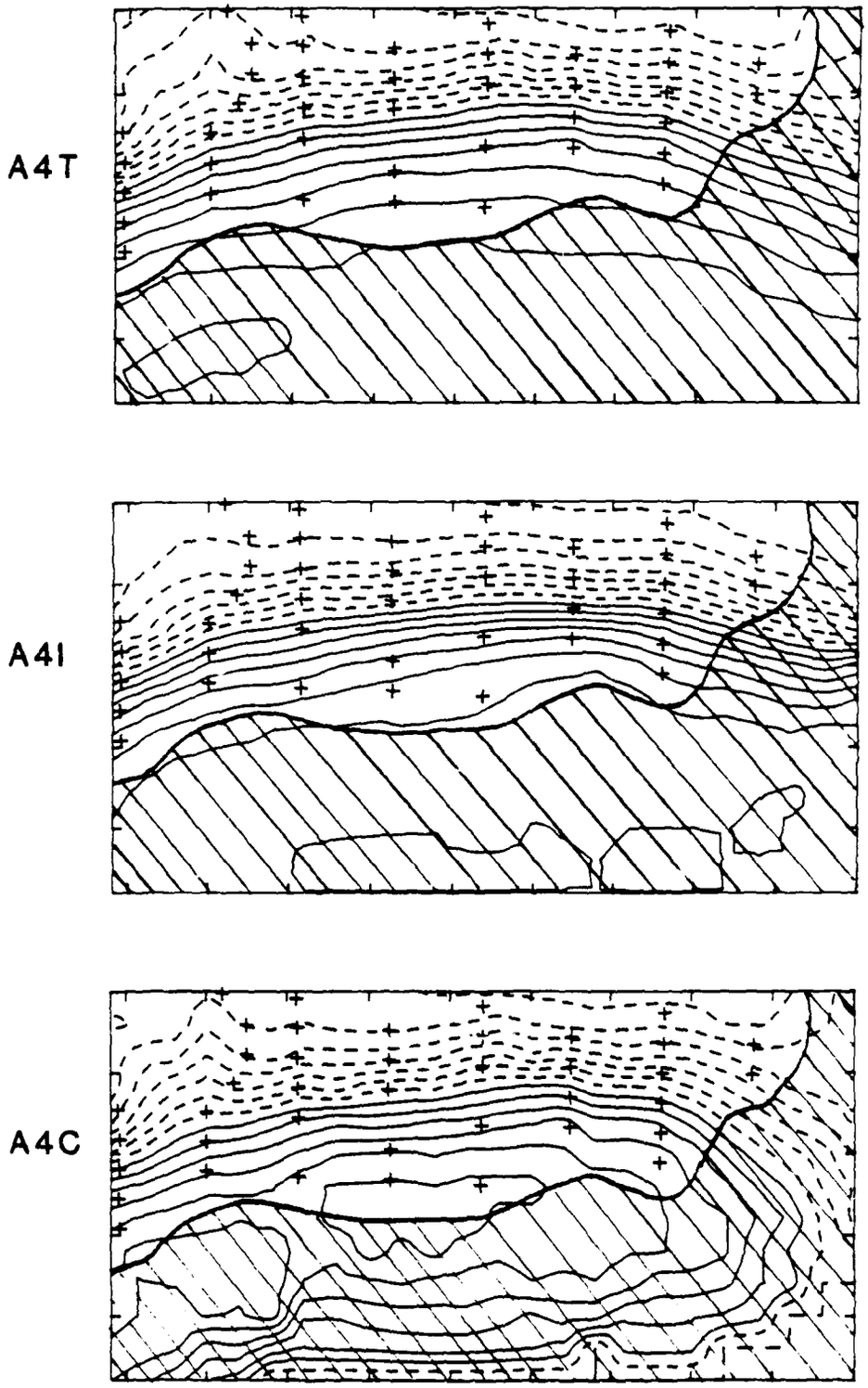

Figure 3.2 AXBT OA maps for survey 4 (12 June 1984) produced using three different mean fields: temporal (A4T), instantaneous (A4I), and constant (A4C). The Z_{12} field is contoured at 50 m intervals, and depths shallower than 500 m are dashed. Hatching indicates regions where the estimated errors are $\geq$15%; these regions have been excluded from the comparisons.

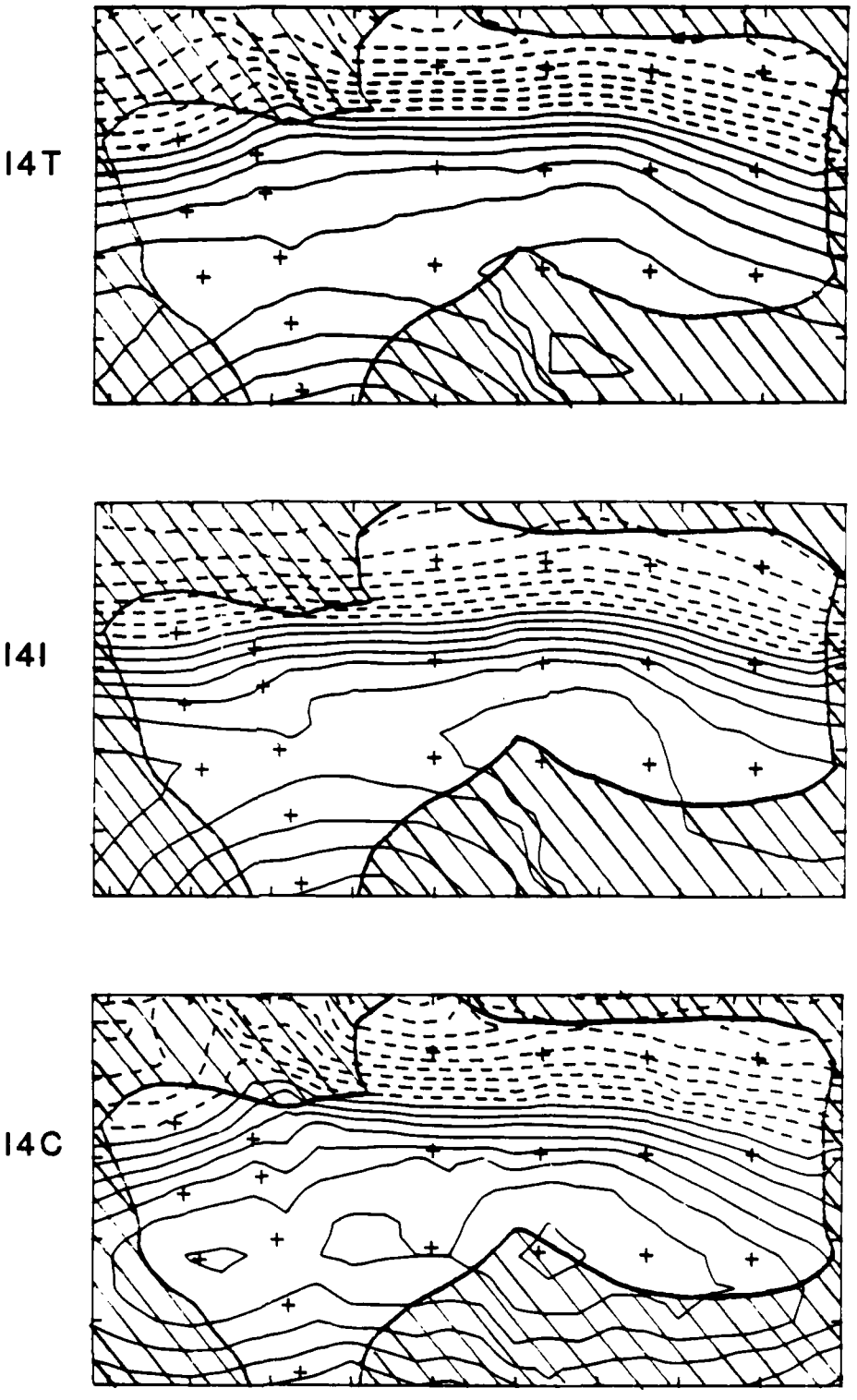

Figure 3.3 IES OA maps for survey 4 (12 June 1984) produced using three different mean fields: temporal (I4T), instantaneous (I4I), and constant (I4C). Contours and hatching are the same as in Figure 3.2.

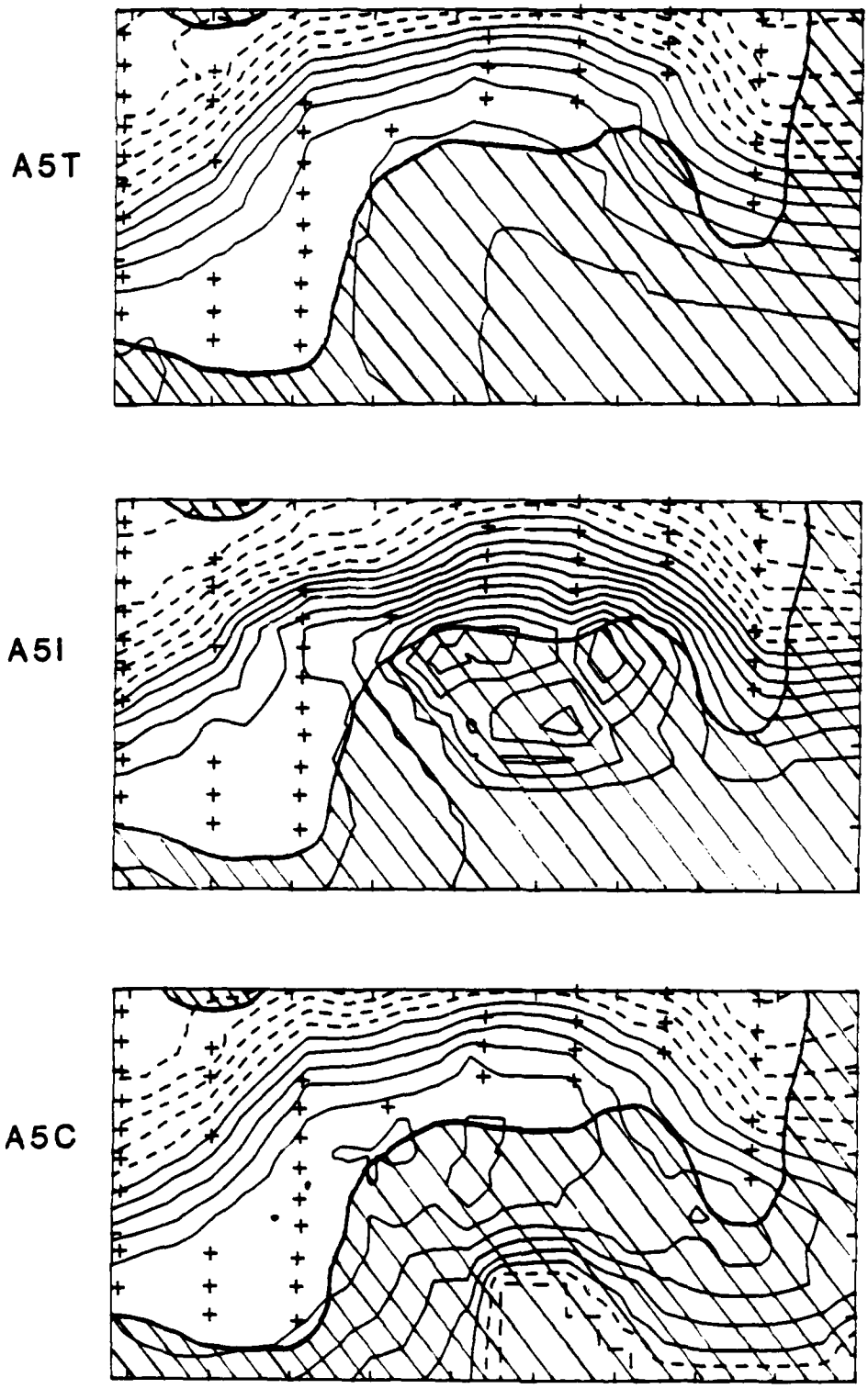

Figure 3.4 AXBT OA maps as in Figure 3.2 except for survey 5 (17 October 1984).

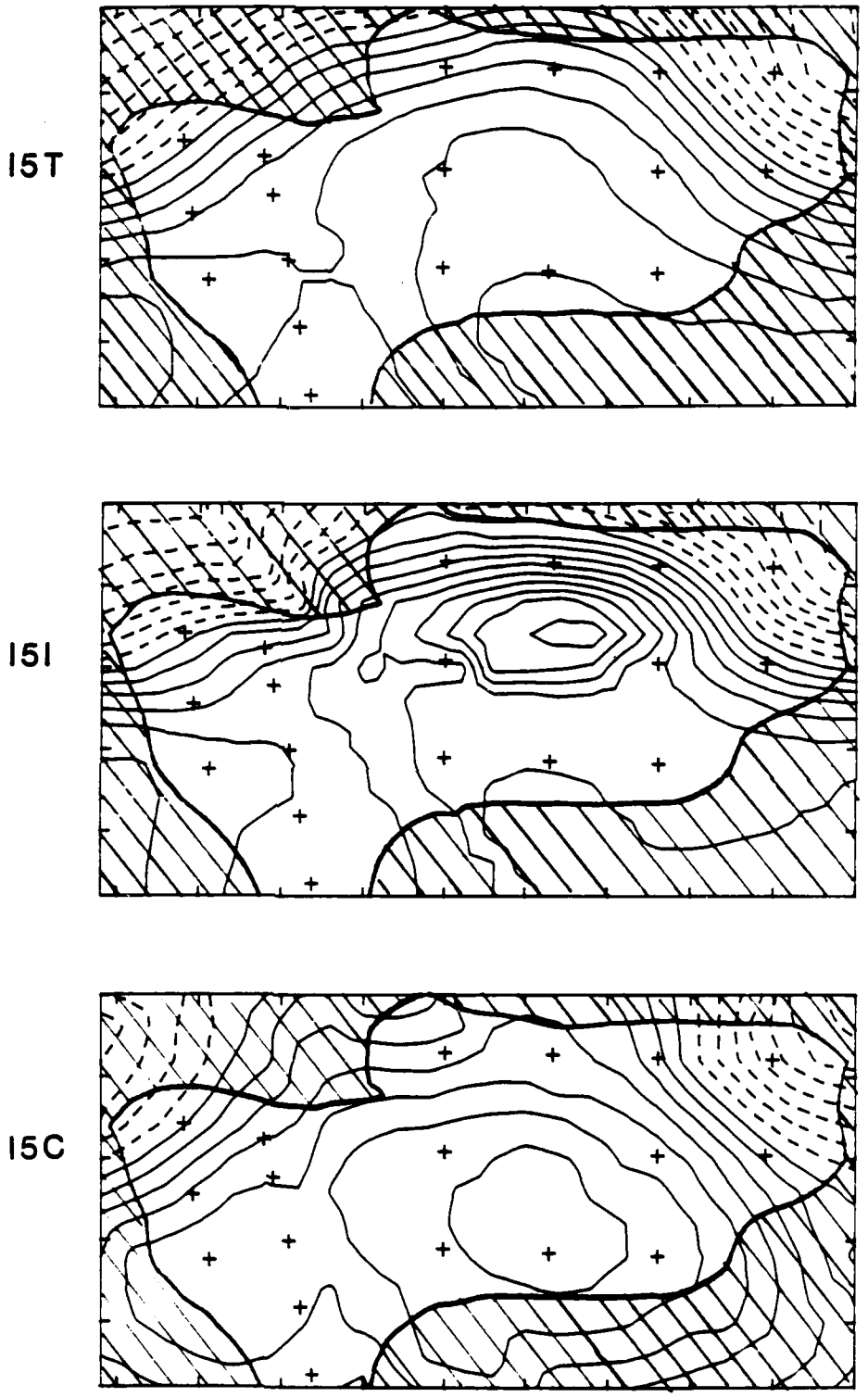

Figure 3.5 IES OA maps as in Figure 3.3 except for survey 5 (17 October 1984).

the instantaneous mean field (Z_I) with the Gulf Stream in a northern location results in a steepening of the thermocline and an 'overshoot' in estimating its depth on the offshore side.

The largest differences between the output maps occur in the extrapolated areas, outside the instrument sites. Much of this area has been masked out (indicated by hatching), because the objectively estimated error field is high. However, one of the main purposes for using the OA method is to estimate the field throughout a broader geographic region extending beyond the IES sites. Hence, we wish to test how well the OA method works in the extrapolated but low-estimated-error region. Additionally, the interpolated areas are affected to some extent by these extrapolated fields. Therefore, we examine the full region of low estimated error. In the following discussions, we describe some of these differences, which result from the different mean fields.

As mentioned above, the usage of the Z_I can result in an overestimation ('overshoot') of the thermocline depth. Whereas the overshoot occurs in the extrapolated area of the densely sampled AXBT map (A5I in Figure 3.4), it also occurs within the interpolated region of the IES map (I5I in Figure 3.5), where there was a large distance separating the instrument sites. Although the loss of one IES in the middle of the array appears to be an important factor in the occurrence of the overshoot, WT85 observed similar overshoots during February 1984 with a full array of instruments. In I5I, the overshoot appears as an isolated pool of deep water. The Gulf Stream path must deviate around this pool in order for the output map to agree with the input measurements. Except for these overshoots, the extrapolated areas

appear to be typical of the Gulf Stream region, even resolving the nearby rings.

A characteristic of the OA method is that the estimated output field, away from the input measurements, will return to the mean field. Clear examples of this are the OA maps A4C, A5C, I4C, and I5C, produced using the constant mean field, Z_C. The contours of constant 12°C isotherm depth thus form unrealistic closed features in the thermal structure. These isolated pools are pronounced along the northern edge of the mapped region in I5I (Figure 3.5). The thermocline depth is grossly underestimated on the offshore side of the Gulf Stream. Additionally, the cold-core Gulf Stream ring is not resolved in the maps for 12 June (A4C and I4C). As a result, the usefulness of the OA maps produced using Z_C is limited because the accurate region of extrapolation is minimal.

The OA maps A4T, A5T, I4T, and I5T produced using the temporal mean field, Z_T, appear to give the most accurate representation of the true temperature structure. Neither the overshoots nor the closed thermal features introduced by Z_I and Z_C are present in these maps. [However, the OA maps shown in Tracey and Watts (1986b) for February 1984 do show some smaller-scale (≤100 m) overshoots.] Also, the thermocline asymptotically reaches reasonable depths in the extrapolated regions.

3.2.3 Internal consistency

The comparisons of the AXBT OA maps, evaluated at all the observation sites, with the actual observations at those sites are given in Table 3.2. Similar comparisons are reported in Table 3.3 for the IES OA maps.

Regardless of which mean field was used, the agreements between the estimated and observed values are good. (Recall that since smoothing is

Table 3.2 AXBT OA Maps Evaluated at AXBT Sites for the Three Choices of Mean Fields

OBS-OA	Range*	Mean**	RMS†	NPTS††
OBS-A4I	57	0	12	61
OBS-A4C	79	0	16	61
OBS-A4T	46	-1	11	61
OBS-A5I	102	-1	15	73
OBS-A5C	60	0	11	73
OBS-A5T	53	0	10	73

* Range = $\max(Z_{OBS} - Z_{OA}) - \min(Z_{OBS} - Z_{OA})$

** Mean = $\frac{\Sigma(Z_{OBS} - Z_{OA})}{NPTS}$

† RMS = $\left[\frac{\Sigma(Z_{OBS} - Z_{OA})^2}{NPTS}\right]^{1/2}$

†† NPTS = Number of comparison points

Table 3.3 IES OA Maps Evaluated at IES Sites for the Three Choices of Mean Fields*

OBS-OA	Range	Mean	RMS	NPTS
OBS-I4I	26	2	8	15
OBS-I4C	43	-3	10	15
OBS-I4T	32	2	8	15
OBS-I5I	49	-3	10	18
OBS-I5C	82	-5	8	18
OBS-I5T	26	1	7	18

* Parameters defined as in Table 3.2

permitted, the estimated values need not agree exactly with the measurements.) The RMS differences of ≤15 m are comparable in size to the measurement errors of the instrumentation.

The best agreements between OA maps and observations (RMS 7-11 m) are obtained with the maps produced using the temporal mean thermocline field, Z_T. For both AXBT and IES measurements on both survey dates, the instantaneous and constant thermocline fields, Z_I and Z_C, produced OA maps with slightly greater range and RMS differences. Hence the Z_T mean field gives the best internal consistency.

3.2.4 Comparison of the AXBT OA maps

The three AXBT OA maps for each day are compared in Table 3.4. Differences are calculated at all mapped grid points within the 15% estimated error contour. Within this expanded region, interpolated and extrapolated from the measurement sites, the range and standard deviation (STD) are roughly 2 to 4 times greater than the range and RMS listed in Table 3.2, which were at the measurement sites only. (The RMS is the same as the STD in the earlier case, where the mean difference was essentially zero.) The largest differences generally occur at the outer boundary of the extrapolated field.

The maps produced using Z_T and Z_C are the most similar in that the range and STD values are the smallest. For these two AXBT surveys, the signs of the mean differences are negative, indicating that maps produced using Z_I are slightly deeper than the others. These results confirm the visual impressions of these maps, in which the thermocline slope appeared much steeper when Z_I was used. (However, mean differences less than about STD/5, or ~10 m, are not statistically significant.) When the Gulf Stream was located to the north (survey 5), the STD values of about 60 m are double those obtained when it flowed

Table 3.4 Differences Between AXBT OA Maps Generated Using Three Choices of Mean Fields

OA_2-OA_1	Range*	Mean**	RMS†	STD††	NPTS@
A4C-A4I	192	-7	33	32	152
A4T-A4I	151	-4	25	25	152
A4T-A4C	109	3	15	15	152
A5C-A5I	399	-11	64	63	159
A5T-A5I	392	-10	61	60	159
A5T-A5C	97	1	16	16	159

* Range = $\max(Z_{OA_2} - Z_{OA_1}) - \min(Z_{OA_2} - Z_{OA_1})$

** Mean = $\dfrac{\Sigma(Z_{OA_2} - Z_{OA_1})}{NPTS}$

† RMS = $\left[\dfrac{\Sigma(Z_{OA_2} - Z_{OA_1})^2}{NPTS}\right]^{1/2}$

†† RES = $[(RMS)^2 - (MEAN)^2]^{1/2}$

@ NPTS = Number of comparison points

Table 3.5 Differences Between IES OA Maps Generated Using Three Choices of Mean Fields*

OA_2-OA_1	Range	Mean	RMS	STD	NPTS
I4C-I4I	235	5	33	33	180
I4T-I4I	154	-3	29	28	180
I4T-I4C	95	-9	22	20	180
I5C-I5I	413	-4	67	66	177
I5T-I5I	368	-20	60	56	177
I5T-I5C	137	-16	28	23	177

* Parameters defined in Table 3.4

through the middle of the mapping region (survey 4). These larger differences for maps produced using Z_I are the result of an overshoot in estimating the thermocline depth on the southern side of the Gulf Stream.

3.2.5 Comparison of the IES OA maps

The IES OA maps for each day are compared in Table 3.5, at all grid points within the region where the estimated error is <15%. The results of these comparisons are very similar to those obtained for the AXBT OA maps in Section 3.2.4. Generally the maps produced using Z_T and Z_C are the most similar, whereas those produced using Z_C and Z_I are the most different. For each survey the range of the differences between Z_T and Z_I is more than double the range of the Z_T and Z_C differences.

3.2.6 Intercomparison of the AXBT and IES OA maps

The AXBT and IES OA maps, produced using identical mean fields, are compared in Table 3.6. Differences were calculated at all grid points within the intersection of their regions of estimated error <15%. The maps produced using Z_T consistently have the smallest ranges and STD values, indicating that they are the most similar. When the Gulf Stream flowed through the middle of the mapping region (survey 4), the largest differences between the maps were obtained using Z_C. However, when the Gulf Stream was far to the north (survey 5), the overshoots, obtained using Z_I, produced even bigger discrepancies between the AXBT OA and IES OA maps.

3.3 Standard Deviation Field Selection

3.3.1 Description of the test

The observed standard deviations (σ) of the IES Z_{12} measurements varied systematically, depending on the proximity of the instrument sites to the mean Gulf Stream location. Higher variance was located

Table 3.6 Intercomparisons of the AXBT OA and IES OA Maps Using Three Choices of Mean Fields*

OA_2-OA_1	Range	Mean	RMS	STD	NPTS
A4I-I4I	228	12	37	37	100
A4C-I4C	232	0	50	50	100
A4T-I4T	195	8	36	35	100
A5I-I5I	343	-5	59	58	100
A5C-I5C	220	-31	54	44	100
A5T-I5T	149	-15	42	39	100

* Parameters defined in Table 3.4

near the mean Gulf Stream center as a result of the steep thermocline slope in that region. Lower values were found both to the north and to the south, where the thermocline slope was reduced.

We represented the observed standard deviations with two different approximations. Both of these were defined as functions of the mean field depth; thus, each had to be applied to the data with its associated mean field. The first of these, σ_T, was described by a Gaussian function of the form:

$$\sigma_T(x,y) = A + B \exp -\left[\frac{Z_T(x,y) - Z_e}{C}\right]^2$$

where A is 50 m, B is (200 m - A), $Z_T(x,y)$ is the temporal mean thermocline depth at location (x,y), Z_e is 470 m, and C is 200 m. This function was chosen to be representative of all the IES records obtained in the Gulf Stream. For the second approximation, we chose the same functional form used by WT85 in which the field σ_I was taken to be the first derivative of the mean field Z_I, scaled to agree in magnitude with the observed values. Both σ_T and σ_I are shown in Figure 3.6 in plan view.

Since σ_T and σ_I are functions of the mean field depths, it was difficult to define a test that could adequately determine the robustness of the OA method to their selection only. Thus, in order to assess the effects of σ variations, we defined a third, very different, constant standard deviation field, σ_{CS} = 100 m, to be independent of the mean depth. Objective maps of the AXBT and IES data were then prepared using the temporal mean field, Z_T, and either σ_T or σ_{CS}.

3.3.2 Description of the AXBT and IES OA maps

The AXBT and IES OA maps for survey 4 (12 June 1984) are shown in Figure 3.7. The corresponding maps for survey 5 (17 October 1984) are

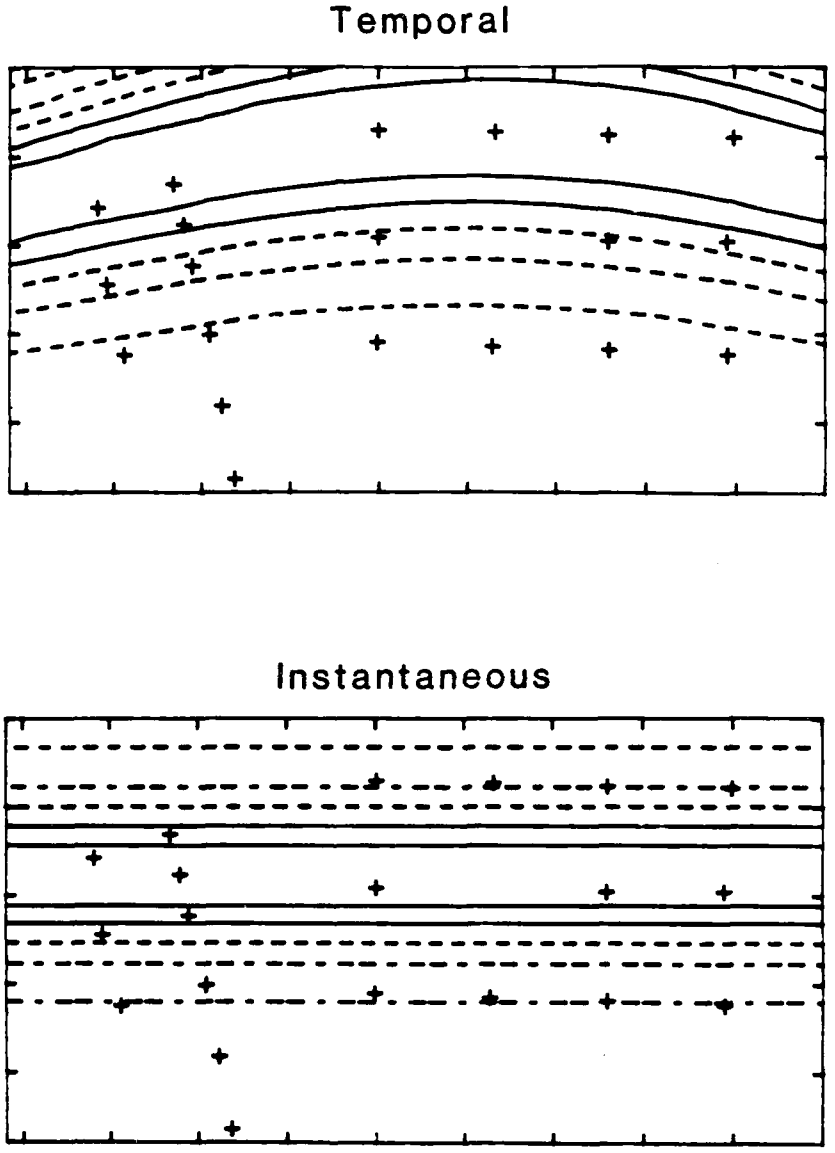

Figure 3.6 The temporal standard deviation field, σ_T (top), and the instantaneous standard deviation field, σ_I (bottom), are shown in plan view. The contour interval is 25 m, with the dashed contours indicating standard deviations of less than 150 m RMS.

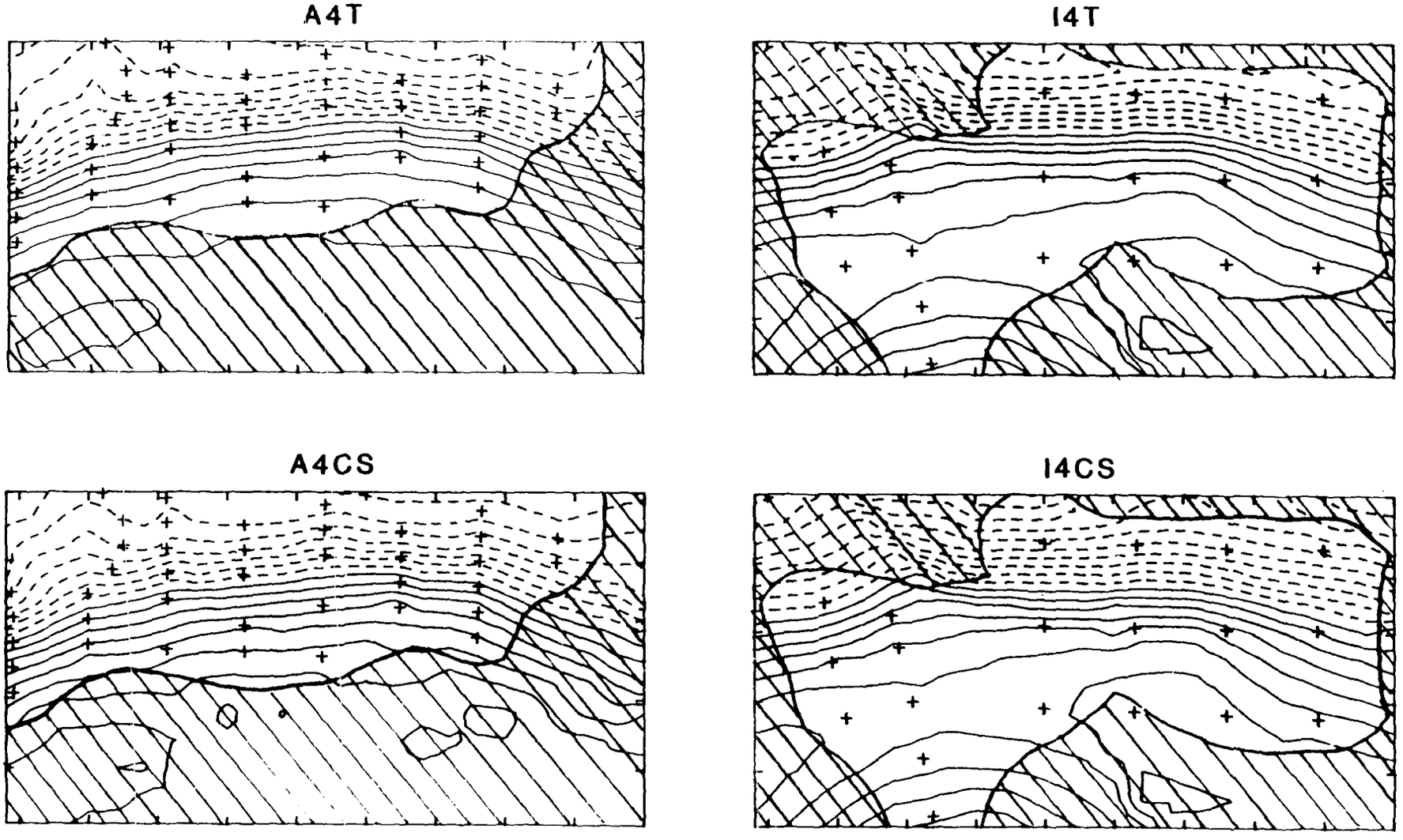

Figure 3.7 AXBT (left) and IES (right) OA maps for survey 4 (12 June 1984), produced using two different standard deviation fields: temporal (A4T and I4T) and constant (A4CS and I4CS). Contours and hatching are the same as in Figure 3.2.

shown in Figure 3.8. Each figure displays the maps produced using the two σ field choices.

Unlike the maps produced with the different mean field selections (Figure 3.3-5), the overall impression of the corresponding OA maps for the two surveys (Figures 3.7-8) is that they are very similar. The distinctions between them occur primarily in the small-scale features, such as the smoothness of the Z_{12} contours and the presence or absence of isolated pools of water.

The slope of the thermocline tends to be more linear in the maps produced using σ_{CS} (OA maps A4CS, A5CS, I4CS, and I5CS in Figures 3.7 and 3.8), as seen from the more uniform spacing of their Z_{12} contours. The linearity is most apparent along the upper edges of the mapping regions. For example, a comparison of the IES OA maps for survey 5 (Figure 3.8) reveals that the thermocline in I5CS is shallower than that in I5T when the depth is less than 300 m. Conversely, the thermocline in I5T is shallower for depths greater than 300 m.

3.3.3 Internal consistency

The AXBT OA maps evaluated at the AXBT sites are compared with the AXBT observations themselves in Table 3.7. The corresponding values for the IES OA maps and IES observations are listed in Table 3.8.

The estimated and observed values agree very well, with RMS differences of about 10 m. This is true no matter which standard deviation field was used. The range and RMS values for the AXBT comparisons are larger than those for the IES comparisons; however, this discrepancy is probably due to the fact that four times as many AXBT sites as IES sites were evaluated.

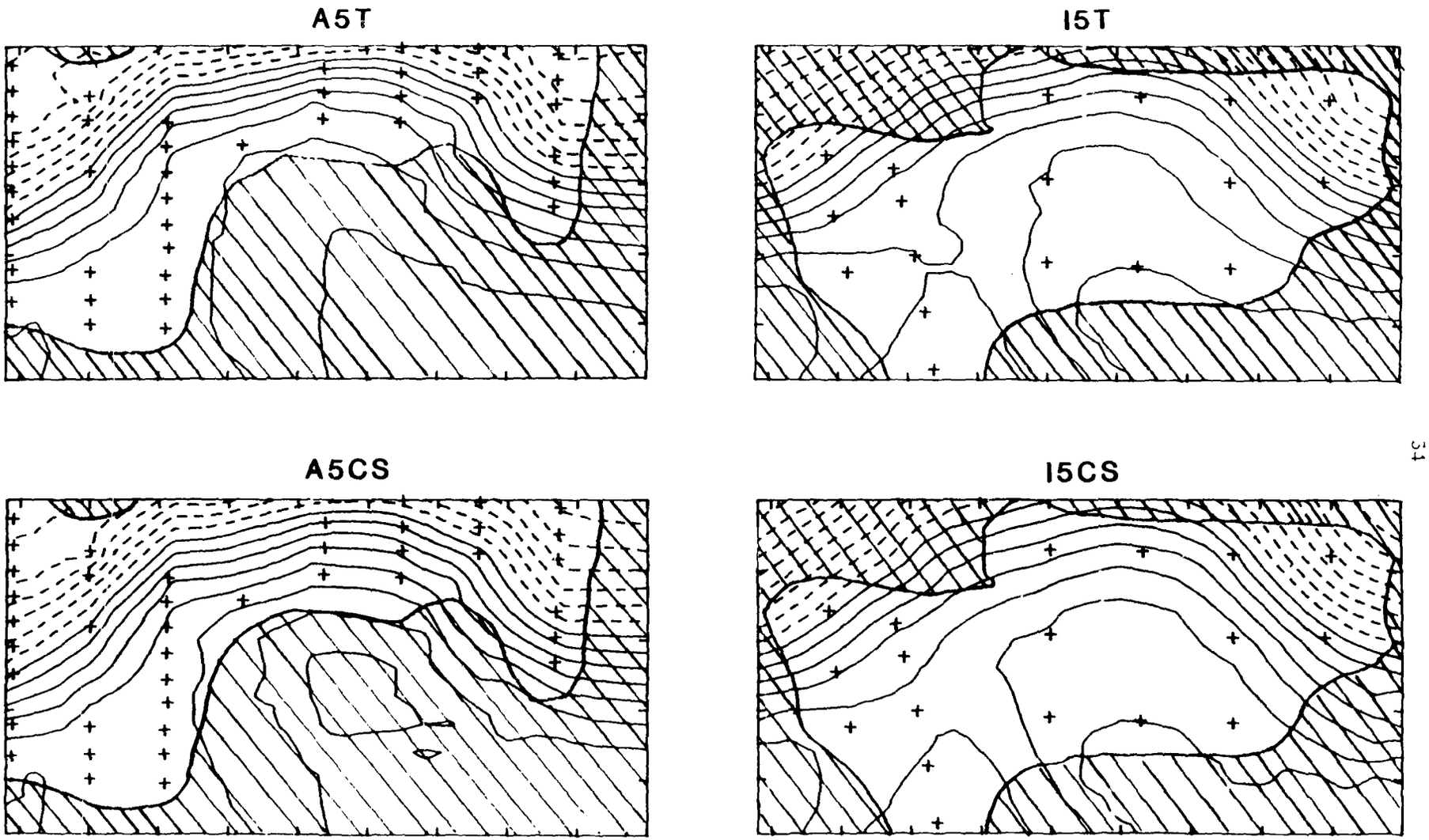

Figure 3.8 AXBT (left) and IES (right) OA maps as in Figure 3.7 except for survey 5 (17 October 1984).

Table 3.7 AXBT OA Maps Evaluated at AXBT sites for Two Choices of Standard Deviation Fields*

OBS-OA	Range	Mean	RMS	NPTS
OBS-A4CS	63	0	14	61
OBS-A4T	46	-1	11	61
OBS-A5CS	49	0	10	73
OBS-A5T	53	0	10	73

* Parameters defined in Table 3.2

Table 3.8 IES OA Maps Evaluated at IES sites for Two Choices of Standard Deviation Fields*

OBS-OA	Range	Mean	RMS	NPTS
OBS-I4CS	37	3	9	15
OBS-I4T	32	2	8	15
OBS-I5CS	27	1	6	18
OBS-I5T	26	1	7	18

* Parameters defined in Table 3.2

3.3.4 Comparison of the AXBT OA maps

The AXBT OA maps produced for each day are compared in Table 3.9a. The STD differences between the maps produced using σ_T and σ_{CS} are small (13 m), indicating that the maps are quite similar. The ranges (56 and 92 m, respectively) are roughly factors of two to four times smaller than those encountered when the mean field was varied (Table 3.4). This implies that the OA method is not as sensitive to the σ field selection as it is to the choice of mean field.

The biggest differences occur in the upper left portion of the mapped region, where the station spacing is somewhat larger (Figures 3.7 and 3.8). Typically, the thermocline depths there are slightly shallower for the maps produced using σ_C.

3.3.5 Comparison of the IES OA maps

Table 3.9b lists the differences between the IES OA maps produced using the two σ field choices. There is good agreement between the output maps since the STD values are not very large (less than 15 m). Additionally, the STD and range values are considerably less than those obtained with variations in the mean field (cf. I5T-I5I in Table 3.5).

The statistics in Table 3.9 indicate that there are bigger differences between the maps for survey 4 than between those for survey 5. Maps I4CS and I4T (Figure 3.7) differ primarily along the northern edge of the region.

3.3.6 Intercomparison of the AXBT and IES OA maps

The AXBT and IES OA maps, produced using the same standard deviation fields, are compared in Table 3.10. The maps produced using σ_T tend to have slightly smaller STD and range values, indicating that they are more similar than the maps using σ_{CS}. However, since the values for σ_{CS}

Table 3.9 Differences Between OA Maps Generated Using Two Choices of Standard Deviation Fields*

OA_2-OA_1	Range	Mean	RMS	STD	NPTS
a) AXBT OA Maps					
A4T-A4CS	56	-1	13	13	152
A5T-A5CS	92	-2	13	13	159
b) IES OA Maps					
I4T-I4CS	88	5	15	14	180
I5T-I5CS	92	-3	11	10	177

* Parameters defined in Table 3.4

Table 3.10 Intercomparisons of the AXBT and IES OA Maps Using Two Choices of Standard Deviation Fields*

OA_2-OA_1	Range	Mean	RMS	STD	NPTS
A4CS-I4CS	254	-19	47	43	100
A4T-I4T	195	8	36	35	100
A5CS-I5CS	158	-11	40	39	100
A5T-I5T	149	-15	42	39	100

* Parameters defined in Table 3.4

are not substantially different, the OA method is apparently not very sensitive to the choice of standard deviation field.

Since the standard deviation field is used to normalize the data prior to applying the OA method (and also to renormalize afterwards), the regions that have the largest perturbations are most affected by the choice of σ. Typically, large perturbations occur either when the output map differs substantially from the mean field or in the extrapolated portions of the output map. For example, in survey 4 (Figure 3.7), the Gulf Stream followed a relatively straight path through the center of the IES array, whereas the mean field (Z_T in Figure 3.1) was arched. Hence, the resulting perturbations are large. As can be seen in Figure 3.7, the thermocline depth in the OA maps from the IES data is shallower where it is extrapolated to the upper edge of the mapped region than it is for the AXBT data, where the survey was centered. This difference is slightly exaggerated for the maps produced using σ_{CS}.

3.4 Correlation Function Selection

3.4.1 Description of the test

Three space-time correlation functions (ρ) were selected for this test of the OA method. Two of these were presented in WT85 and the third was adapted from the autocorrelations given in Halliwell and Mooers (1983).

WT85 determined an empirical correlation function (ρ_{EMP}) from the set of Gulf Stream IES measurements made between 1979 and 1984. A complete explanation of the method used to calculate ρ_{EMP} is given in the Appendix of this report. Briefly, the instruments were grouped into cross-stream, along-stream, and diagonal pairs and the correlations of each group were calculated separately. The correlation function at zero

time lag was found to be isotropic. Figure 3.9 shows ρ_{EMP} in plan view for time lags out to 4 days.

The observed correlations were also approximated by an analytic function of the form:

$$\rho_{WT} = F_o \exp(- t' /T_o) \exp(-r/A) \cos(\pi r/2B)$$

where F_o = 1.0, t' is the lag time, T_o = 9.3 days, $r^2 = (x'-ct')^2 + y'^2$, x' and y' are the spatial separations, c = 12 km/day, A = 391 km, and B = 171 km. This function was chosen such that the temporal decay rate of the central peak was similar to the observed values and that the spatial decay rate was the same as that observed for zero time lag. Figure 3.9 shows ρ_{WT} in plan view for the same time lags as for ρ_{EMP}.

For the third correlation function, we selected one that was determined independently of our data, yet was still appropriate for the Gulf Stream region. Halliwell and Mooers (1983) presented space-time correlations for propagating meanders that were calculated from measurements of the Gulf Stream surface thermal front. We assigned to the function ρ_{HM} the same analytic form as ρ_{WT} but specified the parameters from those given in Halliwell and Mooers (1983). The function ρ_{HM}, shown in Figure 3.9, results from defining F_o = 0.8, T_o = 18.3 days, c = 7 km/day, A = 300 km, and B = 125 km.

For the previous tests of the OA method (Sections 3.2 and 3.3), we limited the OA map comparisons to include only those grid points for which the estimated errors were <15%. However, larger estimated error fields (described below) are produced for ρ_{EMP} and ρ_{HM}; consequently, the number of grid points lying within this specified error limit is reduced. Thus, for this test, we extended our comparisons to include grid points with estimated errors of <35%. All hatched regions (shaded

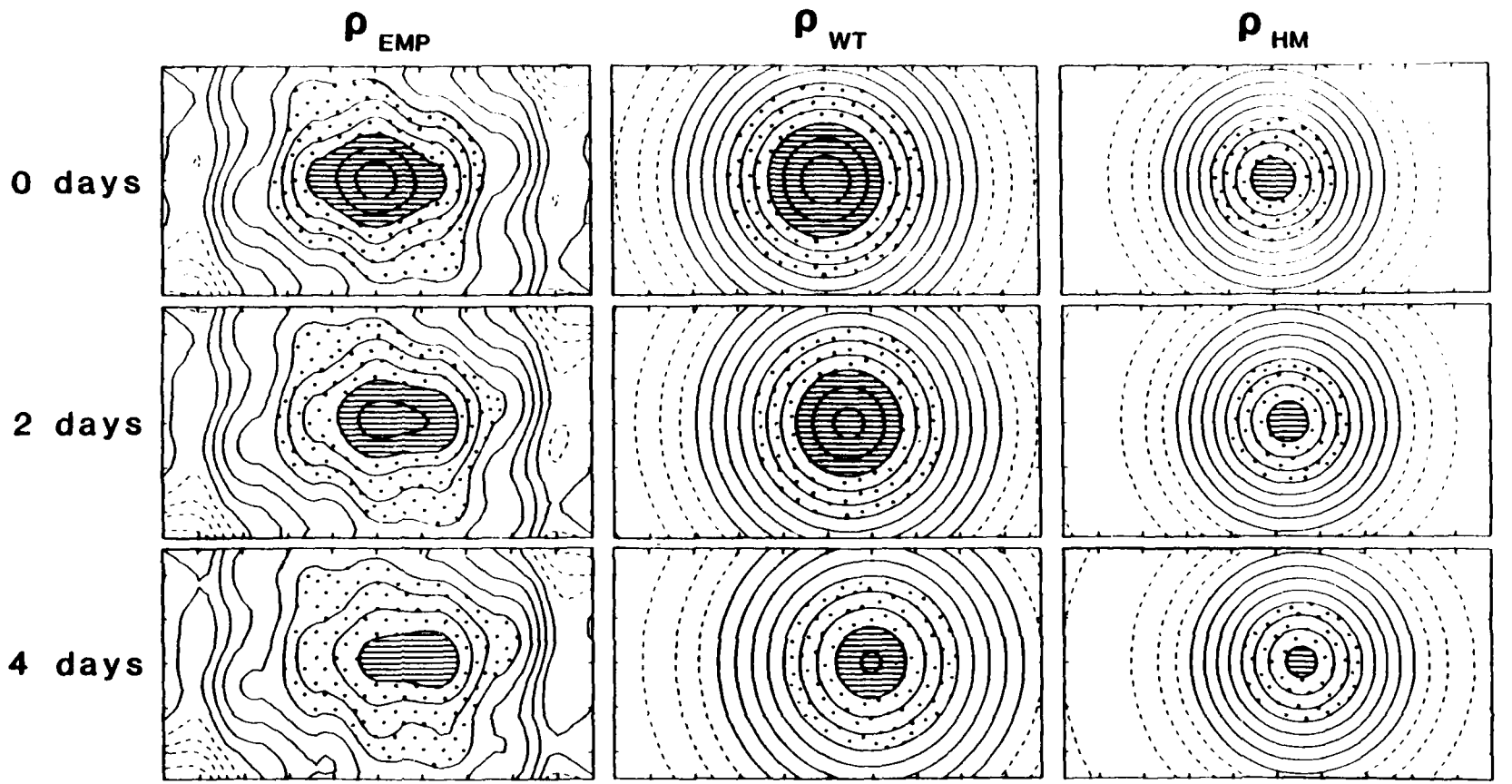

Figure 3.9 Three correlation functions, ρ_{EMP} (left), ρ_{WT} (center), and ρ_{HM} (right), contoured in plan view for time lags of 0, 2, and 4 d. For negative time lags, note that ρ is implicitly given by the symmetry relation $\rho(-x,-y,-t) = \rho(x,y,t)$. The contour interval is 0.1 and negative contours are dashed. Areas with hatching indicate $\rho \geq 0.7$; dotted areas indicate $0.7 \geq \rho \geq 0.4$.

by a single set of parallel lines) in Figures 3.10-13 have errors ≥15%; the crosshatching indicates that the errors exceed 35%.

3.4.2 Description of the AXBT and IES OA maps

The AXBT and IES OA maps for survey 4 (12 June) are shown in Figures 3.10 and 3.11, respectively. The corresponding maps for survey 5 (17 October) are shown in Figure 3.12 and 3.13. Each figure displays the three maps produced using the three different choices of ρ.

The most striking feature of the maps is the difference in the sizes of the two estimated error fields. The error fields for maps A4HM, A5HM, I4HM, and I5HM, all produced using ρ_{HM}, are the largest, with errors greater than 15% predicted throughout the entire mapping region. The error fields associated with ρ_{EMP} and ρ_{WT} are the most similar in size, yet the differences between them are apparent in the IES OA maps (Figure 3.11 and 3.13), where the spacing between instruments sites is coarser. The smallest estimated error fields are obtained with ρ_{WT}.

The large estimated error fields associated with ρ_{HM} are to be expected because the central peak of ρ_{HM} at zero time lag reaches only 0.8. Additionally, both the faster spatial decay rate and the slower temporal decay rate of the central peak may contribute to the larger errors, particularly for the sparse spatial and dense temporal sampling from the IES array.

One reason that ρ_{EMP} is associated with a larger error field than ρ_{WT} is that the shape of ρ_{EMP} is not as smooth as tnat of the analytic function (Figure 3.9). Another reason is that the central peak of ρ_{EMP} broadens at greater time lags (Figure 3.9). Thus, the input data would appear to be less independent to the OA method, resulting in a larger estimated error field.

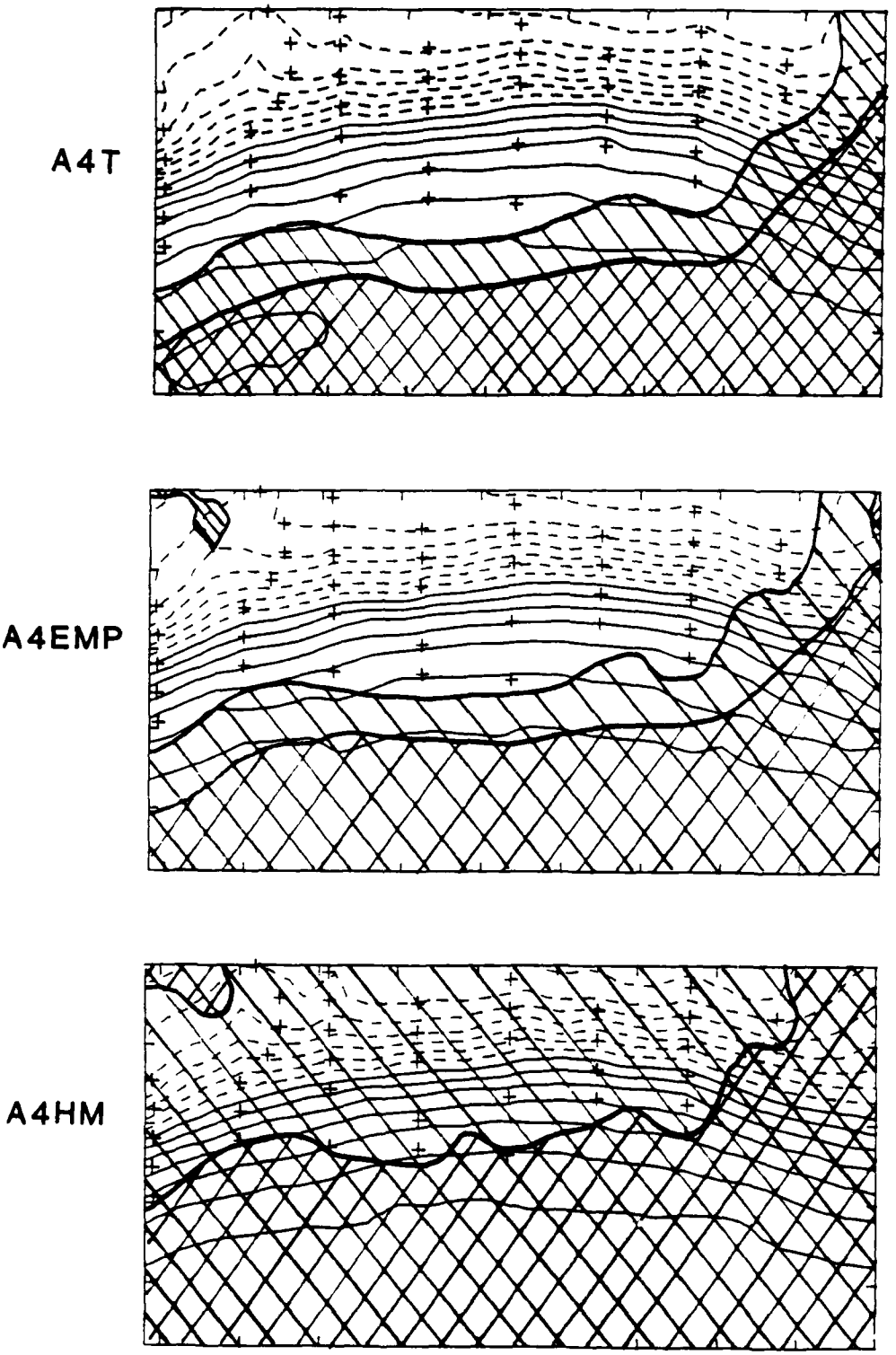

Figure 3.10 AXBT OA maps for survey 4 (12 June 1984), produced using three different correlation functions: ρ_{WT} (A4T), ρ_{EMP} (A4EMP), and ρ_{HM} (A4HM). Areas with hatching correspond to regions of $\geq$15% estimated error and the crosshatching designates areas where the estimated errors exceed 35%. Z_{12} contours and contour interval are the same as in Figure 3.2.

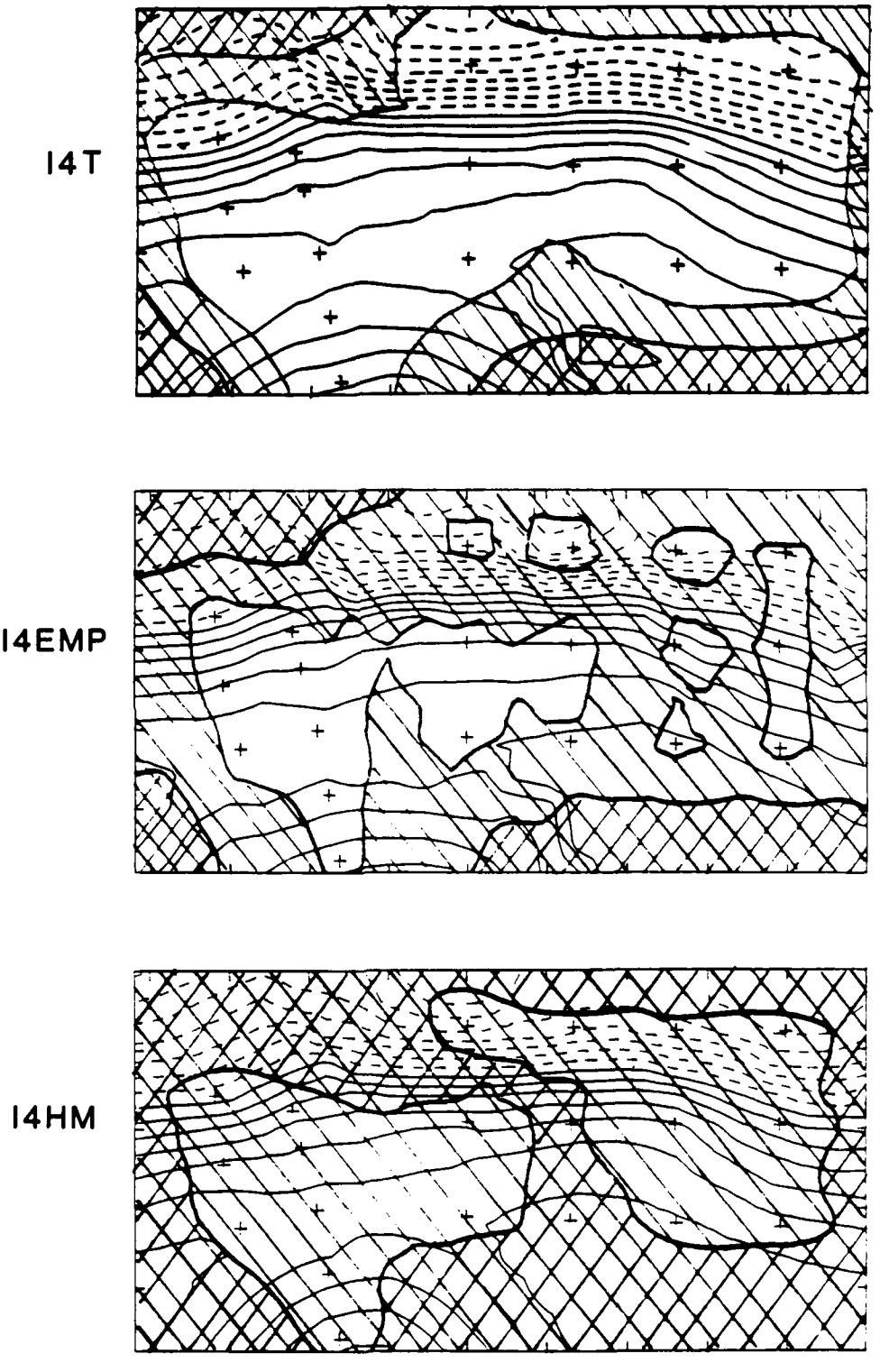

Figure 3.11 IES OA maps for survey 4 (12 June 1984), produced using three different correlation functions: ρ_{WT} (I4T), ρ_{EMP} (I4EMP), and ρ_{HM} (I4HM). Contours, hatching, and crosshatching are the same as in Figure 3.10.

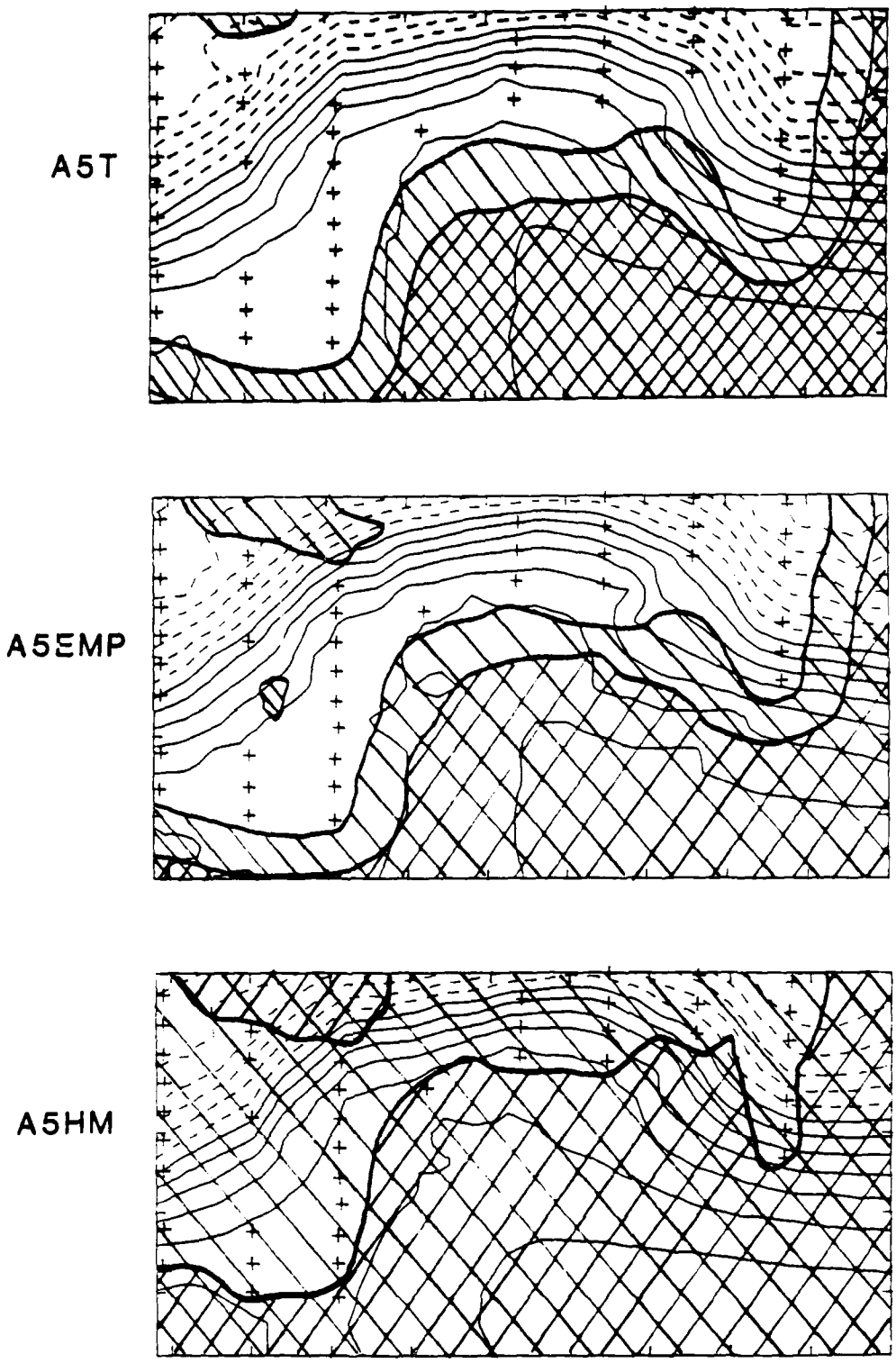

Figure 3.12 AXBT OA maps as in Figure 3.10 except for survey 5 (17 October 1984).

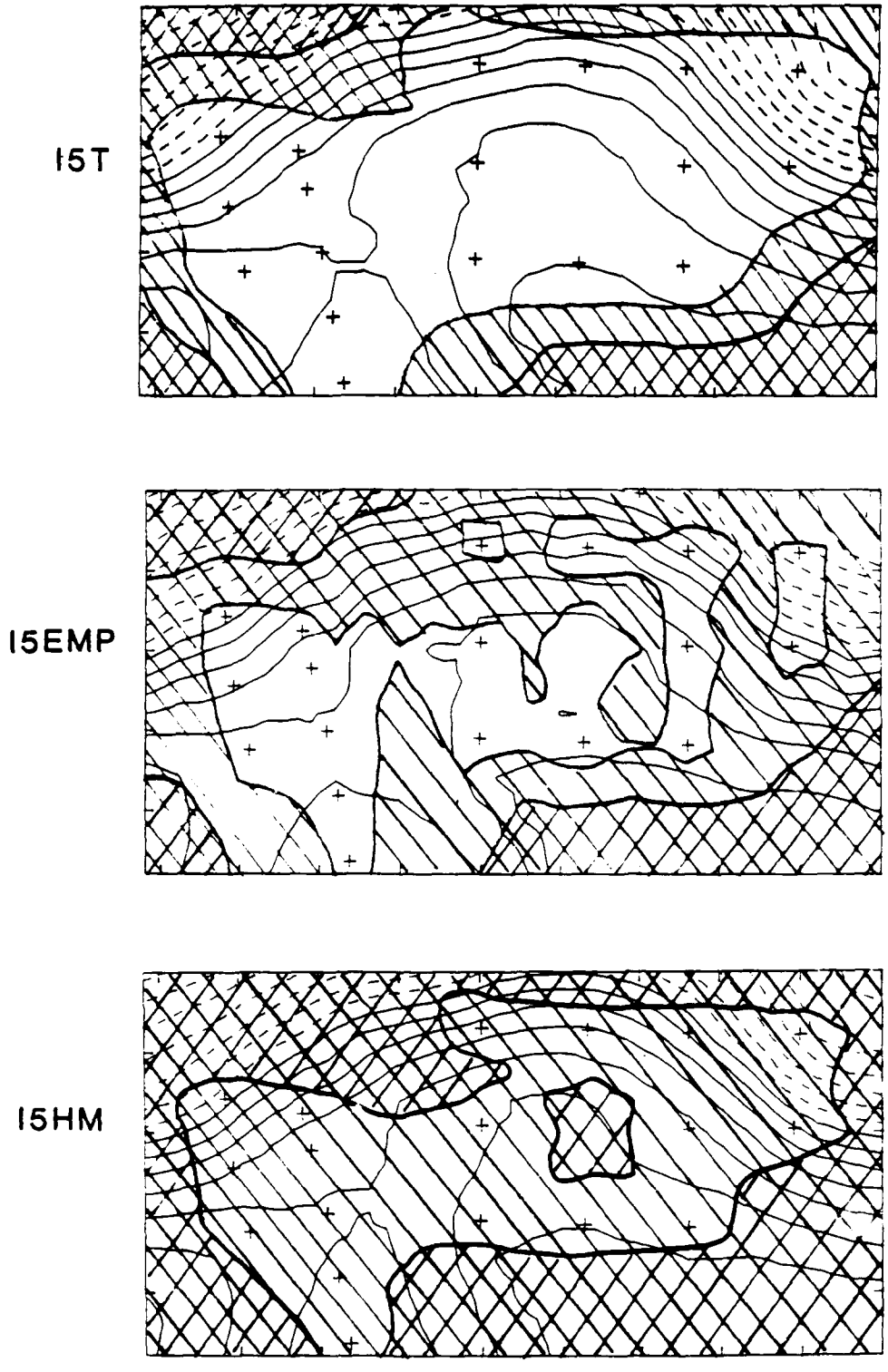

Figure 3.13 IES OA maps as in Figure 3.11 except for survey 5 (17 October 1984).

The rest of this report uses ρ_{WT} as the standard correlation function because it was an analytic function with good qualities (i.e., positive definite correlation matrix) that was a close fit to data from the same type of instruments in the same geographic region. Tests against independent data in Section 4 confirm that the error fields generated from ρ_{WT} produce good estimates of the true errors.

Aside from the estimated error fields, the OA maps of the Z_{12} field produced with the different ρ choices look very similar. The biggest differences occur along the upper edges of the mapped regions in Figures 3.10-13. Another distinction between the output maps in Figure 3.11 is the shape of the cold-core eddy entering the area at the southwest. In I4EMP, the shape is almost rectangular, extending about 265 km along stream and only about 60 km cross stream. However, in I4HM, the eddy is more circular, with a length-to-width ratio of nearly 1. The Z_{12} field in that corner is mapped mainly from the two southernmost IESs, and the differences between the maps arise from the propagation characteristics of the different ρ fields.

3.4.3 Internal consistency

Table 3.11 lists the comparisons between the AXBT OA maps and the input measurements. Similar comparisons are reported in Table 3.12 for the IES OA maps. The resulting errors at all the input sites were small despite the differences in the sizes of the error fields. The number of input points (NPTS) compared remained the same for the three choices of correlation function.

As was seen in Figure 3.9 and Section 3.4.1, the correlation function ρ_{HM} is smaller than either ρ_{EMP} or ρ_{WT}; this results in less smoothing in the objective analyses. The input data that are far away, both spatially and temporally, from the output grid point do not

Table 3.11 AXBT OA Maps Evaluated at AXBT sites for Three Choices of Correlation Functions*

OBS-OA	Range	Mean	RMS	NPTS
OBS-A4HM	21	-1	5	61
OBS-A4EMP	40	-1	9	61
OBS-A4T	46	-1	11	61
OBS-A5HM	22	0	4	73
OBS-A5EMP	43	0	8	73
OBS-A5T	53	0	10	73

* Parameters defined in Table 3.2

Table 3.12 IES OA Maps Evaluated at IES sites for Three Choices of Correlation Functions*

OBS-OA	Range	Mean	RMS	NPTS
OBS-I4HM	16	0	4	15
OBS-I4EMP	26	-1	7	15
OBS-I4T	32	2	8	15
OBS-I5HM	10	0	3	18
OBS-I5EMP	28	2	7	18
OBS-I5T	26	1	7	18

* Parameters defined in Table 3.2

contribute significantly to the estimation at that point. Thus, the best agreements between the OA maps and the observations are obtained with the maps produced using ρ_{HM}. However, since all the RMS values in Tables 3.11 and 3.12 are less than 11 m, there is good agreement between the estimated and observed Z_{ss} values regardless of the choice of correlation function.

3.4.4 Comparison of the AXBT OA maps

Since the estimated error fields associated with ρ_{HM} exceeded 15%, only the AXBT OA maps produced with ρ_{WT} and ρ_{EMP} are compared in Table 3.13a for that error level. However, the three AXBT OA maps for each day are compared in Table 3.13b for all output grid points within the 35% estimated error regions.

At the 35% level, the STD values are small, about 12 m, indicating that the output maps of Z_{ss} are not strongly affected by the choice of correlation function. These STD values are smaller than those in Table 3.4, suggesting that the output maps are influenced more by the choice of mean field than by ρ.

Although the range and STD values at the 35% error level for A5T-A5EMP are the largest, the number of grid points (NPTS) used for the comparisons is almost double those of the other two comparisons. For the map comparisons for survey 4, the NPTS for A4T-A4EMP is 50% larger than the others, yet the range and STD values are of comparable size. Thus, the fields generated from ρ_{WT} and ρ_{EMP} are the most similar, and the biggest differences occur between those produced with ρ_{EMP} and ρ_{HM}.

3.4.5 Comparison of the IES OA maps

The comparisons of the IES OA maps for each day are given in Table 3.14. As described above for the AXBT OA maps, the IES OA maps produced using ρ_{HM} could not be evaluated at the 15% level due to their large

Table 3.13 Differences Between AXBT OA Maps Generated Using Three Choices of Correlation Functions*

OA_2-OA_1	Range	Mean	RMS	STD	NPTS
a) Comparison of regions of less than 15% error					
A4T-A4EMP	57	0	8	8	137
A5T-A5EMP	98	-1	12	12	135
b) Comparison of regions of less than 35% error					
A4EMP-A4HM	66	-1	11	11	122
A4T-A4HM	60	-1	11	11	122
A4T-A4EMP	72	1	10	10	185
A5EMP-A5HM	75	2	13	13	108
A5T-A5HM	56	1	9	9	108
A5T-A5EMP	117	0	14	14	196

* Parameters defined in Table 3.4

Table 3.14 Differences Between IES OA Maps Generated Using Three Choices of Correlation Functions*

OA_2-OA_1	Range	Mean	RMS	STD	NPTS
a) Comparison of regions of less than 15% error					
I4T-I4EMP	180	5	27	27	88
I5T-I5EMP	78	1	14	14	94
b) Comparison of regions of less than 35% error					
I4EMP-I4HM	47	11	31	29	123
I4T-I4HM	71	5	13	12	123
I4T-I4EMP	214	3	25	25	237
I5EMP-I5HM	44	2	13	13	121
I5T-I5HM	72	0	10	10	121
I5T-I5EMP	118	0	17	17	227

* Parameters defined in Table 3.4

error fields. At the 35% error level, the STD differences range from 10-29 m. These are smaller than those given in Table 3.5 for the mean field selection, indicating that the choice for ρ is not as critical.

The smallest STD values were obtained for the comparisons of IES OA maps produced using ρ_{WT} and ρ_{HM}; thus, these maps are the most similar.

3.4.6 Intercomparison of the AXBT and IES OA maps

The differences between the sizes of the error fields result in large differences in the number of grid points available for the AXBT OA and IES OA map comparisons (Table 3.15). At the 15% error limit, the full mapped areas produced by ρ_{HM} were excluded. Also, twice as many grid points were used for the maps produced from ρ_{WT} as for those maps produced using ρ_{EMP}. Even at the 35% error level, there is a large difference in NPTS for all three different choices of correlation function.

At both error levels, the RMS, STD and range values for ρ_{WT} are roughly as good as or better than the values for the other two ρ choices. Thus, ρ_{WT} maps a larger region with less error. Although the RMS differences at the 35% error level for ρ_{WT} and ρ_{EMP} are also comparable in size to those obtained for the mean field selection (Table 3.6), the mapping areas being compared are substantially greater.

3.5 Decimation Time Selection

3.5.1 Description of the test

Observations from N input points are used to estimate the value at a single output grid point. They are selected from the input data based on their correlations (ρ). Those with the highest ρ are chosen since they result in the smallest estimated errors for the output value. Higher correlations are obtained for the data with the smallest separation distances, either spatial or temporal, from the output grid

Table 3.15 Intercomparisons of the AXBT and IES OA Maps Using Three Choices of Correlation Functions*

OA_2-OA_1	Range	Mean	RMS	STD	NPTS
a) Intercomparison of regions of less than 15% error					
A4EMP-I4EMP	228	16	53	50	42
A4T-I4T	195	8	36	35	100
A5EMP-I5EMP	123	-1	32	32	50
A5T-I5T	149	-15	42	39	100
b) Intercomparison of regions of less than 35% error					
A4HM-I4HM	224	4	31	31	85
A4EMP-I4EMP	350	6	50	50	153
A4T-I4T	278	1	44	44	180
A5HM-I5HM	156	-12	40	38	49
A5EMP-I5EMP	186	-10	43	42	162
A5T-I5T	197	-12	45	43	188

* Parameters defined in Table 3.4

points (Figure 3.9). However, these observations are also correlated with each other, and hence do not contribute completely independent degrees of freedom to the estimates at the output grid points (i.e., the error estimates must be larger). Thus, a balance must be obtained in which the input data are separated far enough from each other to be relatively independent, yet not so far from the output point that they no longer supply adequate information for estimating its value.

In this test of the OA method, we assess the importance of the choice of separation time. Because the IES data consist of time series of daily Z_{is} measurements at fixed locations, we can test the effects of temporal separation by subsampling at different intervals. For this test, we chose decimation times (δt) of 1, 4, and 8 d in addition to the 2 d interval used to produce the standard maps. The IES output maps are compared to the standard AXBT OA maps for which all the sampling occurred within a few hours on one flight. (Since the AXBT surveys were intermittent, no corresponding test could be conducted for those data.)

In conjunction with the δt variations, it was also necessary to adjust the number of input values (N) and the maximum time lag (T). In order to determine the most appropriate values, we tested several different combinations of N and T with each choice of δt. We chose the maximum N for a given T for which the OA mapping, which depends upon inverting the matrix of correlations, remained stable. If the determinant of this matrix becomes too small, the matrix is singular and the mapping quality would become poor. For the maps produced using the longer decimation times (4 and 8 d), T was changed from ±4 d to ±8 d. Additionally, for maps I48D and I58D, N was increased to eleven points. For the maps produced using δt = 1 d, N was reduced to seven and T was changed to ±1 d. These selections are summarized in Table 3.1.

3.5.2 Description of the IES OA maps

The IES OA maps for survey 4 (12 June) produced with the four choices of δt are shown in Figure 3.14. Those for survey 5 (17 October) are displayed in Figure 3.15. In general, the output maps are very similar. The major features, such as the cold-core ring (Figure 3.14) and the shape of the Gulf Stream path, are resolved in all of the maps.

The maps differ from one another, however, in that the contours of Z_{12} become progressively smoother as δt increases. For example, the fine-scale structure is more evident in I51D, produced using δt = 1 d, than in I58D, where δt = 8 d. The size of the cold-core eddy (Figure 3.14) is also affected by the choice of δt. The eddy appears almost circular in I41D, with a radius of about 100 km. As δt increases, the dimensions of the eddy enlarge. In maps I4T and I44D, the eddy extends 280 km downstream and 200 m in depth. In I48D, the increased smoothing diffuses the cross-stream thermal gradients. Thus, fewer Z_{12} contours close and the eddy actually appears smaller.

As in the test of the correlation function selection (Section 3.4), the most obvious differences between these maps occur with their estimated errors. However, the differences between the sizes of the error fields are not as great as those obtained in that previous methodology test. The smallest error fields are associated with the standard maps, I4T and I5T, for which δt = 2 d. The largest errors are obtained when δt = 8 d. The two intermediate error fields, associated with maps produced using δt = 1 d (I41D and I51D) and δt = 4 d (I44D and I54D), are comparable in size.

3.5.3 Internal consistency

Table 3.16 lists the comparisons between the actual observations and the estimated outputs of the IES OA maps evaluated at the measurement

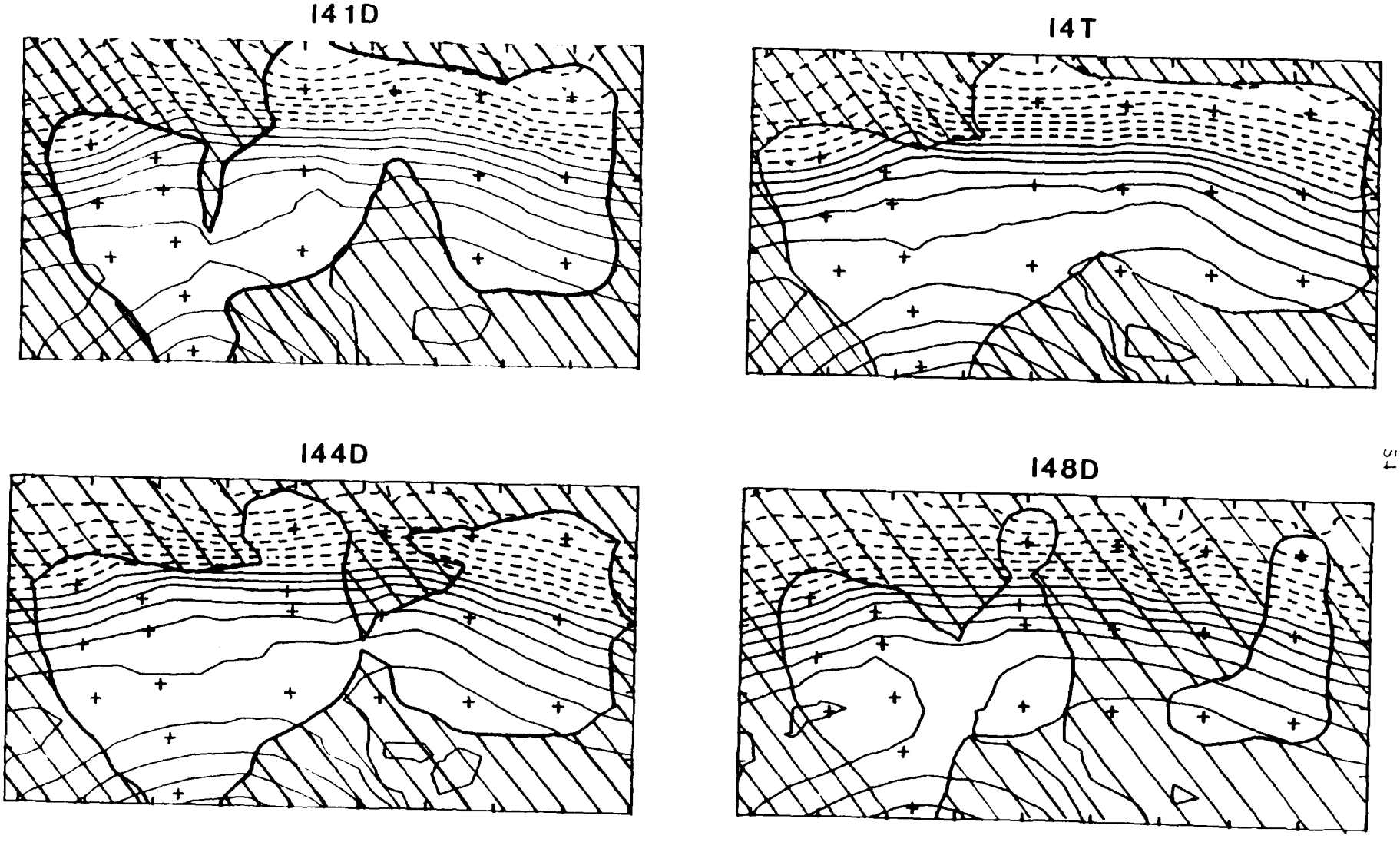

Figure 3.14 IES OA maps for survey 4 (12 June 1984), produced using four different decimation times: 1 d (I41D), 2 d (I4T), 4 d (I44D), and 8 d (I48D). Contours and hatching are the same as in Figure 3.10.

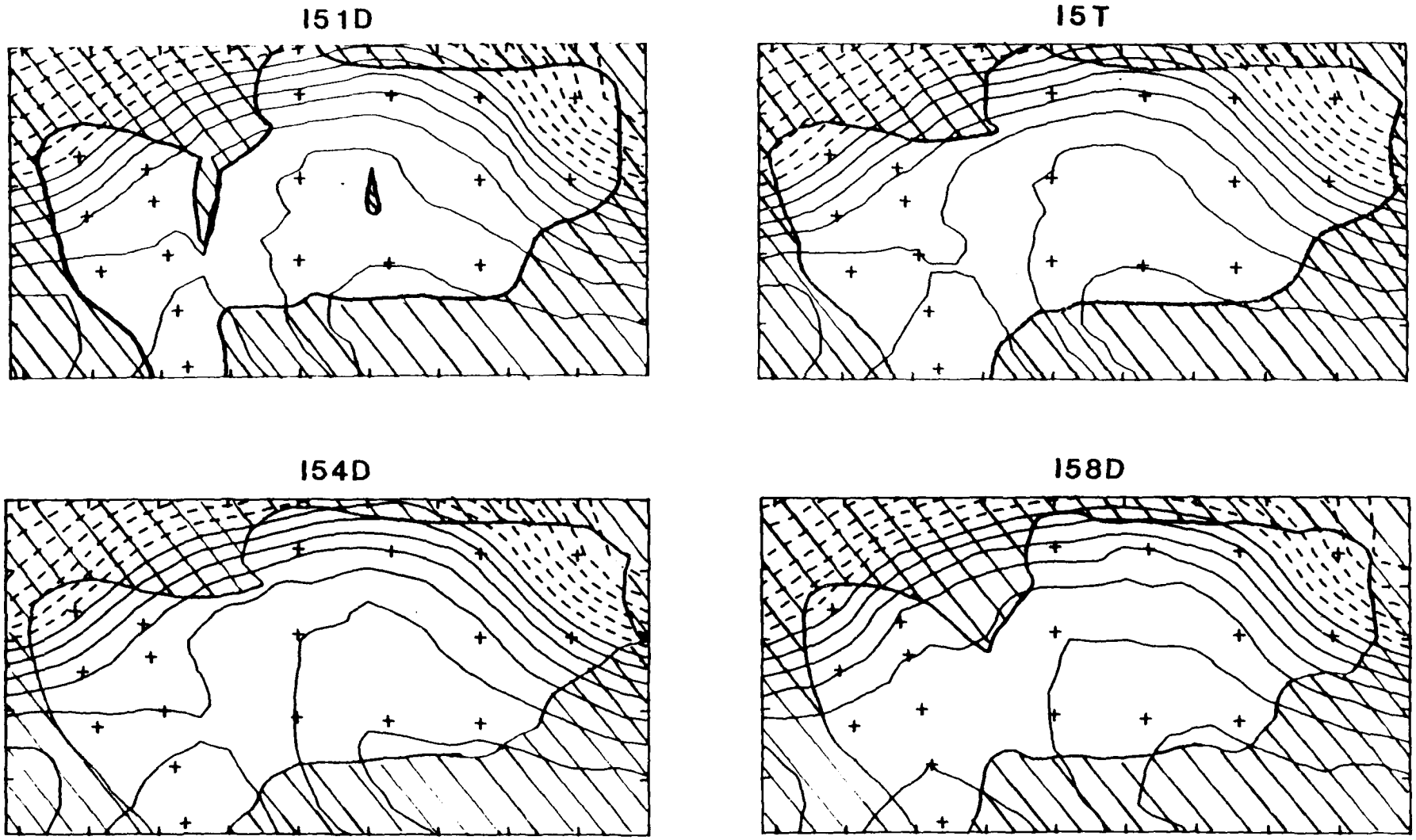

Figure 3.15 IES OA maps as in Figure 3.14 except for survey 5 (17 October 1984).

Table 3.16 IES OA Maps Evaluated at IES Sites for Four Choices of Decimation Times*

OBS-OA	Range	Mean	RMS	NPTS
OBS-I41D	26	1	7	15
OBS-I4T	32	2	8	15
OBS-I44D	47	0	12	15
OBS-I48D	48	0	12	15
OBS-I51D	18	1	5	18
OBS-I5T	26	1	7	18
OBS-I54D	23	2	7	18
OBS-I58D	35	2	10	18

* Parameters defined in Table 3.2

Table 3.17 Differences Between IES OA Maps Generated Using Four Choices of Decimation Times*

OA_2-OA_1	Range	Mean	RMS	STD	NPTS
I4T-I41D	105	-4	18	18	150
I4T-I44D	90	1	12	12	148
I4T-I48D	73	-1	16	15	92
I5T-I51D	47	0	8	8	158
I5T-I54D	47	1	9	9	166
I5T-I58D	72	2	16	15	146

* Parameters defined in Table 3.4

sites. As expected, both the range and RMS values increase as δt becomes larger; the comparisons of instantaneous observations with estimated outputs should worsen as more and more averaging is done. For δt = 1 d, the range (18-26 m) and RMS (5-7 m) of the differences are smaller than those obtained for any of the previous tests of the OA methodology. The corresponding values for the remaining three δt selections are also among the smallest. Thus, there is excellent agreement between the observed and the estimated values for all the decimation intervals.

3.5.4 Comparison of the IES OA maps

The IES OA maps for both surveys are compared in Table 3.17. The STD values (8-18 m) are small and nearly uniform. However, the standard maps (I4T and I5T) and those produced using δt = 4 d are the most similar in that the STD values are consistently smaller.

Additionally, the range and STD values in Table 3.17 are also among the smallest obtained for any of the OA methodology tests. Thus the choice of δt does not strongly affect the estimated output maps. However, it is important to note that this type of comparison does not reveal if there has been a loss of high-frequency signals, which may be of scientific interest, as δt increases. Because the best agreement with the observations is obtained for the maps produced using δt = 1 d, there is an indication of some signal loss at the larger decimation intervals.

3.5.5 Intercomparison of the AXBT and IES OA maps

Table 3.18 compares the IES OA maps with the standard AXBT OA maps (Figures 3.10 and 3.12) for the same survey dates. The range and STD are essentially the same for all comparisons, indicating that there is

Table 3.18 Intercomparisons of the AXBT and IES OA Maps Using Four Choices of Decimation Times*

OA_2-OA_1	Range	Mean	RMS	STD	NPTS
A4T-I41D	159	8	32	31	87
A4T-I4T	195	8	36	35	100
A4T-I44D	183	8	32	31	74
A4T-I48D	132	6	32	31	41
A5T-I51D	158	-18	43	39	91
A5T-I5T	149	-15	42	39	100
A5T-I54D	149	-11	40	39	92
A5T-I58D	155	-13	42	40	82

* Parameters defined in Table 3.4

very little difference between the IES OA maps generated with different decimation times.

The differences in the sizes of the error fields result in a wide range in the number of grid points used in the intercomparisons. NPTS ranges from ~40 for I48D to 100 for the standard maps. Since it is desirable to map accurately the largest area possible, decimation times of either 1 d or 2 d appear to be good choices.

3.6 Summary of Results

We have examined the robustness of the objective mapping technique to the choices of four control parameters: (a) the mean field, (b) the standard deviation field, (c) the correlation function, and (d) the decimation time. Output maps of both IES and AXBT data were produced by varying just one of these control parameters at a time, keeping all others the same.

For each test, we checked the internal consistency of the output maps by evaluating them at all the observation sites and comparing them with the actual observations at those sites. In all cases, the RMS differences were $\leq$15 m, which are comparable to the measurement errors of the instrumentation. Thus, the output maps agreed well with the observations, regardless of the choice of control parameter.

The OA mapping technique was most sensitive to the mean field selection. We produced output maps using: (a) a time-averaged mean field, (b) an instantaneous mean field, and (c) a constant mean field. Of these three, both the instantaneous and constant mean fields introduced unrealistic thermal structures (overshoots and circular features) to the extrapolated areas of the output maps, whereas the time-averaged mean field did not. Additionally, the IES OA maps produced using the temporal mean field gave the best internal

consistency (RMS differences of 8-10 m) and the best intercomparisons with the AXBT OA maps (STD differences of 35-40 m). Thus, the most accurate representation of the true temperature structure was obtained for the maps produced using the temporal mean field.

The choice of the space-time correlation function had the most pronounced effect on the estimated error fields associated with the output maps. The largest estimated error fields were obtained with the independently derived analytic function, ρ_{HM}, based on surface observations of the Gulf Stream thermal front (Halliwell and Mooers, 1983). The analytic function, ρ_{WT}, based on four years of IES data from the same region of the Gulf Stream, gave the smallest error fields. The estimated error fields associated with the maps produced using an empirical function, ρ_{EMP}, were intermediate between these other two. All of the AXBT and IES OA maps agreed well ($\leq$10 m RMS) with the observations, no matter which correlation function was used.

Intercomparisons of the AXBT OA and IES OA maps were made for two levels of estimated error (15 and 35%). Although fairly uniform RMS values (35-45 m) were obtained for all three correlation functions, the analytic function ρ_{WT} is considered to be the best choice because it mapped the largest area with the least error. Also, the error fields generated from ρ_{WT} were shown to produce good estimates of the true errors.

Since only slight changes in the thermocline slope were observed, variations in the standard deviation field selection produced virtually no differences between the output maps. Thus, the OA method is apparently not very sensitive to the choice of σ. We have chosen σ_T because it is most similar to the observed standard deviation field, and

should produce the most accurate output maps of the true thermocline depth field.

Variations in the selection of the decimation time, δt, produced only minor differences in the output maps of the thermocline depth field. The output maps prepared by varying δt gave the best agreement with the observations, with RMS differences as low as 5 m. Comparing the IES OA maps with the AXBT OA maps also gave small STD values (30-40 m). These values are considerably smaller than those when the mean field was varied (35-60 m STD).

The decimation time selection may be more critical than these results indicate, however. At larger δt intervals, increased smoothing occurs, which may result in the loss of the high-frequency perturbations. Since there is little difference between the output maps of the thermocline depth field, it is desirable to choose δt such that these fluctuations may be resolved. We have selected both δt = 1 d (high temporal resolution) and δt = 2 d ("standard") because smoothing is kept to a minimum. Also, the estimated errors associated with both of these selections are low; thus, the output $Z_{1,2}$ maps produced have the largest areas of accurate mapping.

SECTION 4. TESTS OF THE IES OA MAPS AGAINST INDEPENDENT DATA

4.1 General Information

4.1.1 Motivation for the test

The principal purpose of this section of the report is to compare the IES OA maps with independent but concurrent measurements of Z_{12} from XBTs and AXBTs. We examine the results of these comparisons in order to determine the accuracy of the mapped Z_{12} fields.

Two cases are presented here. Two sets of OA maps have been produced, in which different amounts of temporal smoothing were used in calculating the output Z_{12} values. For case A, the OA maps were produced using the standard map parameters (in particular, the decimation time was δt = 2 d and the maximum time lag was T = ±4 d) described in Section 3 of this report. These same parameters were used to produce the OA maps shown in the data reports by Tracey and Watts (1986b), Tracey et al. (1985), and Friedlander et al. (1986). The second set of OA maps (case B) were produced with a higher temporal resolution (δt = 1 d and T = ±1 d) and, therefore, less averaging was performed. We compare XBT and AXBT Z_{12} values with both sets of maps to determine the map accuracy and to assess the effects of different amounts of temporal smoothing.

In addition to the daily maps of the Z_{12} field, estimated error fields were also produced daily by the OA technique. Each error field is a statistical measure (percent standard deviation) of how well the Z_{12} field has been estimated from the input data. Figure 4.1 (top) shows the case A (standard map parameters) error field for a representative date (19 January 1985). The mapped area corresponds to

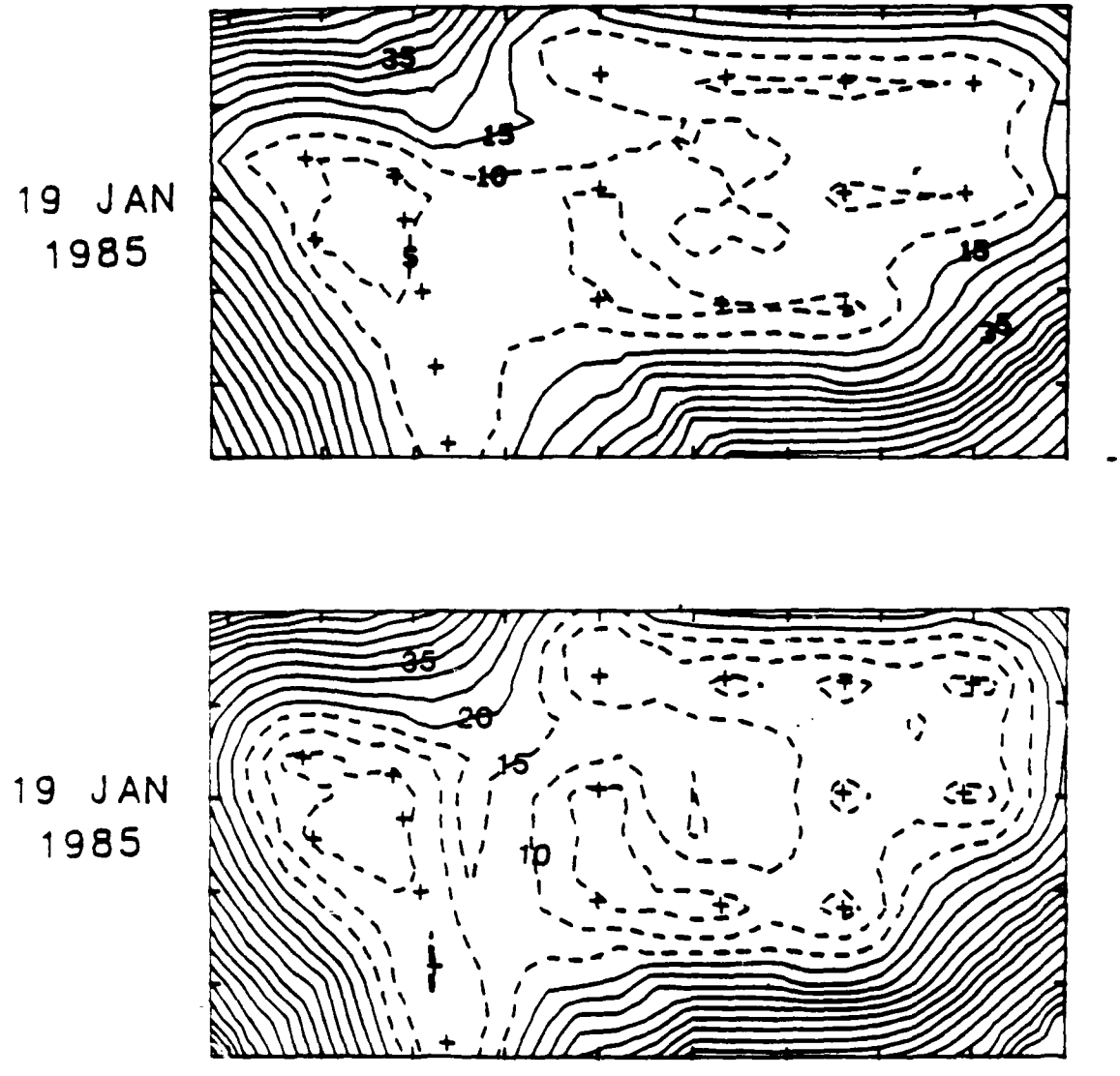

Figure 4.1 The error fields (% standard deviation) on 19 January 1985 for two decimation times: case A (top; σt = 2 d), with dashed contours indicating <15% error; and case B (bottom; σt = 1 d), with dashed contours indicating <20% error. Contour intervals are 5%.

the boxed area of Figure 2.1. The estimated errors are low (≤5%) near the IES measurement sites and increase with distance from those sites. Figure 4.1 (bottom) shows the error field, for the same date, associated with the Z_{12} map produced using the higher temporal resolution parameters (case B). Note that the estimated errors are slightly larger for case B than case A.

The OA technique is used to estimate the Gulf Stream Z_{12} field over a large continuous area by extrapolating outside the IES array. The error fields have been used qualitatively to mask out extrapolated areas of the Z_{12} fields where the map quality is predicted to be poor. For example, WT85 subjectively chose to mask out all extrapolated regions where the errors were ≥15%. That error level was chosen because it combined low predicted errors with a large mapping area that extended beyond the instrument sites. We would now like to select, objectively, the largest area of accurate mapping by comparing the OA maps against independent measurements of the Z_{12} field. These comparisons are made first for the standard maps (Section 4.2) and then for the high temporal resolution maps (Section 4.3).

4.1.2 Distribution of the data

On five cruises in the study area during 1982 to 1985, a total of 402 XBTs were taken. Of these, XBTs taken outside the boxed region of Figure 2.1 were not used in this test. Additionally, XBTs were also excluded if they were located in regions where the water was either too warm or too cold to measure Z_{12}. Finally, XBTs taken in the mapping region with ≥35% error are excluded.

Thus, of the 402 XBTs taken over the three-year period, 295 of them were used in comparison with the standard IES OA maps. The locations of the XBTs used are shown in Figure 4.2, where the outer box is the same as

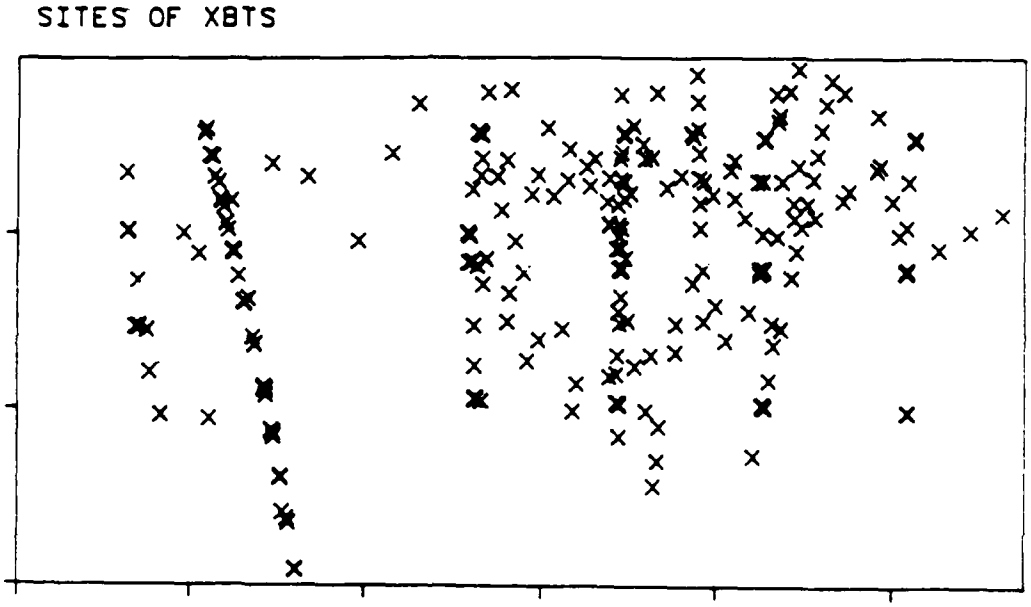

Figure 4.2 Locations of the 295 XBTs used, superimposed for all five cruises during the study period.

that outlined in Figure 2.1. Since the primary purpose of the XBT surveys was to calibrate the IESs, the XBT drop sites were concentrated near the instrument sites. Eighty-nine percent (262) of the 295 XBTs taken within the standard map (case A) region delineated by the 35% error limit also occurred within the region of ≤15% error. In Figure 4.3a, the histograms show that the number of XBTs used in this test increased by eleven percent as the standard map estimated error increased from 15 to 35%.

For the high temporal resolution map (case B) comparisons, there were a total of 284 XBTs that satisfied the criteria. The histograms (Figure 4.3c) illustrate that the drop sites are concentrated near the IES sites, with eighty-six percent (245) of the XBTs falling within the map region delineated by the 15% error limit.

A total of 512 AXBTs were dropped on six flights between 1 June and 13 November 1984. Of these, 195 met the same criteria described above for the XBTs and were used in the standard map (case A) comparisons. For the high temporal resolution map (case B) comparisons, 164 AXBTs met the criteria. The probe drop-sites are shown in Figure 4.4.

The survey flights were centered on the Gulf Stream thermal front position; thus, they did not always coincide with the fixed IES array. During several of the survey flights, the Gulf Stream path was located to the north of the IES array due to the presence of a large-amplitude meander. The AXBT sites were also shifted northward, and were concentrated along the upper edge of the mapped region. Consequently, the AXBTs were more evenly distributed throughout the mapping regions delineated by the 10 to 35% error levels.

Of the 195 AXBTs available for the standard map (case A) comparisons, 80 probes were in the region between the 15% and 35% error

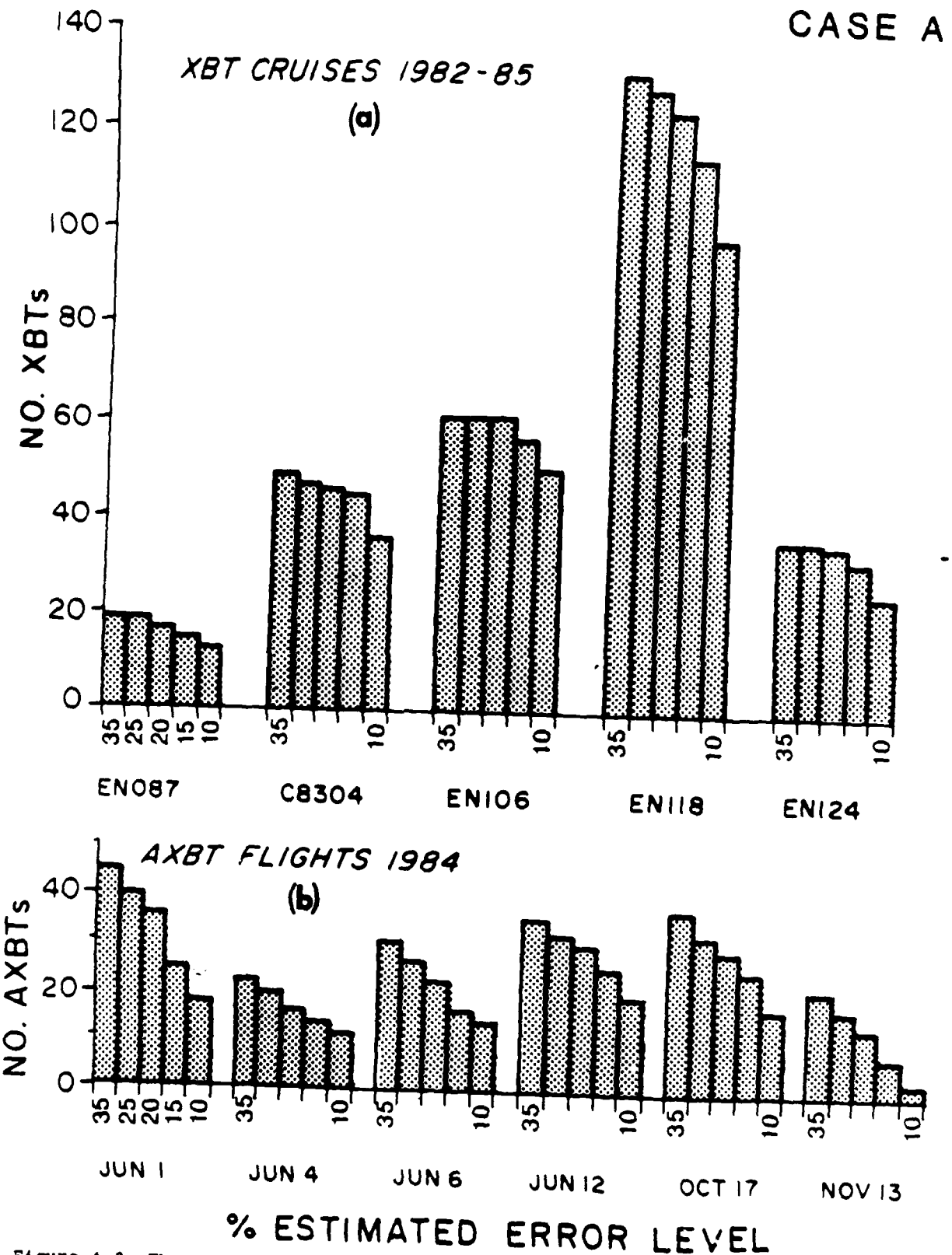

Figure 4.3 The number of comparisons made at five levels of estimated error. For case A (σt = 2 d), comparison is between IES OA maps and (a) XBTs for each cruise and (b) AXBTs for each flight. For case B (σt = 1 d), comparison is between IES OA maps and (c) XBTs for each cruise and (d) AXBTs for each flight.

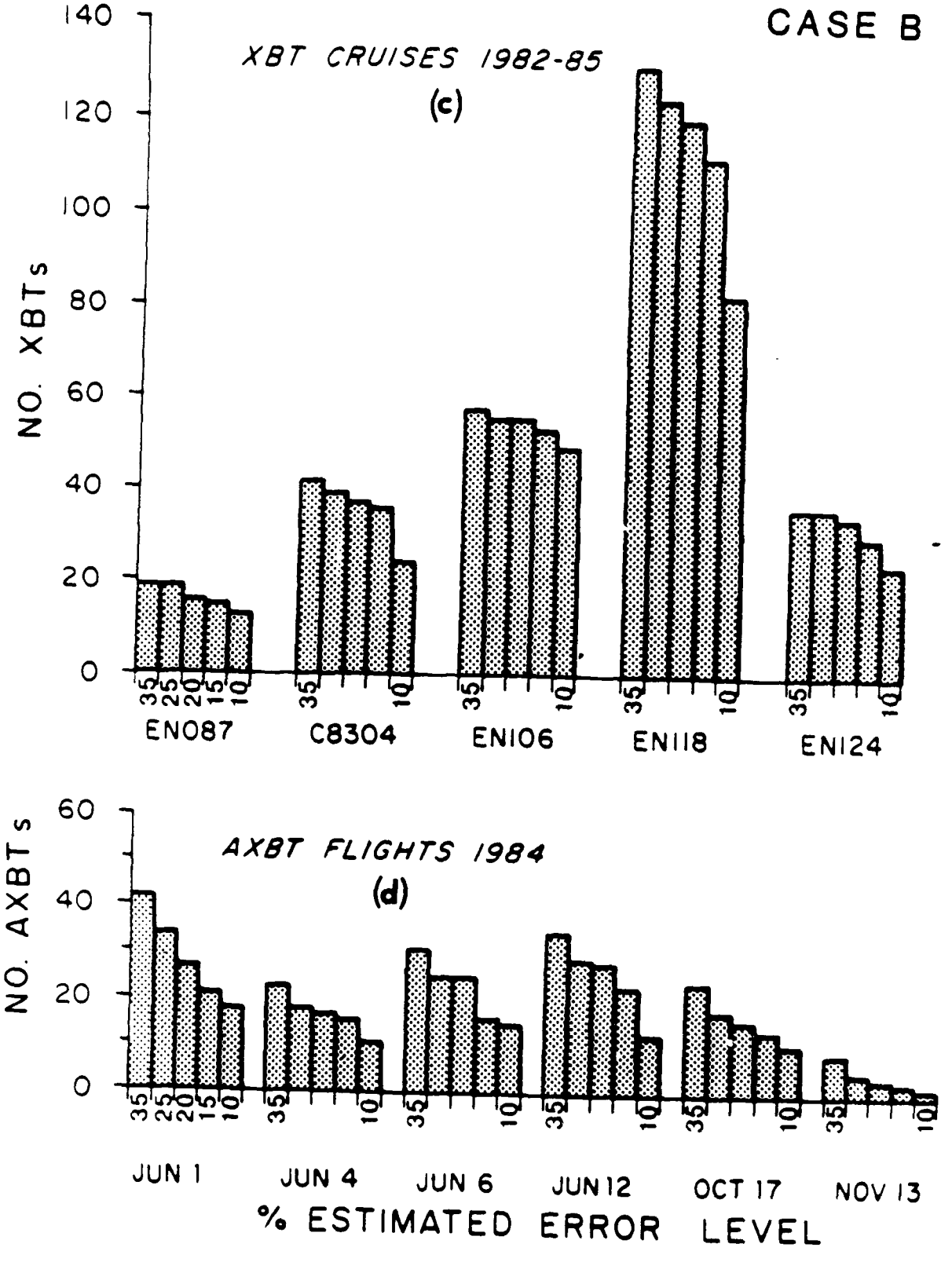

Figure 4.3, continued.

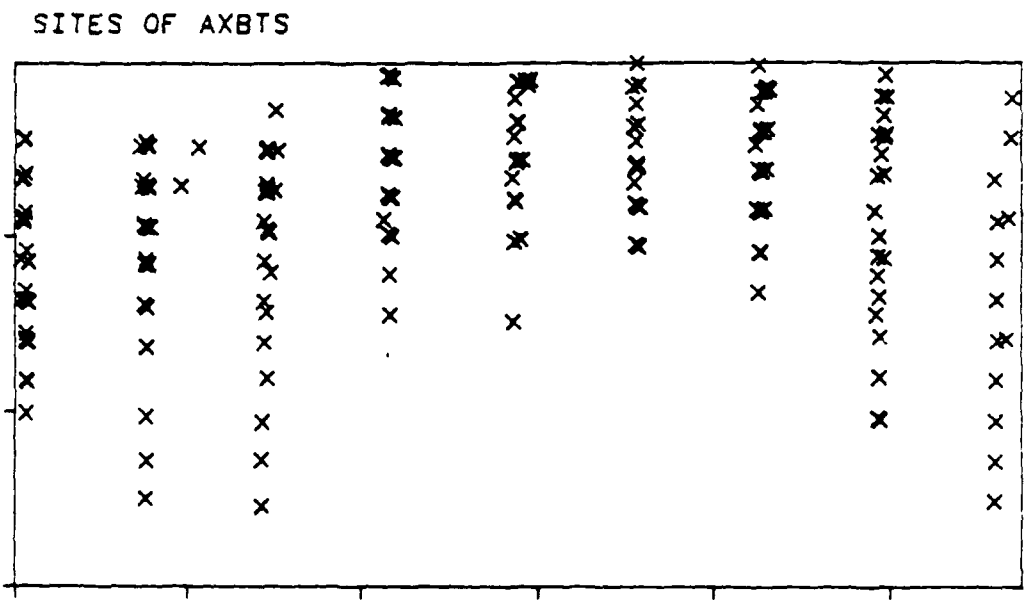

Figure 4.4 Locations of the AXBT drop sites, superimposed for all six flights during the study period.

levels and 115 probes were in the region of ≤15% error (Figure 4.3b). For the high temporal resolution map (case B) comparisons, 71 probes were in the region between 15% and 35% error levels and 93 probes were in the region of ≤15% error (Figure 4.3d).

4.1.3 Description of the test

First, the depth of the 12°C isotherm was extracted from each of the XBTs and AXBTs. If temperature inversions (associated with lower-salinity Slope Water) resulted in the occurrence of more than one Z_{12} value, the deepest one was chosen.

Next, the estimated Z_{12} values were determined from the IES OA maps for the same locations as the probe drop sites. For any XBT or AXBT site not located at a grid point, the Z_{12} value was determined by linear interpolation. Since the IES OA maps were produced for 1200 GMT on each day from July 1982 to May 1985, the Z_{12} value was extracted from the map that was closest in time to the probe launch. For case A, the output maps for the three-year period were produced using the standard map parameters described in Section 3. For case B, the high temporal resolution maps were produced specifying δt = 1 d and T = ±1 d, retaining all other standard map parameters.

The estimated Z_{12} values from the IES OA maps were plotted against the observed XBT Z_{12} values from all five cruises. Two plots were produced, one for all XBTs occurring within the map region delineated by the 35% error level, and the other for only these XBTs within either the 15% error level (case A, standard maps) or 20% error level (case B, high temporal resolution maps).

The differences, ΔZ, between the Z_{12} values from the IES OA maps and the XBTs were calculated as:

$$\Delta Z = (\text{OA } Z_{12}) - (\text{XBT } Z_{12})$$

For each cruise, the mean and root-mean-square differences (RMS) of the number of comparisons (NPTS) were determined as:

$$\text{mean} = \frac{\Sigma(\Delta Z)}{NPTS}$$

$$\text{RMS} = \left[\frac{\Sigma(\Delta Z^2)}{NPTS}\right]^{1/2}$$

The ΔZ differences were divided into groups, according to the locations of the XBTs within geographic regions delineated by five levels of OA map error. For this analysis, we used the 10, 15, 20, 25, and 35% error levels. Then the RMS differences of each group were calculated separately.

The mean and RMS calculations were repeated for the comparisons of the IES OA maps with the AXBTs. To determine ΔZ, the XBT Z_{12} values in the above equation were replaced with AXBT Z_{12} values.

Additionally, the navigation systems on the ship and aircraft are different. Thus, systematic offsets could occur in the locations of the AXBT drop sites relative to the IES array location. These navigation offsets would differ from flight to flight. To determine if these offsets occurred on any of the six surveys, the standard deviations (STD) for all five error levels were calculated as:

$$\text{STD} = [(\text{RMS})^2 - (\text{Mean})^2]^{1/2}$$

If the position of the aircraft had actually been shifted to the north of the array, the Z_{12} values from the AXBTs would be shallower than those from the IESs and the mean ΔZ would be positive. Conversely, if the aircraft had been offset to the south, the mean ΔZ would be negative. To eliminate these biases, the mean ΔZ for each flight was removed from the Z_{12} values of the IES OA maps. These residual OA Z_{12} values were then plotted against the Z_{12} values of the AXBTs at the 15

and 35% error levels for the standard maps (case A) and at the 20 and 35% error levels for the high temporal resolution maps (case B).

To check for possible navigation offsets between ship cruises, the standard deviations (STD) were also determined for the XBTs. We expected these offsets to be negligible since the IESs were deployed by the same ships that dropped the XBTs.

4.2 Comparison of the IES OA maps with XBT and AXBT Data: Case A (δt = 2 d)

4.2.1 Results of the XBT comparison

For each XBT located within the mapping region delimited by the 15% error level, the depth of the 12°C isotherm is plotted against the OA Z_{12} estimate (Figure 4.5). The scatter about the line of perfect agreement represents a RMS difference of 47 m. Figure 4.6 shows the same comparison of Z_{12} values but extended to include all XBTs within the 35% estimated map error level. A RMS difference of 50 m was calculated for all 295 XBTs at the 35% map error level. These RMS differences are relatively small, indicating that there is good agreement between the estimated and observed Z_{12} values.

The RMS differences at the 10, 15, 20, 25 and 35% map error levels are plotted by cruise in Figure 4.7. This figure illustrates that as we extrapolate farther away from the IES sites (i.e., extending out to areas of increased estimated mapping error), the RMS differences worsen. On three cruises (C8304, EN106 and EN118), the RMS differences were relatively constant as the estimated map error increased. However, the RMS differences for two cruises, EN087 and EN124, increased sharply before levelling off. The RMS differences were also calculated for the combined XBTs from all five cruises (Figure 4.7, right). In Figure 4.7, the combined RMS results increase uniformly from 44 m to 50 m as the estimated map error increased from 10% to 35%. This overall increase in

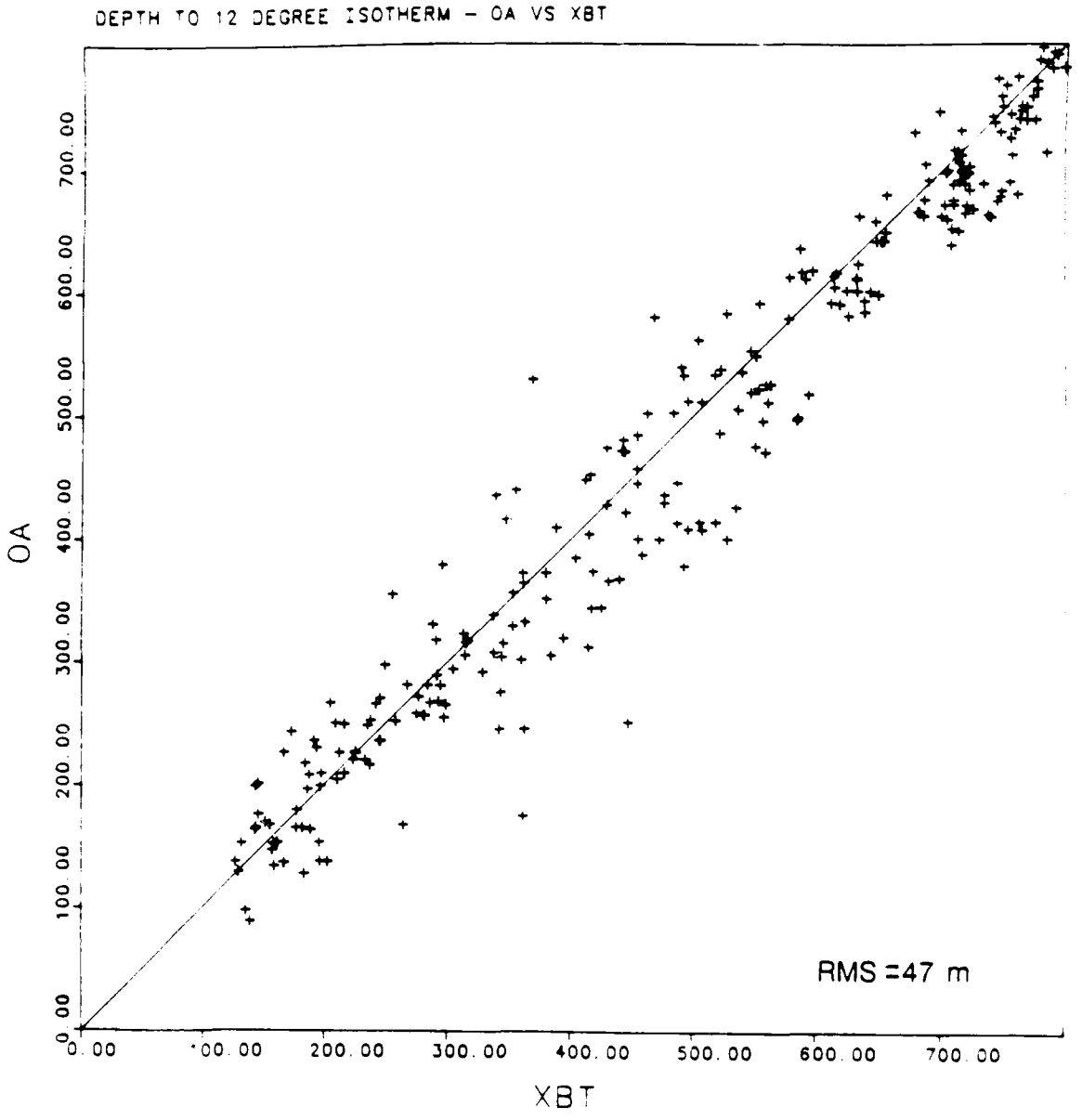

Figure 4.5 Comparison of the Z_{12} from XBTs versus the Z_{12} from IES OA maps within the region where mapping error is <15 % for case A (δt = 2 d). The solid line represents the line of perfect agreement.

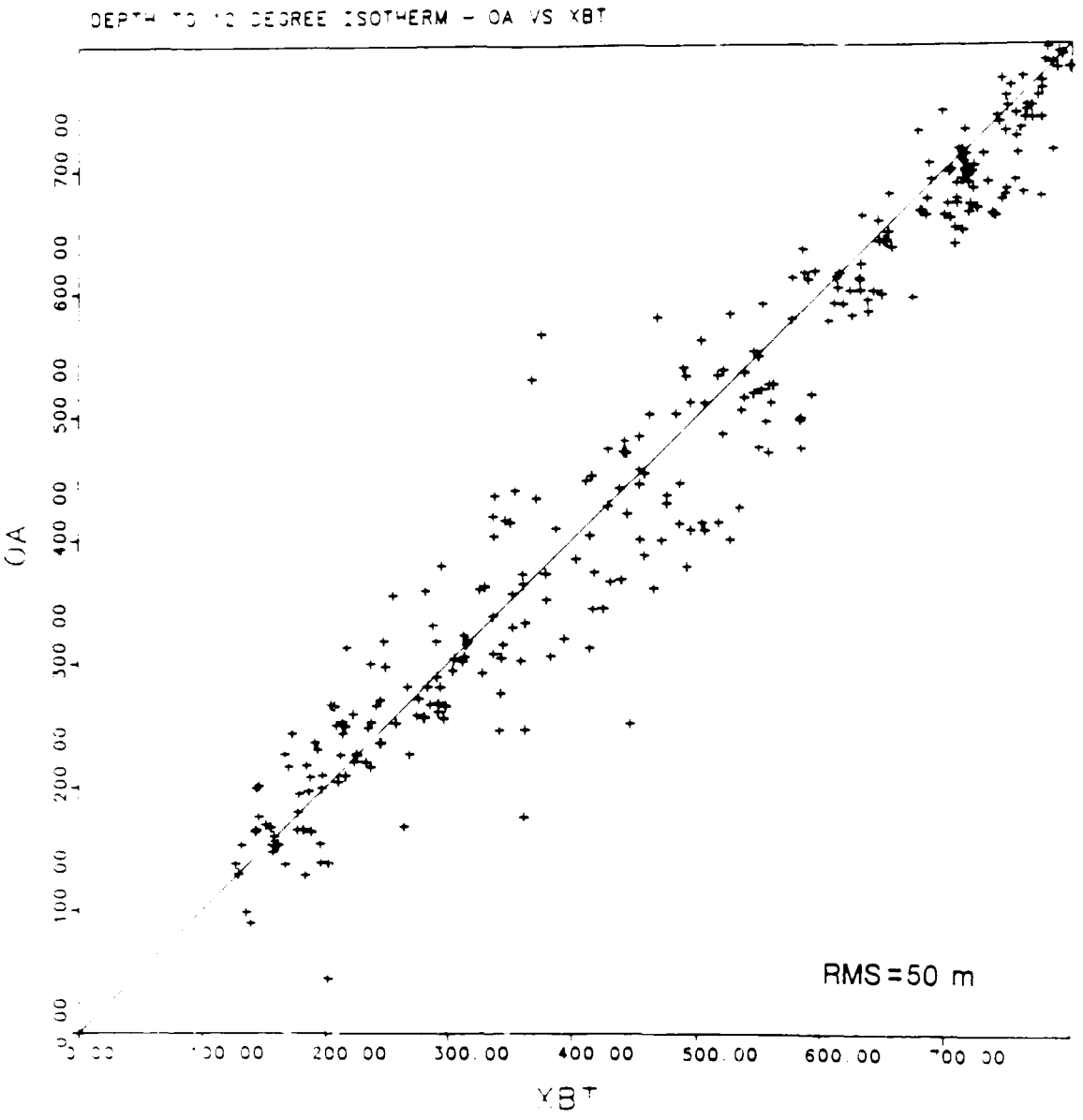

Figure 4.6 Same as Figure 4.5 except within the <35% error region.

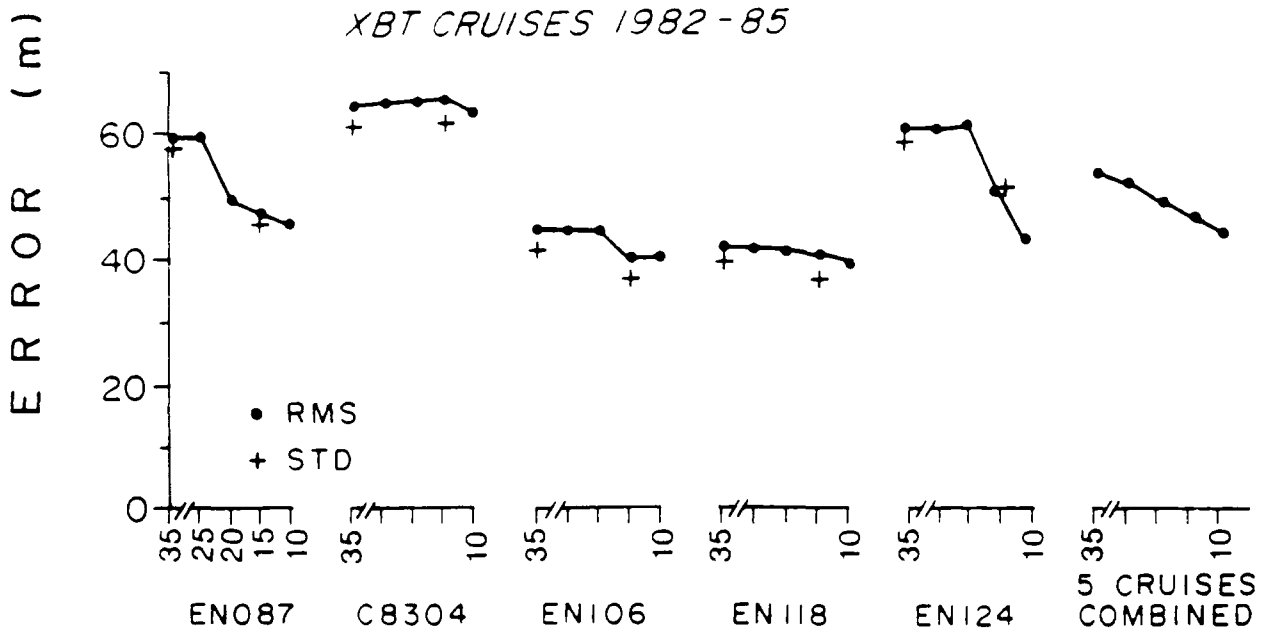

Figure 4.7 The RMS difference (•) and STD difference (+) for Z_{12} values from IES OA maps compared with Z_{12} values from XBTs within five levels of estimated error for case A (δt = 2 d) for five cruises individually and for all five cruises combined.

the RMS differences is small because the distribution of the XBTs (discussed in Section 4.1.2) biases the data toward the low mapping error region.

The corresponding STD values at the 15% and 35% error levels are also plotted in Figure 4.7. They are very similar to the RMS values, indicating that no biases were introduced due to navigation offsets on any of the cruises.

4.2.2 Results of the AXBT comparison

The depth of the 12°C isotherm of each AXBT within the region of the 15% error limit is plotted against the residual estimated OA Z_{12} value in Figure 4.8. A STD of 53 m was calculated for those AXBTs within the 15% error level. Figure 4.9 shows the same comparison of Z_{12} values but including all AXBTs within the 35% estimated map error level. A STD of 68 m was calculated for the IES OA map and AXBT comparison at the 35% error level.

The navigation offsets between the ship and the aircraft are apparent in Figure 4.10. Both the RMS and STD differences for each flight are plotted at the five map error levels (from 10 to 35%). The navigational offsets (about 2 km cross stream) are apparent as the differences between the curves for the flights on June 1, June 6 and November 13. The two curves are almost identical for the other three flights, indicating that no offsets occurred.

The STD differences were composited for all six flights. They increase from 39 m at the 10% estimated map error level to 68 m at the 35% estimated error level. The rapid increase in STD differences from 39 m to 53 m to 66 m as the mapping area was extended to include the regions of 10% to 15% to 20% estimated error, respectively, suggests the need to limit the extent of extrapolation beyond the IES sites.

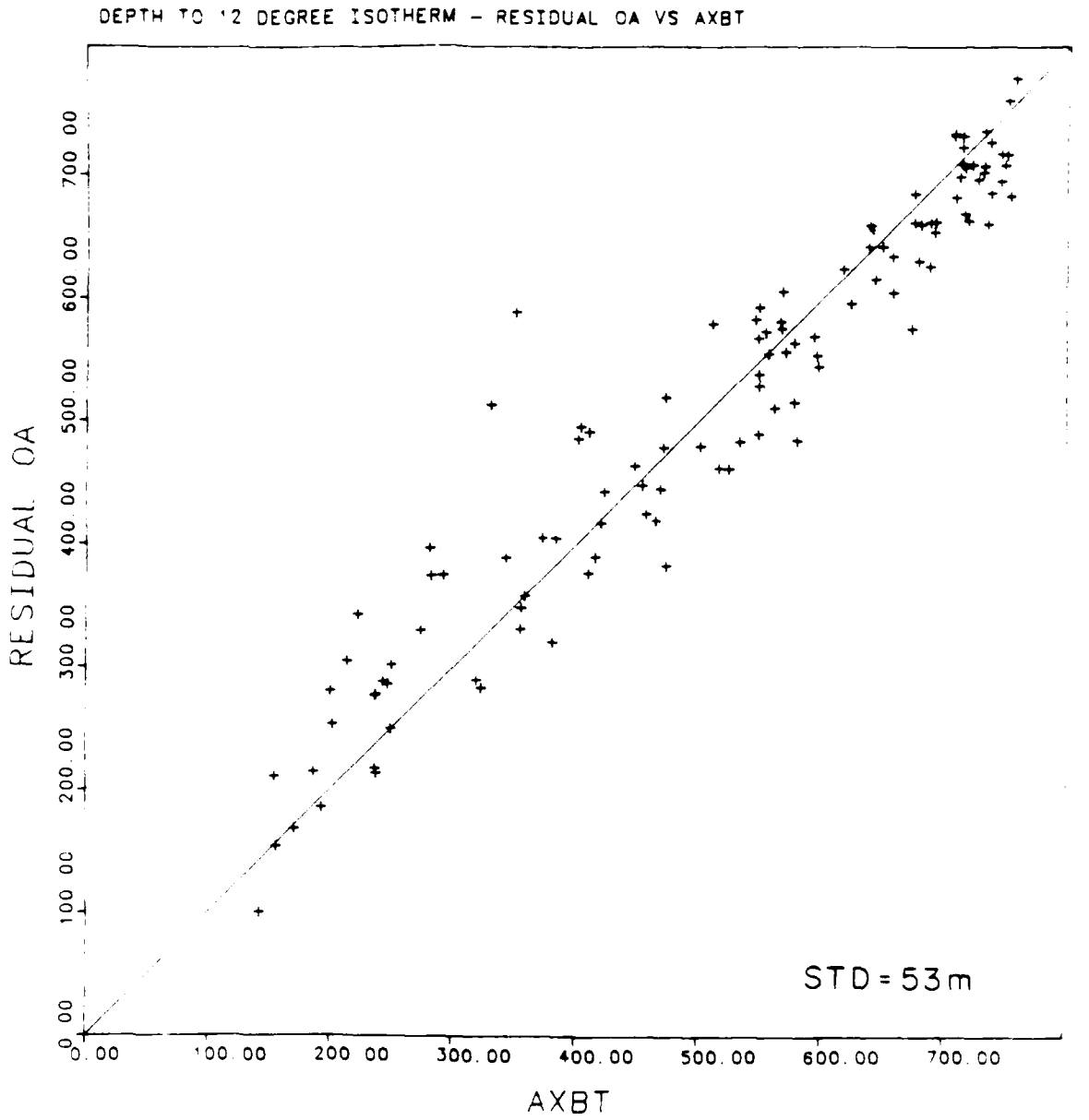

Figure 4.8 Same as Figure 4.5 except for AXBTs.

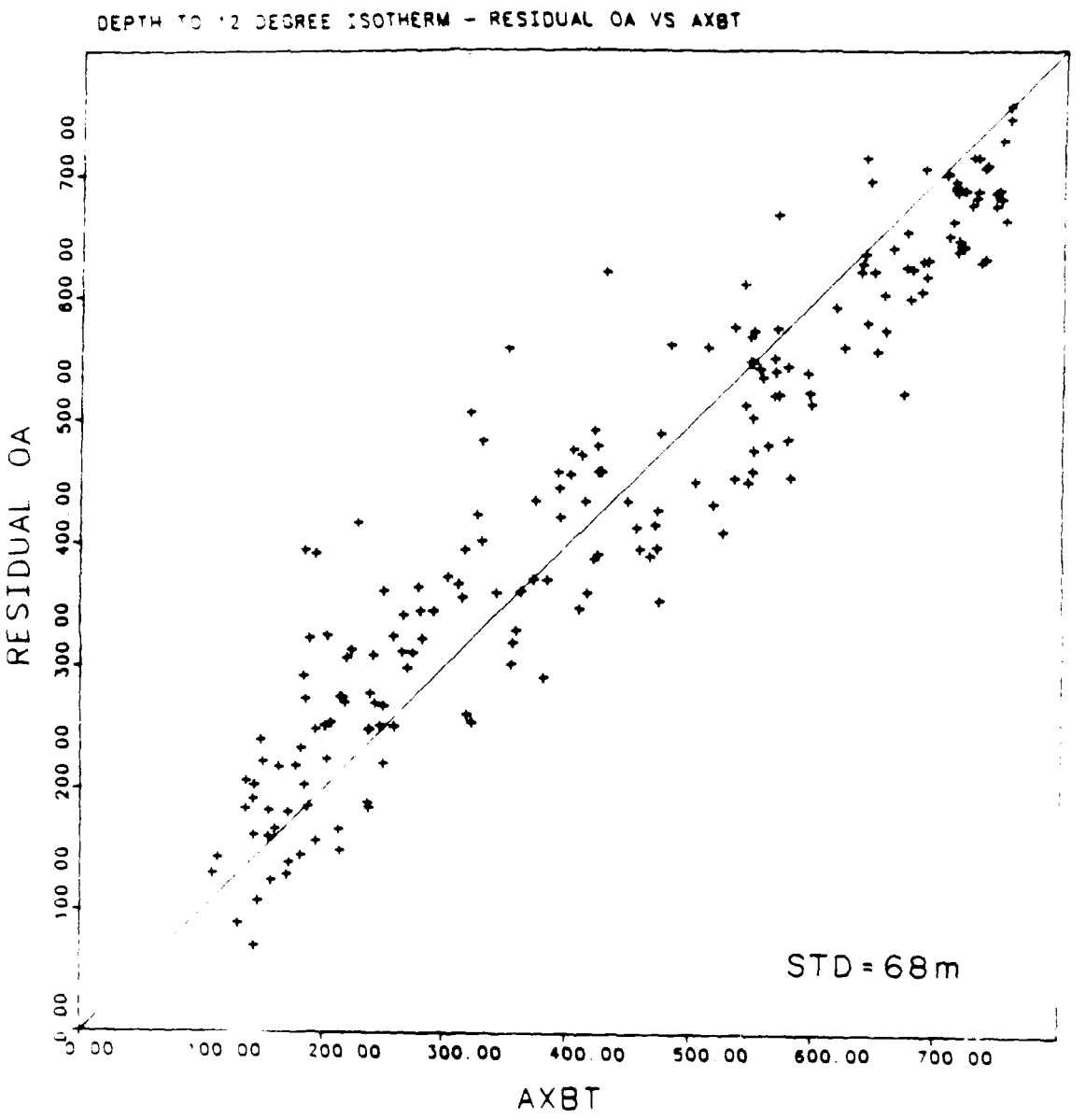

Figure 4.9 Same as Figure 4.6 except for AXBTs.

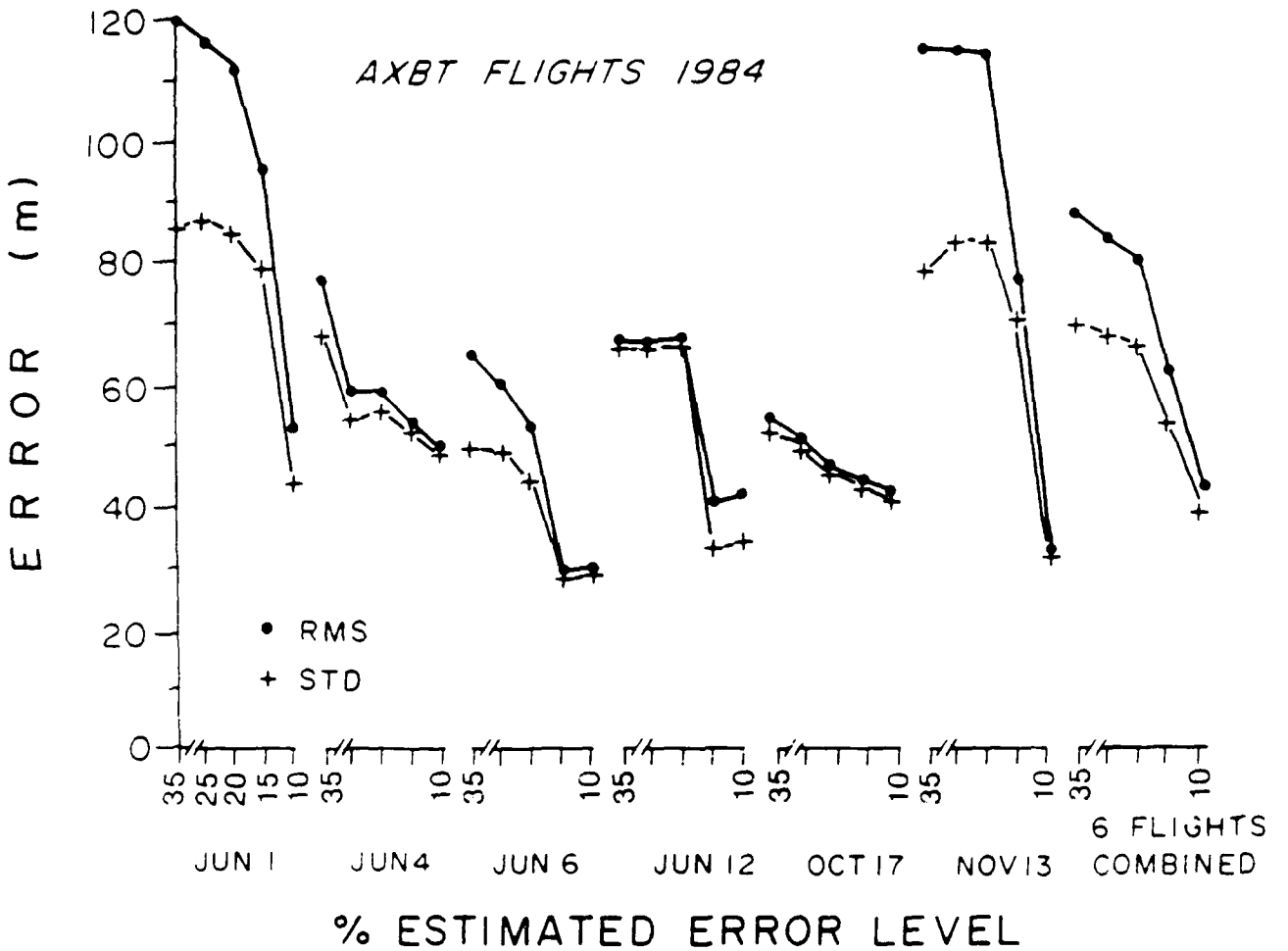

Figure 4.10 Same as Figure 4.7 except for AXBTs for six flights individually and for all six flights combined.

4.3 Comparison of the IES OA maps with XBT and AXBT Data: Case B (δt = 1 σ)

4.3.1 Results of the XBT comparison

For each XBT located within the map region delimited by the 20% error level, the depth of the 12°C isotherm is plotted against the OA Z_{12} estimate in Figure 4.11. The scatter represents a RMS difference of 47 m. Figure 4.12 shows the same Z_{12} comparison but includes all XBTs within the 35% estimated map error level with a corresponding RMS difference of 50 m.

The RMS differences are plotted in Figure 4.13 by cruise for estimated map error levels ranging from 10% to 35%. EN106 had almost a constant RMS difference as the estimated map error increased. For C8304 and EN118 there was a sharp rise in RMS difference and then a leveling off as map error levels increased further. Two cruises (EN087 and EN124) had a steady RMS increase as map error levels increased. The combined RMS differences for all 5 cruises increase uniformly from 40 m to 50 m as the map error increased from 10% to 35%.

The corresponding STD values are also plotted in Figure 4.13. There is little difference from RMS values, again indicating that no navigational biases were introduced.

4.3.2 Results of the AXBT comparison

The depth of the 12°C isotherm at each AXBT site is plotted against the residual estimated OA Z_{12} value for all AXBTs within the region of the 20% and 35% error limits in Figure 4.14 and Figure 4.15, respectively. The STD differences increase from 47 m at the 20% error level to 74 m at the 35% error level. The range of these results exceeds that for the standard map comparisons (case A) in which a minimum STD of 53 m and a maximum STD of 68 m were obtained at the 15% and 35% error levels, respectively. The range for case B is greater due

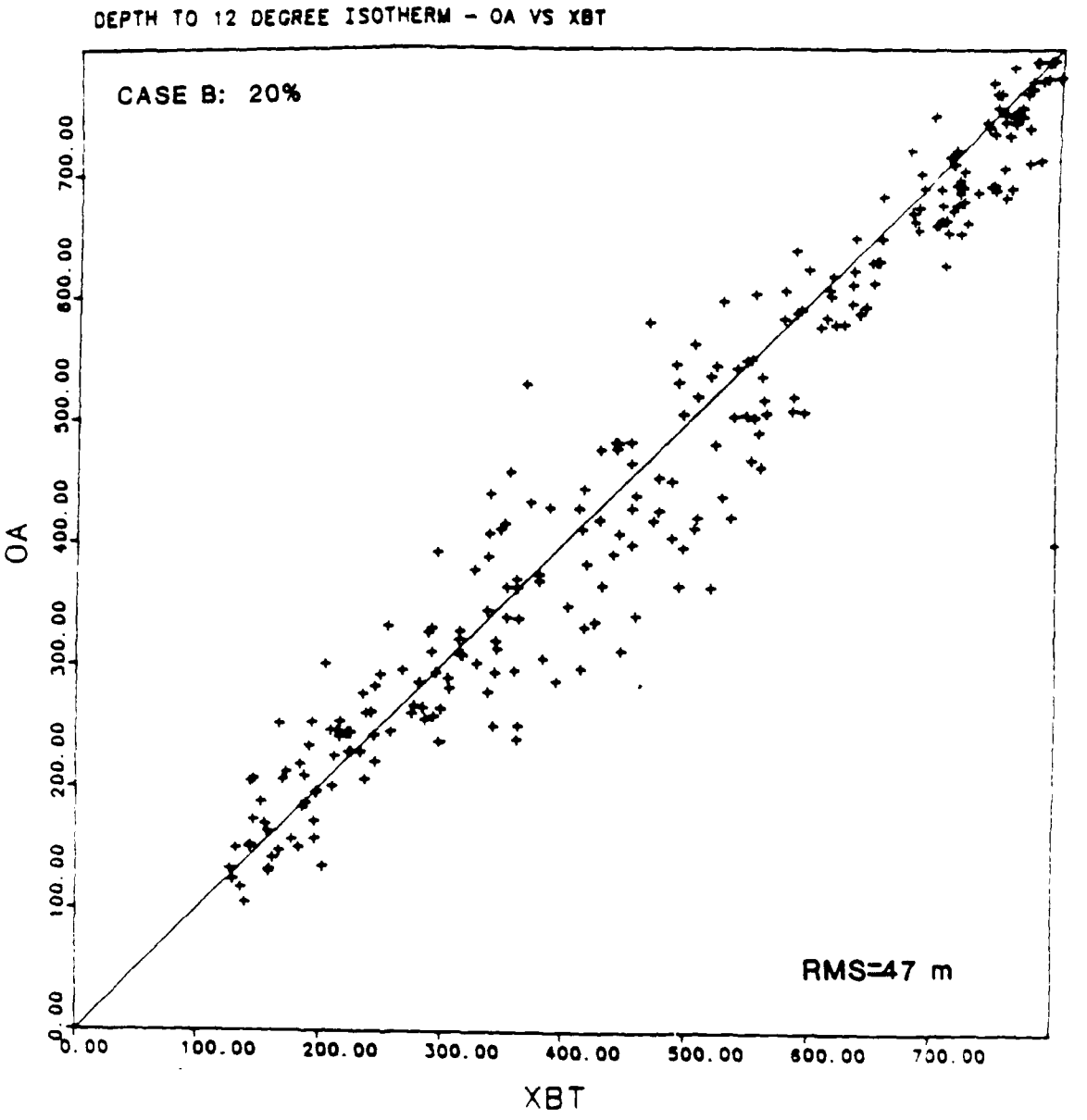

Figure 4.11 Same as in Figure 4.5 except for case B (δt = 1 d) and <20% error.

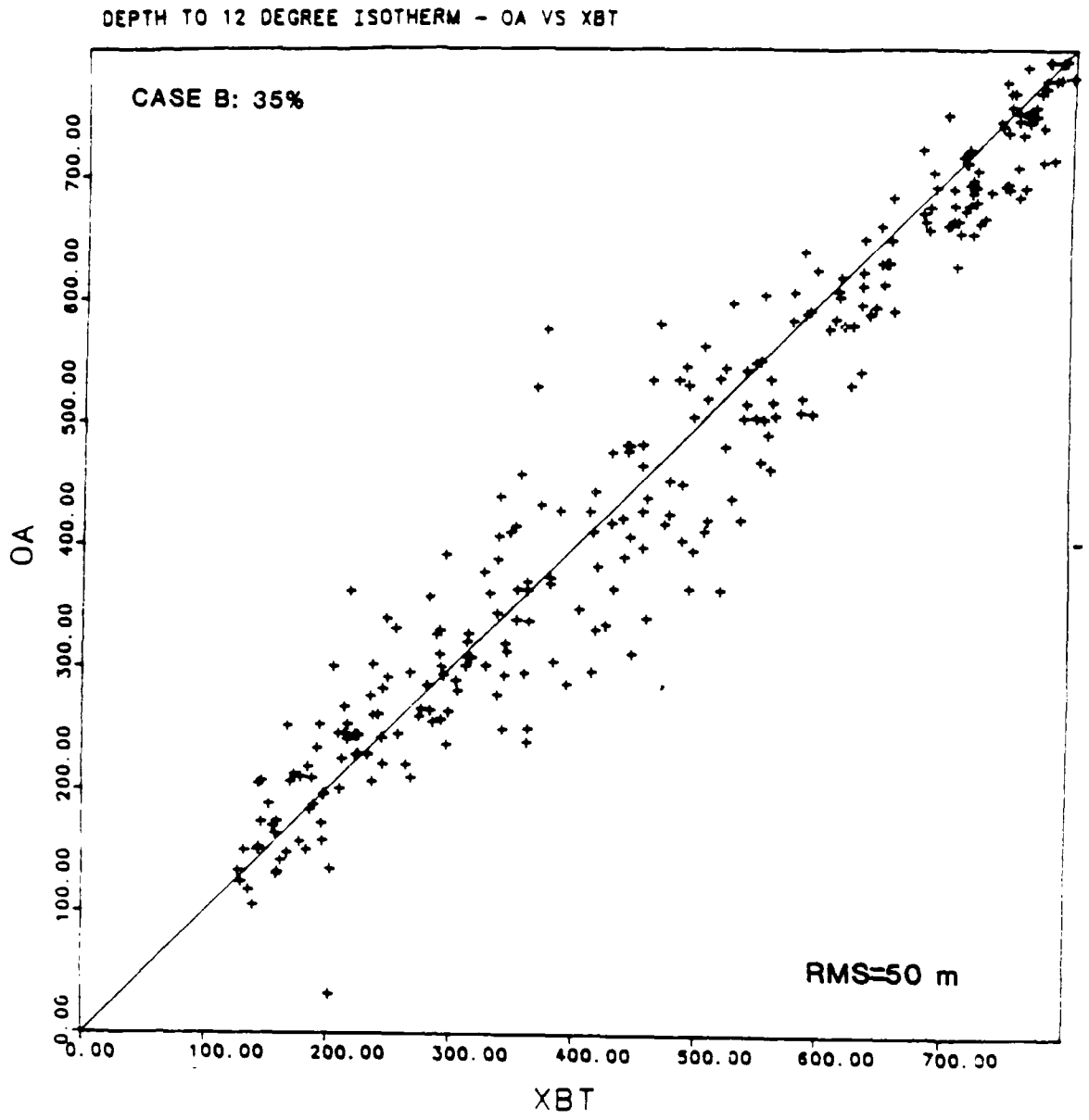

Figure 4.12 Same as Figure 4.6 except for case B.

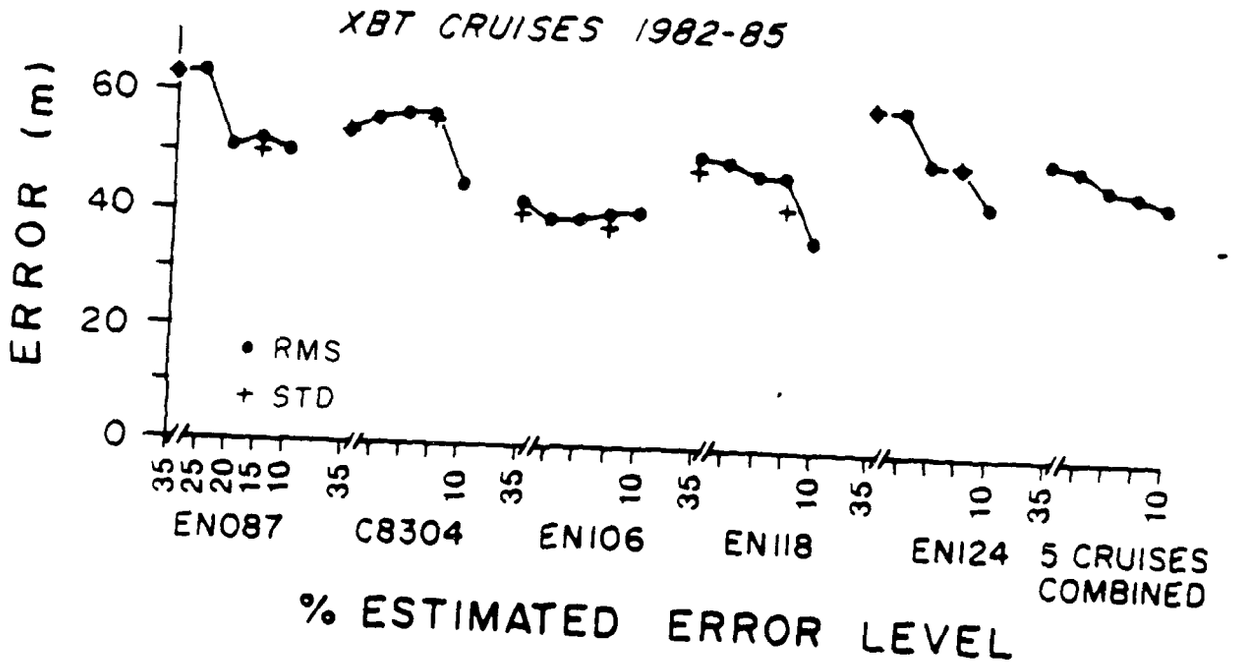

Figure 4.13 Same as Figure 4.7 except for case B.

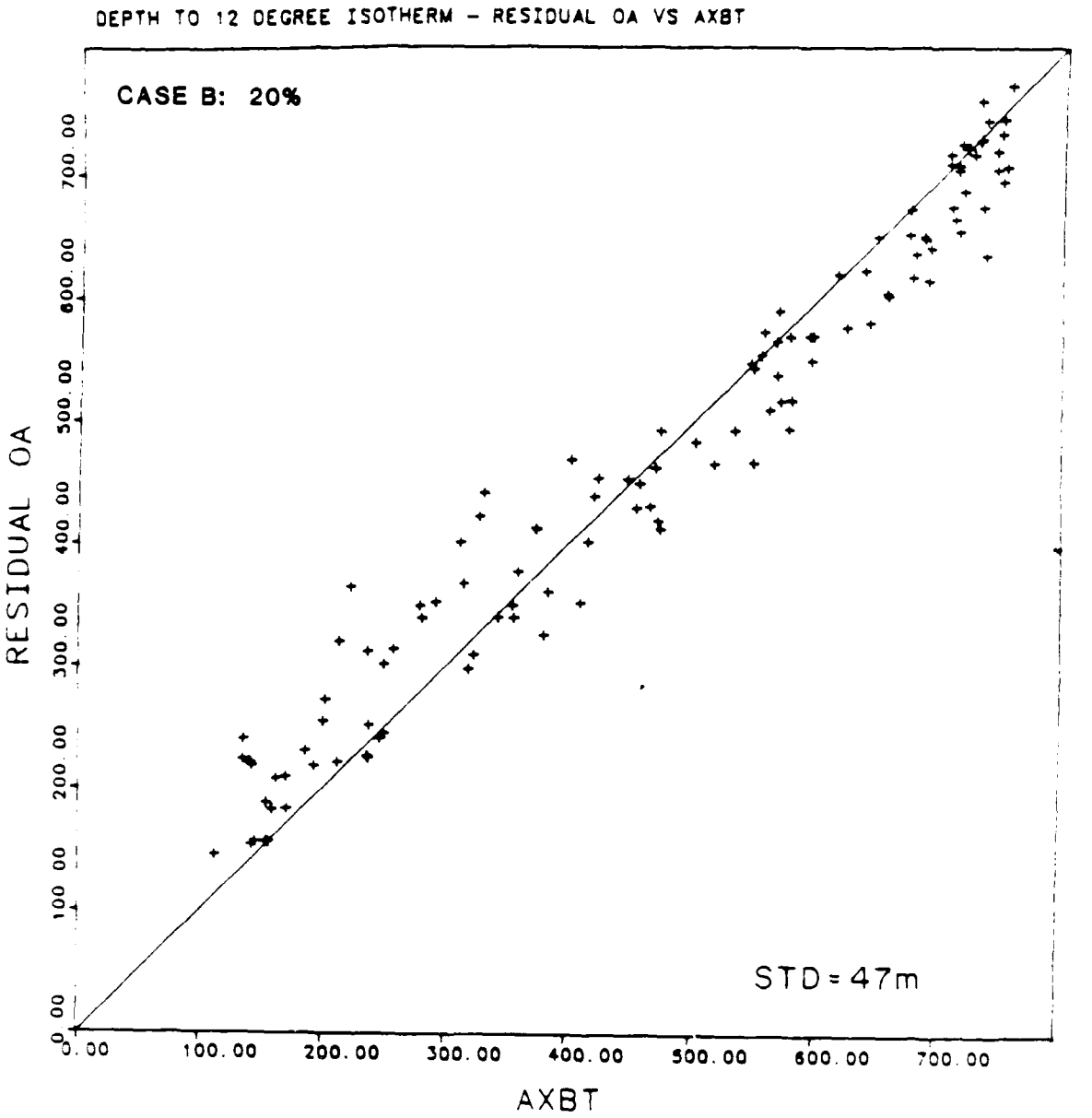

Figure 4.14 Same as Figure 4.5 except for AXBTs and case B (δt = 1 d) at the 20% error level.

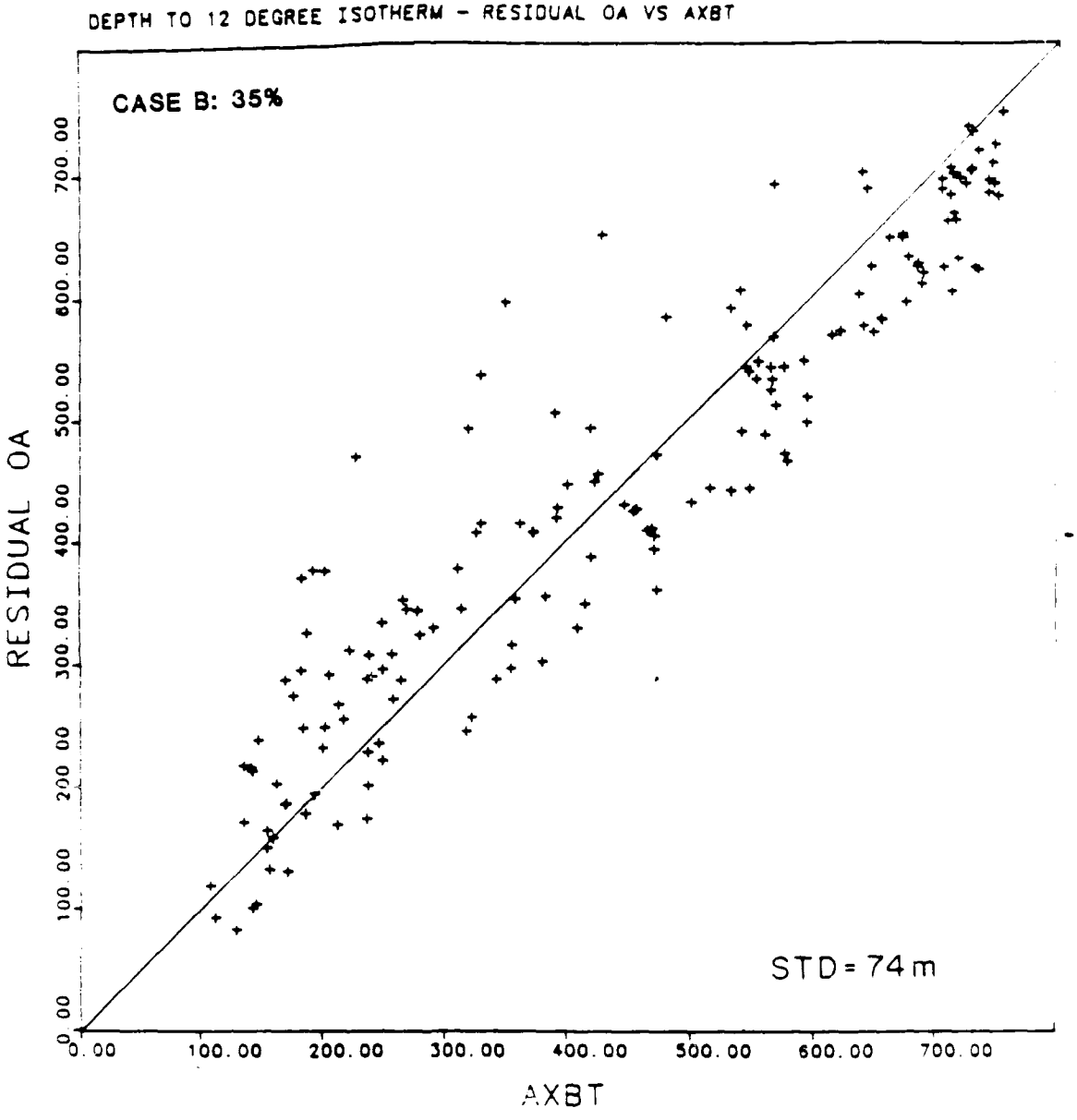

Figure 4.15 Same as Figure 4.6 except for AXBTs and case B.

to the redistribution of some AXBTs within the five error levels. As the error fields increased in size from case A to case B, some of the AXBT drop-sites shifted into map regions with higher estimated errors.

The navigational offsets between the ship and aircraft are apparent also in Figure 4.16, where the RMS and STD differences for error levels ranging from 10% to 35% are plotted for each flight. The differences between the two curves for 1 June, 6 June, 17 October, and 13 November indicate such an offset. The two curves for the 4 June and 12 June flights are almost identical, indicating no navigational bias.

The composite STD values for all six flights increases from 34 m at the 10% estimated map error level to 74 m at the 35% error level. As in the comparison with the standard maps, there is a rapid increase in STD differences as the mapping area was extended from regions of 10 to 35% estimated error.

4.4 Accounting for the RMS differences

Finally, we attempt to account for all the factors contributing to the observed RMS (40-50 m) and STD (34-74 m) differences between the IES OA maps and the XBTs and AXBTs found in both cases A and B. Three sources of error contribute to these differences: (a) the XBT and AXBT probes, (b) the inverted echo sounders, and (c) the objective analysis method.

Sippican Corporation reports a depth accuracy for the XBTs of 5 m plus 2% of the depth, which, when combined with a 0.2°C temperature accuracy, yields an ϵ_{XBT} = 15 m RMS XBT error in Z_{12} for an average Gulf Stream Z_{12} of 400-500 m. The accuracy of the deep AXBTs was determined to be 11 m, resulting from the combination of a 0.2°C temperature accuracy and ±5 m depth accuracy (Boyd, 1986).

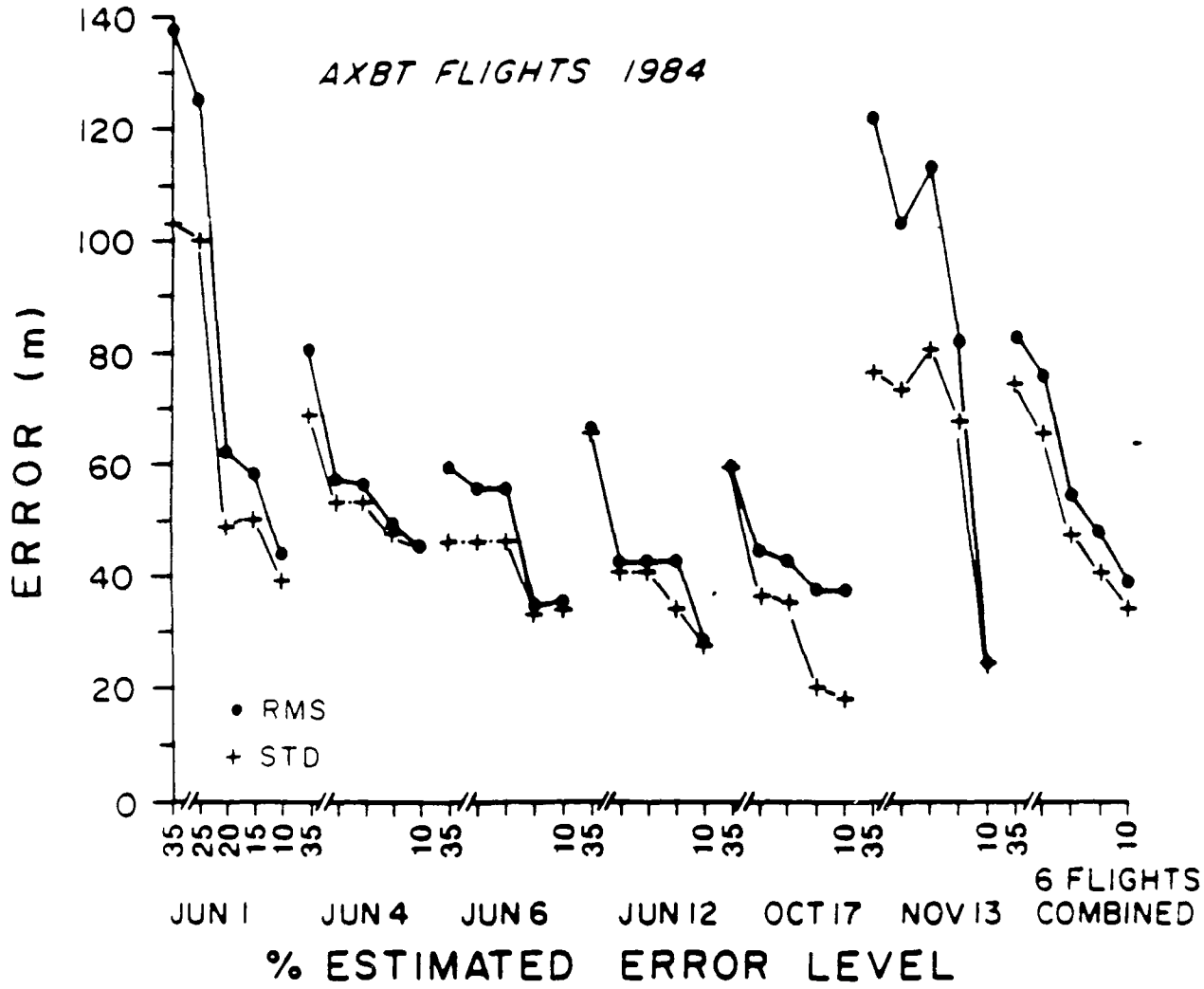

Figure 4.16 Same as Figure 4.7 except for AXBTs and case B.

Tracey and Watts (1986a) report a Z_{12} accuracy of ϵ_{IES} = 25 m RMS for the IESs. This was obtained by directly comparing the Z_{12} values measured by IESs with those of XBTs dropped right at the IES sites. This difference results from the differences in the types of measurements made by the two instruments. The IES Z_{12} value is an integrated measurement, throughout the full water column, and as such is not sensitive to small-scale vertical features such as internal waves. The XBT, however, records the instantaneous Z_{12} which results from fluctuations on all vertical scales. Typically, the comparison of an integral measurement with a point measurement produces some disagreement.

In general, any amount of interpolation will cause the output values to differ from the input measurements. Two different amounts of temporal smoothing were used to produce the OA maps for cases A and B. The output Z_{12} values were estimated from several (N = 9) input values within separation distances R = 120 m and lag times of T = ±4 d for the standard maps with decimation time δt = 2 d (case A). For the high temporal resolution maps (case B), lag times were changed to T = ±1 d, the decimation time was reduced to δt = 1 d, and N was decreased to seven input values. In both cases, the OA method tends to smooth the small-scale horizontal and temporal fluctuations in the Z_{12} field. The amount by which the outputs differ from the inputs can be estimated by:

$$\epsilon_{OA} = e^{1/2} * \sigma$$

where e is the error at the output grid point estimated by the OA method and σ is the standard deviation of Z_{12} at that point. Assuming a typical value for σ in the Gulf Stream of 100 m (Figure 3.6) within the map region of 15% estimated error, we obtain ϵ_{OA} = 38 m. The value of

ϵ_{OA} ranges from 32 m at the 10% error level within the IES array to 59 m at the 35% map error level in the outer fringes of the OA maps.

The total expected RMS difference between the IES OA maps and the XBTs and AXBTs is the square root of the sum of the squares of these three uncorrelated contributers $(\epsilon_{XBT}^2 + \epsilon_{IES}^2 + \epsilon_{OA}^2)^{-1/2}$. Using ϵ_{OA} = 38 m for the 15% error level, we obtain an expected error of 48 m. The expected RMS difference ranges from 42 m for the 10% error level to 67 m at the 35% error level. These expected errors are close to the observed RMS and STD differences between the Z_{12} values of the IES OA maps (for both cases A and B) and the XBTs (40-50 m) and the AXBTs (34-74 m). Although the XBT RMS difference of 50 m for the 35% error level seems low, it can be attributed to the concentration of the XBT drop sites near the IES sites. Thus, the AXBTs, with more evenly distributed drop sites, give a better estimace of the true STD differences at the 35% error level. The good agreement between the expected RMS differences of 42-67 m and the observed RMS and STD differences of 34-74 m assures us that we have accounted for all the error.

4.5 Summary of Results

Comparisons of estimated IES OA Z_{12} values with the Z_{12} measured independently by XBTs and AXBTs were made in order to determine how well the OA technique maps the thermocline depth field. RMS and STD differences between the Z_{12} values determined from IES OA maps and from XBTs and AXBTs were calculated at five estimated error levels ranging from 10-35% for standard maps (case A) and high temporal resolution maps (case B).

To check for biases introduced by navigation offsets between the ship and aircraft, we looked for large discrepancies between the RMS and

STD values. For the XBT comparisons with the IES OA maps, no significant differences were found, confirming that there were no navigation offsets between the ships that dropped the XBTs and those that deployed IESs. Large differences were found, however, for four of the AXBT comparisons, indicating that navigation offsets occurred between the ship and aircraft. In order to minimize these biases, we have used the STD values for the AXBT comparisons.

For the standard maps (case A), the comparison of the IES OA Z_{12} values with those of the XBTs resulted in RMS differences ranging from 40 m at the 10% map error level to 50 m at the 35% error level (Figure 4.7). The AXBT STD differences ranged from 39 m at the 10% error level to 68 m at the 35% error level (Figure 4.10).

The comparison of the Z_{12} values from the high temporal resolution maps (case B) with those of the XBTs yielded RMS differences of 39 m at the 10% map error level to 50 m at the 35% error level (Figure 4.3). The AXBT comparisons with these maps produced STD differences ranging from 34 m at the 10% error level to 74 m at the 35% error level (Figure 4.16).

For both cases A and B, the AXBT STD values spanned a greater range than the XBT RMS values. The difference can be attributed to differences in the drop-site locations of the XBTs and AXBTs; the AXBTs were more evenly distributed throughout the regions delimited by the five error levels.

It is interesting to note that the RMS and STD values at the 15% error level for case A (standard maps) are nearly the same as those at the 20% error level for case B (high temporal resolution maps). This is true for both the XBTs and AXBTs. For case A, the RMS and STD values at the 15% error level were 47 m for the XBTs and 53 m for the AXBTs. The

XBT and AXBT RMS and STD differences were identical (47 m) at the 20% error level for case B. Inspection of the estimated error fields shown in Figure 4.1 reveals that the area outlined by the 15% error level for case A is very similar to that described by the 20% error level for case B. Thus, the subsets of probes used for these tests were nearly the same. In either case, the RMS and STD differences of less than 50 m indicate that there is good agreement between the estimated (from the OA maps) and observed (from the XBTs and AXBTs) Z_{12} values.

For the IES OA standard (case A) maps, we chose the region delimited by the 15% error level as the largest area of accurate mapping. Correspondingly, we chose the region defined by the 20% error level for the high temporal resolution (case B) maps. There are several reasons why we believe that the map quality within these areas is good. First, the observed RMS differences between the IES OA maps and the XBTs and AXBTs were only 47 m. For both cases, large increases in RMS error were obtained for each 5% error increase beyond these limits, while the mapping areas were only slightly increased. Secondly, having identified three contributing sources of error, we can account for the observed RMS differences. Additionally, the observed RMS differences are less than the contour interval used for the Z_{12} maps. This corresponds to a small (~5 km) error in the lateral displacement of the Z_{12} depth. Finally, the error of 47 m represents less than 8% of the total thermocline depth variation of 700 to 800 m found in the Gulf Stream.

SECTION 5. CONCLUSIONS

Watts and Tracey (1985) modified the objective analysis method presented in Carter (1983) and Carter and Robinson (1987) in order to extend its application to the thermal frontal region of the Gulf Stream. In this report, we present the results from a series of tests which assessed the sensitivity of the technique to variations in the control parameter selections. Having chosen the parameters that produce the best output maps of the thermocline depth field, we then determined the accuracy of these maps by comparing them against concurrent measurements of the temperature field made by XBTs and AXBTs.

We tested the robustness of the methodology to the selection of the mean field, standard deviation field, correlation function, and decimation time. Despite variations in these parameters, the interpolated areas (between the instrument sites) of all the output maps are very similar. All output maps, evaluated at the measurement sites, differed from the actual observations by less than 15 m RMS, regardless of the control parameter chosen. The extrapolated regions (away from the instrument sites) were strongly affected by the choice of mean field, with two of the three fields introducing unrealistic thermal features to the output maps. Variations in the choice of correlation function produced little effect on the output maps themselves, but the sizes of the estimated error fields associated with them varied considerably between the three functions tested. Only minor differences in the output Z_{12} maps were produced by the decimation time and the standard deviation field. However, large subsampling intervals result in increased smoothing, which in turn may result in the loss of the high-frequency fluctuations that are of scientific interest.

We found that the best output maps were obtained by using the temporal mean (Z_T) and standard deviation (σ_T) fields. Subsampling the input data at either one-day (δt = 1 d) or two-day (δt = 2 d) intervals appeared to resolve many of the important fluctuations while keeping smoothing to a minimum. The analytic correlation function based on IES measurements in the Gulf Stream, ρ_{WT}, predicted the smallest errors, and these agreed well with the observed differences from independent data.

One of the purposes of applying the OA technique on the IES Z_{12} measurements is to map accurately (i.e., with minimal estimated errors) the Gulf Stream thermocline depth field over a large area. In order to objectively choose the limits of extrapolation beyond the instrument sites, comparisons of the output maps were made with independent measurements of Z_{12} obtained from XBTs and AXBTs. Two cases were tested: Case A evaluated OA maps produced using the standard map parameters (in particular δt = 2 d and T = ±4 d) and case B evaluated maps produced with higher temporal resolution (δt = 1 d and T = ±1 d). RMS and STD differences for both cases were computed at five levels of estimated error ranging from 10-35%. These differences ranged from 34 m at the 10% level to about 74 m at the 35% level. The mapping regions delimited by the 15% error level for case A and the 20% error level for case B were nearly indentical. The observed differences between the IES OA maps and the XBTs and AXBTs were 47 m at the 15% (case A) and 20% (case B) error levels. We have chosen the 15% error level for the standard maps and the 20% error level for the high temporal resolution maps as the limits of the Z_{12} field extrapolation. These were selected because the RMS differences are less than one contour interval on the output Z_{12} maps and represent less than 8% of the total thermocline depth change (700-800 m) across the Gulf Stream.

ACKNOWLEDGEMENTS

This research program was funded by the National Science Foundation under grants OCE82-01222 and OCE85-17746 and by the Office of Naval Research under contract N00014-81-C-0062. John Bane of the University of North Carolina provided the AXBT data used for the comparisons. Skip Carter supplied the basic objective mapping and contouring programs. We thank Julie Rahn for editorial assistance.

REFERENCES

Boyd, J.D. 1986. Improved depth and temperature conversion equations for Sippican AXBTs. NORDA Report 156. NSTL, Mississippi.

Bretherton, F.P., R.E. Davis, and C.B. Fandry. 1976. A technique for objective analysis and design of oceanographic experiments applied to MODE-73. Deep-Sea Res. 23: 559-582.

Carter, E.F. 1983. The statistics and dynamics of ocean eddies. Ph.D. Thesis. Harvard University.

Carter, E.F. and A. R. Robinson 1987. Analysis models for the estimation of oceanic fields. J. Atmos. Oceanic Technol. 4: 49-74.

Freeland, H.J. and W.J. Gould. 1976. Objective analysis of meso-scale ocean circulation features. Deep-Sea Res. 23: 915-923.

Friedlander, A.F., K.L. Tracey, and D.R. Watts. 1986. The Gulf Stream Dynamics Experiment: Inverted echo sounder data report for the July 1982 to April 1983 deployment period. University of Rhode Island. GSO Technical Report 86-5. 101 pp.

Gandin, L.S. 1965. Objective analysis of meteorological fields. Israel Program for Scientific Translations. Jerusalem. 242 pp.

Halliwell, G.R., Jr. and C.N.K. Mooers. 1983. Meanders of the Gulf Stream Downstream from Cape Hatteras 1975-1978. J. Phys. Oceanogr. 13: 1275-1292.

Tracey, K.L., M. Cronin, and D.R. Watts. 1985. The Gulf Stream Dynamics Experiment: Inverted echo sounder data report for the June 1984 to May 1985 deployment period. University of Rhode Island. GSO Technical Report 85-3. 176 pp.

Tracey, K.L. and D.R. Watts. 1986a. On Gulf Stream meander characteristics near Cape Hatteras. J. Geophys. Res. 91: 7587-7602.

Tracey, K.L. and D.R. Watts. 1986b. The Gulf Stream Dynamics Experiment: Inverted echo sounder data report for the April 1983 to June 1984 deployment period. University of Rhode Island. GSO Technical Report 86-4. 228 pp.

Watts, D.R. and W.E. Johns. 1982. Gulf Stream meanders: observations on propagation and growth. J. Geophys. Res. 87: 9467-9476.

Watts, D.R. and H.T. Rossby. 1977. Measuring dynamic heights with inverted echo sounders: Results from MODE. J. Phys. Oceanogr. 7: 345-358.

Watts, D.R. and K.L. Tracey. 1985. Objective analysis of the Gulf Stream thermal front from inverted echo sounders. Gulf Stream Workshop Proceedings. University of Rhode Island. II. 525-548.

APPENDIX

DETERMINATION OF THE CORRELATION FUNCTION

The following discussion, with minor changes, was originally presented in Watts and Tracey (1985).

An essential input to the objective analysis is the space-time correlation function $\rho(x',y',t')$, where primes indicate lag distances in space and time. To estimate $\rho(x',y',t')$, we combined data from previous IES deployment-pairs in the Gulf Stream to estimate the average correlation function $\rho(x',y',t')$, for all (x',y') spatial separations and time lags t' from -16 to +16 d. Fifty-three individual instruments, from 1979 to 1984 in six deployment periods, were used and all the pair separations are plotted in Figure A.1. To check for anisotropy of ρ, we first identified cross-stream and along-stream IES pairs and separately calculated their correlation functions. These were averages in 10 km bins and are showm in Figure A.2 versus distance. At zero time lag, the observations show ρ to be remarkably isotroic, since the functional shapes for instruments spaced in either direction are indistinguishable. Consequently we can approximate $\rho = \rho(r)$. Figure A.3 shows the observed correlation function in plan view for time lags out to 10 days. These have been smoothed by a 50 km Gaussian weighted low-pass filter. At non-zero time lag, the peak of the observed correlation functon moves downstream at 12 km/d, decays slowly (e.g., exceeding 0.7 at t' = 6 d), and maintains its symmetric shape.

We can approximate ρ by the functional form:

$$\rho(x',y',t') = \exp(-t'/T_0)\exp(-r/A)\cos(\pi r/2B)$$

where $r^2 = (x'-ct')^2 + (y')^2$, T_0 = 9.3 d, A = 391 km, B = 171 km, and c = 12 km/d. Figure A.3 also shows the idealized function for the same

time lags as the observed function. We chose this function such that the temporal decay rate of the central peak is similar to the observed values. The spatial decay rate is exactly the same as that observed for zero time lag; thus the idealized function at zero time lag (upper left corner) is another view of $\rho(r)$, which was already shown in Figure A.2. The decay rates of both functions remain similar out to 4 d time lag, but the observed correlations decay more slowly than the idealized function for the longer time lags.

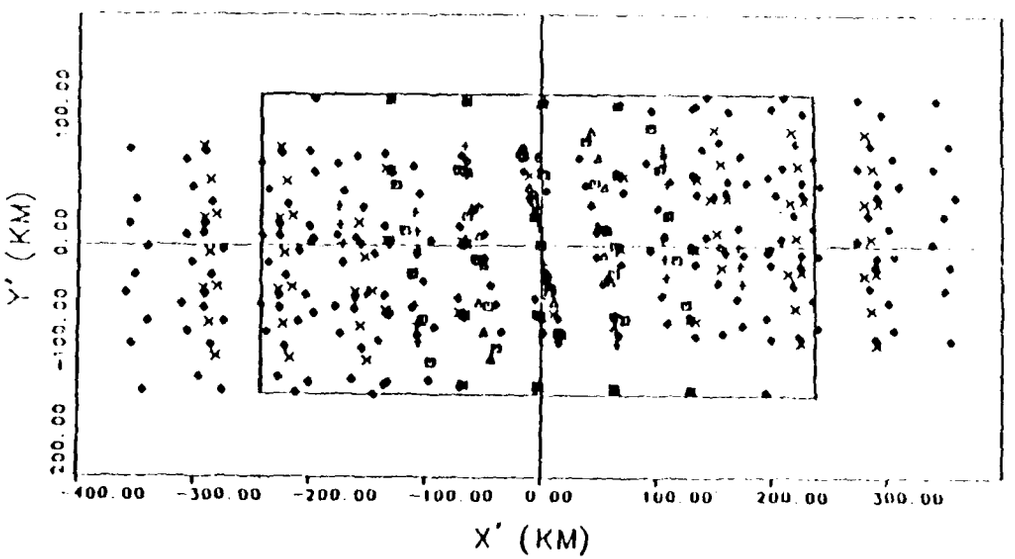

Figure A.1 Plot of all IES pair separations (x',y') with a different symbol used to represent each deployment period. The center box corresponds to the region for which the smoothed $\rho(x',y',t')$ is contoured in Figure A.3.

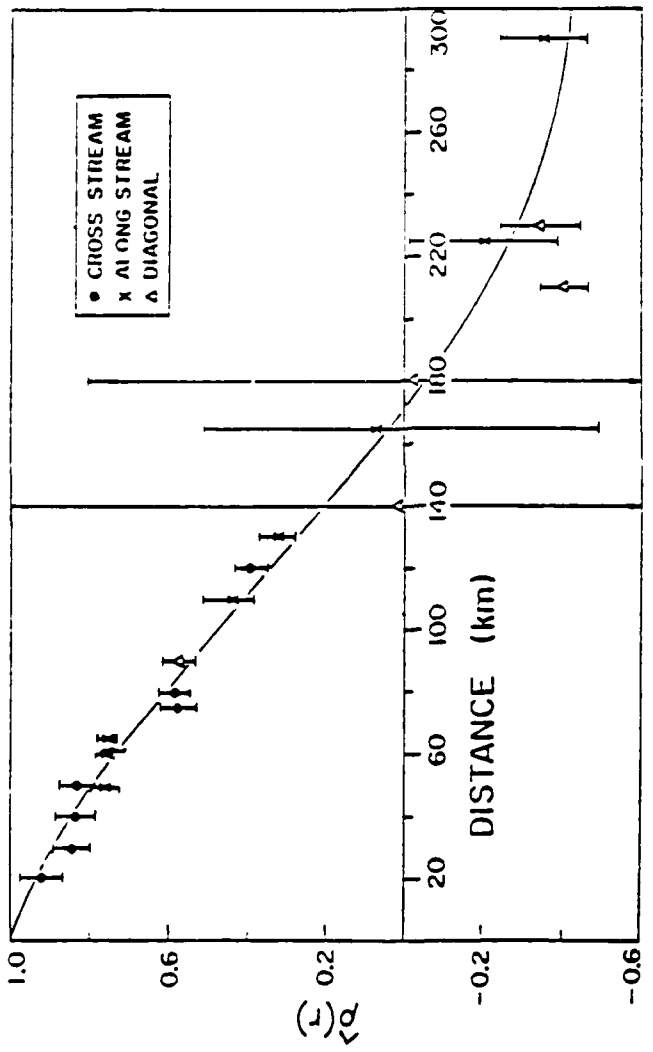

Figure A.2 Correlation functions for cross-stream, along-stream, and diagonal IES pairs versus distance. The solid curve through the values is the idealized $\rho(x',y',t')$ at a time lag of 0 days.

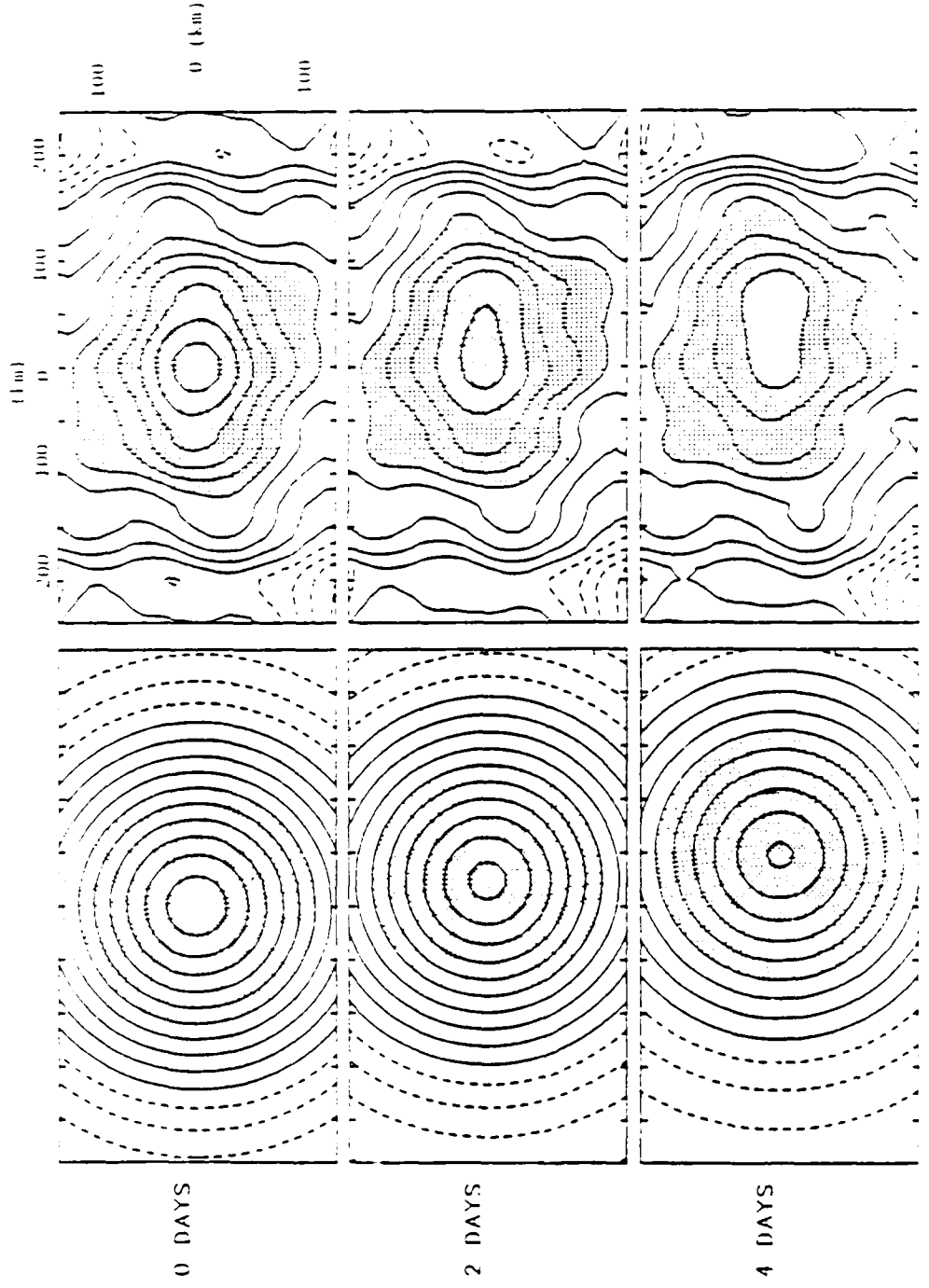

Figure A.3 Idealized (left) and observed (right) correlation functions $\rho(x',y',t')$, contoured in plan view for time lags from 0 to 10 days in 2-day steps. For negative time lags, note that ρ is implicitly given by the symmetry relation $\rho(-x',-y',-t') = \rho(x',y',t')$. Contour interval is 0.1 and negative contours are dashed. Darker shading indicates $\rho \geq 0.7$; lighter shading indicates $\rho \geq 0.4$.

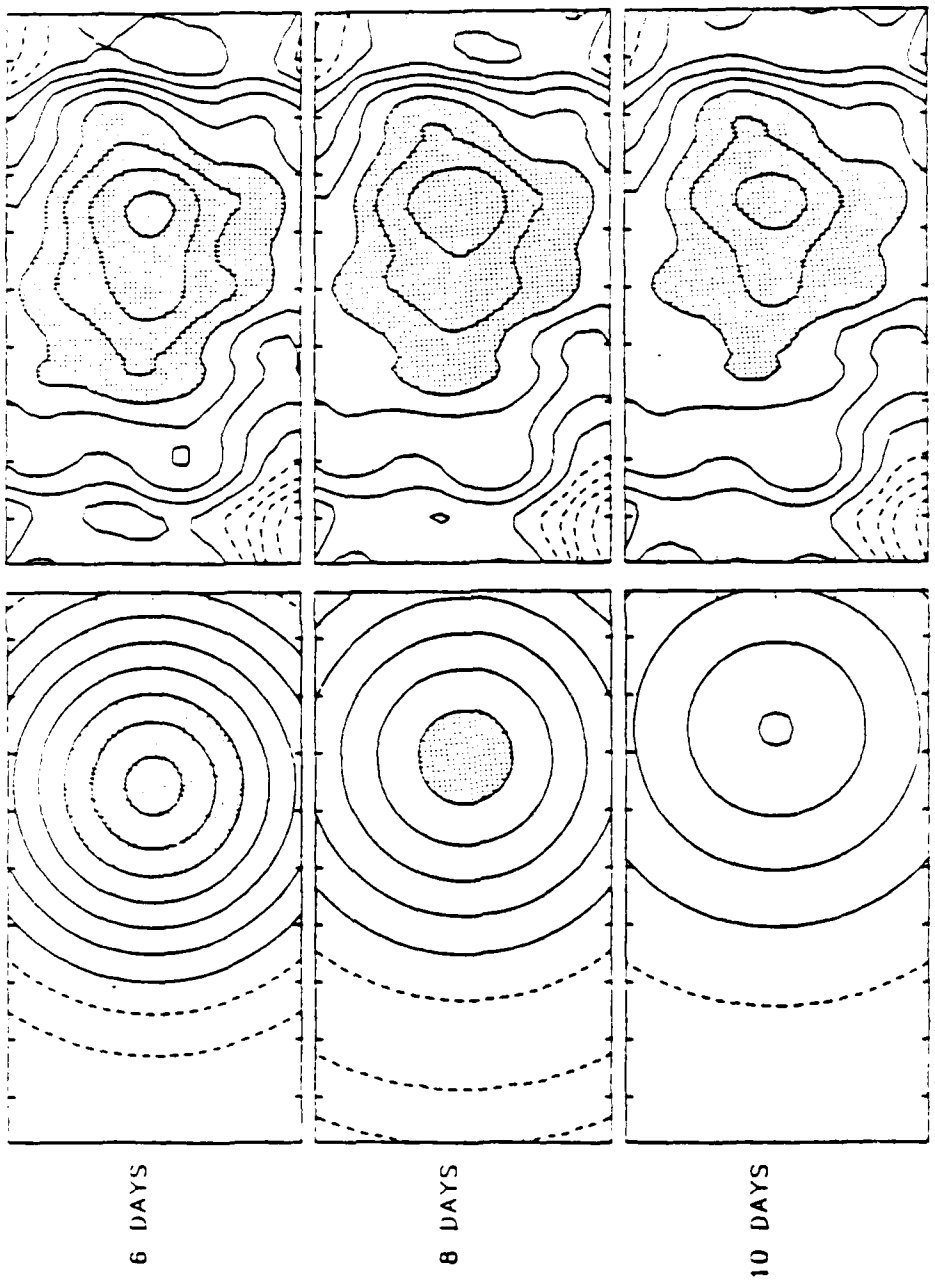

Figure A.3, continued.

Unclassified
SECURITY CLASSIFICATION OF THIS PAGE

REPORT DOCUMENTATION PAGE

1a. REPORT SECURITY CLASSIFICATION: Unclassified	1b. RESTRICTIVE MARKINGS: --
2a. SECURITY CLASSIFICATION AUTHORITY: --	3. DISTRIBUTION/AVAILABILITY OF REPORT: Distribution for public release; distribution is unlimited.
2b. DECLASSIFICATION/DOWNGRADING SCHEDULE: --	
4. PERFORMING ORGANIZATION REPORT NUMBER(S): Graduate School of Oceanography Technical Report 87-2	5. MONITORING ORGANIZATION REPORT NUMBER(S)
6a. NAME OF PERFORMING ORGANIZATION: University of Rhode Island Graduate School of Oceanography; 6b. OFFICE SYMBOL (If applicable)	7a. NAME OF MONITORING ORGANIZATION
6c. ADDRESS (City, State, and ZIP Code): South Ferry Road, Narragansett, RI 02882	7b. ADDRESS (City, State, and ZIP Code)
8a. NAME OF FUNDING/SPONSORING ORGANIZATION: (1) National Science Foundation (2) Office of Naval Research; 8b. OFFICE SYMBOL (If applicable): Physical Oceanography Program, Code 422 PO	9. PROCUREMENT INSTRUMENT IDENTIFICATION NUMBER: OCE82-01222 and OCE85-17746 N00014-81-C-0062
8c. ADDRESS (City, State, and ZIP Code): (1) 1800 G St. NW, Washington D.C. 20550 (2) Code 422 PO, 800 North Quincy, Arlington, VA 22217	10. SOURCE OF FUNDING NUMBERS: PROGRAM ELEMENT NO. / PROJECT NO / TASK NO. / WORK UNIT ACCESSION NO.

11. TITLE (Include Security Classification)
Objective Analysis of the Gulf Stream Thermal Front: Methods and Accuracy (Unclassified)

12. PERSONAL AUTHOR(S)
K.L. Tracey, A.I. Friedlander, and D.R. Watts

13a. TYPE OF REPORT	13b. TIME COVERED	14. DATE OF REPORT (Year, Month, Day)	15. PAGE COUNT
Summary	FROM 7/1982 TO 5/1985	December 1987	104

16. SUPPLEMENTARY NOTATION

17. COSATI CODES			18. SUBJECT TERMS (Continue on reverse if necessary and identify by block number)
FIELD	GROUP	SUB-GROUP	Gulf Stream thermal front; Inverted Echo Sounders; objective analysis

19. ABSTRACT (Continue on reverse if necessary and identify by block number)

The objective analysis (OA) technique was adapted by Watts and Tracey in order to map the thermal frontal zone of the Gulf Stream. Here, we test the robustness of the adapted OA technique to the selection of four control parameters: mean field, standard deviation field, correlation function, and decimation time. Output OA maps of the thermocline depth are most affected by the choice of mean field, with the most realistic results produced using a time-averaged mean. The choice of the space-time correlation function has a large influence on the size of the estimated error fields, which are associated with the OA maps. The smallest errors occur using the analytic function, ρ_{WT}, which is based on four years of inverted echo sounder data collected in the same region of the Gulf Stream. Variations in the selection of the standard deviation field and decimation time have little effect on the output OA maps.

We determined the accuracy of the output OA maps by comparing them with independent measurements of the thermal field. Two cases are evaluated: standard maps and high temporal resolution maps, with decimation times of 2 days and 1 day, respectively. Standard deviations

20. DISTRIBUTION/AVAILABILITY OF ABSTRACT	21. ABSTRACT SECURITY CLASSIFICATION
☒ UNCLASSIFIED/UNLIMITED ☒ SAME AS RPT ☐ DTIC USERS	unclassified
22a. NAME OF RESPONSIBLE INDIVIDUAL	22b. TELEPHONE (Include Area Code) / 22c. OFFICE SYMBOL

DD FORM 1473, 84 MAR — 83 APR edition may be used until exhausted. All other editions are obsolete.

SECURITY CLASSIFICATION OF THIS PAGE

19.

(STD) between the standard maps at the 15% estimated error level and the XBTs (AXBTs) are determined to be 47-53 m. The comparisons of the high temporal resolution maps at the 20% error level with the XBTs (AXBTs) give STD differences of 47 m.